Optimizing the Implementation of Green Technologies Under Climate Change Uncertainty

A Dissertation Presented for the

Doctor of Philosophy

Degree

The University of Tennessee, Knoxville

Mohammad Ramshani

August 2019

© by Mohammad Ramshani, 2019
All Rights Reserved.

To mom and dad, my sister and my brother.

Acknowledgments

I would first like to express my special appreciation and thanks to my advisor, Dr. Xueping Li, for the precious opportunity to be part of his research group, and for his never-ending help and support, and invaluable guidance.

My sincere thanks also goes to Dr. Khojandi, for all the helps, insights, and support without which this dissertation would not be possible.

To my dissertation committee members, Dr. Oleg Shylo and Dr. Jon Hathaway. Thank you for your generously offered time and your insights on this work. Your inputs in the dissertation are highly appreciated.

I also would like to thank my fellow graduate students: Mohit Shukla, Kaike Zhang, Phillip Scruggs, Rodney Kizito, Luis Liu, and Lorna Treffert . Thank them for sharing the graduate school life together here and the supportive team environment.

Abstract

In this study, we aim to investigate the application of the green technologies (i.e., green roofs (GRs), Photovoltaic (PV) panels, and battery integrated PV systems) under climate change-related uncertainty through three separate, but inherently related studies, and utilize optimization methods to provide new solutions or improve the currently available methods

First, we develop a model to evaluate and optimize the joint placement of PV panels and GRs under climate change uncertainty. We consider the efficiency drop of PV panels due to heat, savings from GRs, and the interaction between them. We develop a two-stage stochastic programming model to optimally place PV panels and GRs under climate change uncertainty to maximize the overall profit. We calibrate the model and then conduct a case study on the City of Knoxville, TN.

Second, we study the diffusion rate of the green technologies under different climate projections for the City of Knoxville through the integration of simulation and dynamic programming. We aim to investigate the diffusion rates for PV panels and/or GRs under climate change uncertainty in the City of Knoxville, TN. We further investigate the effect of different and evaluate their effects on the diffusion rate. We first present the agent based framework and the mathematical model behind it. Then, we study the effects of different policies on the results and rate of diffusion.

Lastly, We aim to study a Lithium-ion battery load connected to a PV system to store the excess generated electricity throughout the day. The stored energy is then used when the PV system is not able to generate electricity due to a lack of direct solar radiation. This study is an attempt to minimize the cost of electricity bill for a medium sized household by maximizing the battery package utilization. We develop a Markov decision processes (MDP) model to capture the stochastic nature of the panels' output due to weather. Due to the

minute reduction in the Li-ion battery capacity per day, we have to deal with an excessively large state space. Hence, we utilize reinforcement learning methods (i.e., Q-Learning) to find the optimal policy.

Table of Contents

1 Optimal Planning of the Joint Placement of Photovoltaic Panels and Green Roofs Under Climate Change Uncertainty **1**

1.1 Introduction . . . 2

1.2 Model Formulation . . . 8

1.3 Model Calibration . . . 12

1.3.1 Parameters Estimated From the Literature . . . 12

1.3.2 Parameters Estimated From Data . . . 18

1.4 Computational Study . . . 22

1.4.1 Solution Approach and Additional Metrics . . . 23

1.4.2 Case Study . . . 24

1.4.3 Sensitivity Analysis . . . 28

1.4.4 Robustness Analysis . . . 35

1.4.5 Environmental Insights . . . 37

1.5 Conclusion and Remarks . . . 38

2 Optimizing PV System Integrated Lithium-ion Batteries Return Under Climate Uncertainly **39**

2.1 Introduction . . . 39

2.2 Model Formulation . . . 47

2.3 Structural Properties . . . 51

2.4 Computational Experiments . . . 52

2.4.1 Example Optimal Policies . . . 52

2.4.2 Current Practices and Policies . . . 54

2.4.3 Solution Approach . . . 56
2.4.4 Computational Analyses . . . 60
2.5 Conclusion and Remarks . . . 62

3 An Agent Based Approach to Study the Diffusion Rate and the Effect of Policies on Joint Placement of Photovoltaic Panels and Green Roof under Climate Change Uncertainty 64

3.1 Introduction . . . 64
3.1.1 Photovoltaic Panels and Green Roofs . . . 65
3.1.2 Climate Change . . . 67
3.1.3 Agent Based Modeling and Diffusion Models . . . 67
3.2 Methods . . . 72
3.2.1 Financial Model . . . 73
3.2.2 Attitudinal Model . . . 75
3.2.3 ABM Framework . . . 77
3.3 Model Calibration . . . 81
3.4 Computational Studies . . . 90
3.4.1 Case Study . . . 90
3.4.2 Sensitivity Analyses . . . 90
3.4.3 Policy Evaluation . . . 94
3.5 Conclusion . . . 96

4 Conclusions 97

Bibliography 100

Appendices 126

Vita 139

List of Tables

1.1 Notation used in the two-stage stochastic model. 9

1.2 Parameter values estimated from the literature and industry reports. 18

1.3 Ten coupled general circulation models (CGCMs) generated at Oak Ridge National Laboratory's Climate Change Science Institute [35] using high-performance computing resources, including Titan, America's fastest supercomputer [35]. 19

1.4 Maximum, average and the standard deviation range for daily pairwise comparisons across the projections from ten CGCMs, presented in Table 3.5, over two planning horizons of length $T = 10$ years and $T = 20$ years, starting from January 2011. 20

1.5 The parameter values in the three cases considered in the case study for the City of Knoxville. 25

1.6 Optimal solution for an initial budget of $20 million available for investment over two planning horizons of length $T = 10$ years and $T = 20$ years for the cases presented in Table 1.5. 26

1.7 Area covered by stand-alone GRs, stand-alone PV panels, and GR integrated PV panels under different values for PV panel output, PV system variable cost, percentage energy saving in cooling and heating degree-hours due to GR installation, and percentage efficiency increase in the output of PV panels due to integration with GRs for an initial budget of $20 million available over two planning horizons of length $T = 10$ years and $T = 20$ years. 29

1.8 Area covered by stand-alone GRs, stand-alone PV panels, and GR integrated PV panels under different values of δ, for an initial budget of \$20 million available over two planning horizons of length $T = 10$ years and $T = 20$ years for the cases presented in Table 1.5. 31
1.9 Area covered by stand-alone GRs, stand-alone PV panels, and GR integrated PV panels under different values of $\mathbb{C}^{\kappa}$, for an initial budget of \$20 million available over two planning horizons of length $T = 10$ years and $T = 20$ years for the cases presented in Table 1.5. 33
1.10 Optimal solution for an initial budget of \$20 million available for investment over two planning horizons of length $T = 10$ years and $T = 20$ years for the cases presented in Table 1.5 under the grid-based calibration approach. . . . 35
1.11 Robustness analysis for different parameter combinations for an initial budget of \$20 million available over two planning horizons of length $T = 10$ years and $T = 20$ years. Negative values are enclosed in parentheses. 36
1.12 Total amount of requisite fossil fuels to produce the electricity saved and/or generated under the optimal solution in Cases 1–3 for two planning horizons of length $T = 10$ years and $T = 20$ years. 37

2.1 Notation used in the model. 50
2.2 Case studies to investigate the effects of changes in possible set of peak sunlight hours at day t, $X(t)$, on the results of the model. 53
2.3 Mean, maximum, minimum, and standard deviation for the results from the comparison between the optimal policy from the model versus the benchmark, i.e., charge as much as possible and discharge until the demand is met or the battery is empty, and replace when maximum available capacity is equal to $\underline{\ell}$, for to two cases presented in Table 2.2. 55
2.4 Eight different case studies designed to evaluate the performance of the developed approximate algorithms, where $X(t)$ denotes the possible set of peak sunlight hours at day t. 60

2.5 Average Mean Absolute Percentage Error (MAPE), preparation time and train time for DQN, ADQN, and SADQN for 10,000 episodes (iterations) over a time span of 30 days, i.e., $T_{Max} = 30$. Average MAPE shows the average value of MAPE from the results of following the optimal policies under each DRL algorithm compared to the exact solution method over the time horizon. Prep time is the time to generate the data using the exact solution method for each algorithm, which is equal to 0 for DQN as we do not generate any data for DQN before starting the algorithm. The Train time denotes the time in minutes that is spent on training the DRL algorithm. 62

3.1 Model notation for financial sub-model. 74

3.2 Common social networks utilized in the literature for ABM [126]. 78

3.3 The cost per PV system size in USD for southern U.S. for two different panel output efficiency [106]. 83

3.4 Price of PV systems per Watts from 2014 to 2018 reported by [76]. 83

3.5 Coupled general circulation climate forecast models (CGCMs) provided by Oak Ridge National Laboratory's Climate Change Science Institute [35]. These ten projection models are generated using high-performance computing resources, including Titan, America's fastest supercomputer [35]. 84

3.6 The results from the daily pairwise comparison for the ten CGCMs shown in Table 3.5 over the planning horizon of this study, i.e., $T = 20$, starting from January 2011. 85

3.7 Intercept and slope for monthly regression models for peaks sunlight hours versus precipitation level in mm based on historical data for city of Knoxville, TN, based on the data provided by [159] and [156]. 87

3.8 The independent variables and their corresponding normalized coefficients developed by [243]. 88

3.9 The total number of installed PV system, GRs, and GR integrated PV systems, for the agents in the network for different values for network hyper-parameters, decision threshold, and social interactions over twenty years starting from January 2011. 93

A.1 The energy consumption for different sizes of residential buildings in the U.S. and the state of Tennessee, based on the report by EIA [68]. 127

C.1 The number of constraints, variables, and solution times for the three cases in Table 5. 132

List of Figures

1.1 GR integrated PV panel installed over a rooftop in Hailey, Idaho [208]. . . . 3

1.2 The daily maximum and minimum temperatures for the City of Knoxville, Tennessee from ten different climate projections for the year 2030. The dashed lines present the maximum and minimum temperatures across the ten projections over the year. (For details on the climate projections refer to Table 3.5.) 4

1.3 Example hourly temperature values for the City of Knoxville. 21

1.4 Visual-SOLAR radiation map for the City of Knoxville, Tennessee [121]. . . 22

1.5 Rooftop size and solar insolation for the 209,183 buildings in the City of Knoxville, stratified across rooftop size category. 23

1.6 Heat map for average daily maximum and minimum temperatures over the year 2030 projected by the ACCESS CGCM across 4-kilometer wide grids for the City of Knoxville. 34

2.1 An example of battery integrated PV systems. 41

2.2 Example optimal policy for two different cases shown in Table 2.2, with maximum available capacity replacement threshold, i.e., $\underline{\ell}$, equal to 75%. . . 54

2.3 Example optimal policy for two different cases shown in Table 2.2, with maximum available capacity replacement threshold, i.e., $\underline{\ell}$, ranging between 30% and 75%. The red dashed line shows the day from which possible set of peak sunlight hours at day t, $X(t)$, changes. 55

3.1 A GR integrated PV system on a rooftop in a house in Seattle [62]. 66

3.2 The structure of the proposed framework, including Attitudinal and Income model as well as Agent Based Model. The dashed lines indicate the feedback from interactions and time evolution of model variables which originate from the Agent Based Model and is fed to the models. 82
3.3 Visual-SOLAR radiation map for the City of Knoxville, Tennessee [121]. . . 87
3.4 Historical peak sunlight hours and precipitation data for City of Knoxville over 30 years from 1960 to 1990. 88
3.5 The total number of installed packages for a sample of 0.05% of total number of buildings in city of Knoxville, TN, over 20 years. The highlighted areas are the neighborhoods with the most number of installed green technologies. The image only shows the households with installed packages in order to improve the presentation of the results. 91
3.6 The total number of installed packages under 6 different cases, i.e., ideal world, no policies, 5 year and 25 year ITC, PC, and PC and 20-year ITC, where the dashed lines show the cases with ITC policy, and continuous lines represent the cases with no policies. The Lost Opportunity shows the difference between the ideal installation of green technologies and the results form the policy with the most installations. 95

A.1 Average hourly electricity consumption for space conditioning in the state of Tennessee versus building size, based on the data from [68]. The black line represents the regression line for the hourly energy consumption for space conditioning as a function of building size ($R^2 = 0.9816$). 128
B.1 The monthly average temperatures for the City of Knoxville, Tennessee for the ten different climate projections from January 2018 to December 2030. The dashed lines present the maximum and minimum temperatures across the ten projections. 129

B.2 The yearly average temperatures for the City of Knoxville, Tennessee for the ten different climate projections from January 2011 to December 2050. The dashed lines present the maximum and minimum temperatures across the ten projections. 130
B.3 The daily average temperatures for the City of Knoxville, Tennessee for the ten different climate projections from January 2011 to December 2050. The dashed lines present the maximum and minimum temperatures across the ten projections. 131

Chapter 1

Optimal Planning of the Joint Placement of Photovoltaic Panels and Green Roofs Under Climate Change Uncertainty

Photovoltaic (PV) panels directly convert sunlight into electricity; but, sunlight also heats the panels, negatively impacting their efficiency. Green roofs are vegetative layers grown on rooftops, mainly to provide added insulation on the roof to save energy. Green roofs also cool near-surface air temperature. Hence, the joint installation of PV panels and green roofs may potentially lead to higher efficiency of PV panels in certain climates. We develop a two-stage stochastic programming model to optimally place PV panels and green roofs under climate change uncertainty to maximize the overall profit from energy generated and saved. We calibrate the model using the literature, industry reports, and the data from different, at times conflicting, climate projections. We then conduct a case study for a mid-size city in the U.S., perform extensive sensitivity and robustness analyses and provide insights.

1.1 Introduction

Greenhouse gases are the most important contributing factor to the increase of average global temperatures over time [30]; at the current pace, it is estimated that the global temperature will rise by up to 5.8 degrees Celsius over the next century [181]. Greenhouse gas emissions are primarily caused by burning fossil fuels [195] and without a significant change in energy production policies, specifically to reduce the reliance on fossil fuels, the current concentrations of greenhouse gases in the atmosphere is only expected to grow [105].

Solar power is a clean, free, and promising renewable energy source that helps reduce greenhouse gas emissions and hence, mitigate global warming and climate change. Photovoltaic (PV) panels, which can directly convert sunlight into electricity, are one of the most efficient methods of harnessing solar power. PV panels are the fastest growing renewable technology in the recent years at an annual average rate of 6.8% [73]. The number of panels installed within the U.S. increased by 63% between 2007 and 2008 [194], with an estimated increase of approximately 30% per year from 2013 through 2016 in the residential sector [73]. This rate of growth can be attributed to the decreasing costs of PV panels [82] as well as the incentives provided by state and federal governments. The falling prices of PV panels, coupled with the overall increases in power costs from conventional sources, suggest that PV panels are on track to become a strategically advantageous solution to sustainable energy production [235]. It is, however, important to note that despite the increase in demand and the popularity of PV panels, efficiency of PV panels is still limited and depend mainly on the panels' cell material and their operating temperature. The open circuit voltage shows a drop of 2.3 mV per 1 degree Celsius rise in temperature, which translates to a 0.5% drop in efficiency per degree Celsius rise in temperature [231]. While there is ongoing research into engineering solutions to increase the efficiency of PV panels, this paper explores an immediate operational solution through improved, systemic placement decisions.

According to the U.S. Energy Information Administration (EIA), 47.7% of the energy consumed by residential households and 34% of the energy used by the commercial sector is due to space conditioning (i.e., heating and cooling) [73]. Given an expected average growth rate of 0.4%–1.2% and 0.9%–1.1% in the residential and commercial sectors, respectively,



Figure 1.1: GR integrated PV panel installed over a rooftop in Hailey, Idaho [208].

it is estimated that by 2040 the number of residential households grows to 150 million and the commercial space increases to 110 billion square feet [73]. Hence, any reduction in the energy required for space conditioning can result in substantial cost/energy savings. Green roofs (GRs), which are vegetative layers grown on rooftops, can provide added insulation on the roof and cool near-surface air temperature through decreasing the absorption rate of solar radiation by the building structure [61]. This cooling effect can contribute to an approximately 30% drop in the surface temperature [61]. Several long-term studies are currently underway to quantify the thermal performance of GRs [155, 205] as well as the relationship between GRs and energy savings [50, 180] under different climatic conditions. So far, it is estimated that widespread installation of GRs throughout the U.S. can result in \$7−\$10 billion in savings [61].

In addition to direct savings in space conditioning costs, GRs can contribute to energy production of PV panels if they are jointly installed. Specifically, GRs create a cool micro-climate in hot weather and reduce the temperature of their surrounding area. Hence, their joint installation with PV panels (Figure 1.1) can help cool down the panels, allowing them to function at a higher efficiency. The increase in panel efficiency is consistently reported in the literature; however, the degree of this increase varies from one study to another, ranging between 0.08% and 8.3% across studies of various lengths, conducted in different climates [40, 110, 122, 232].

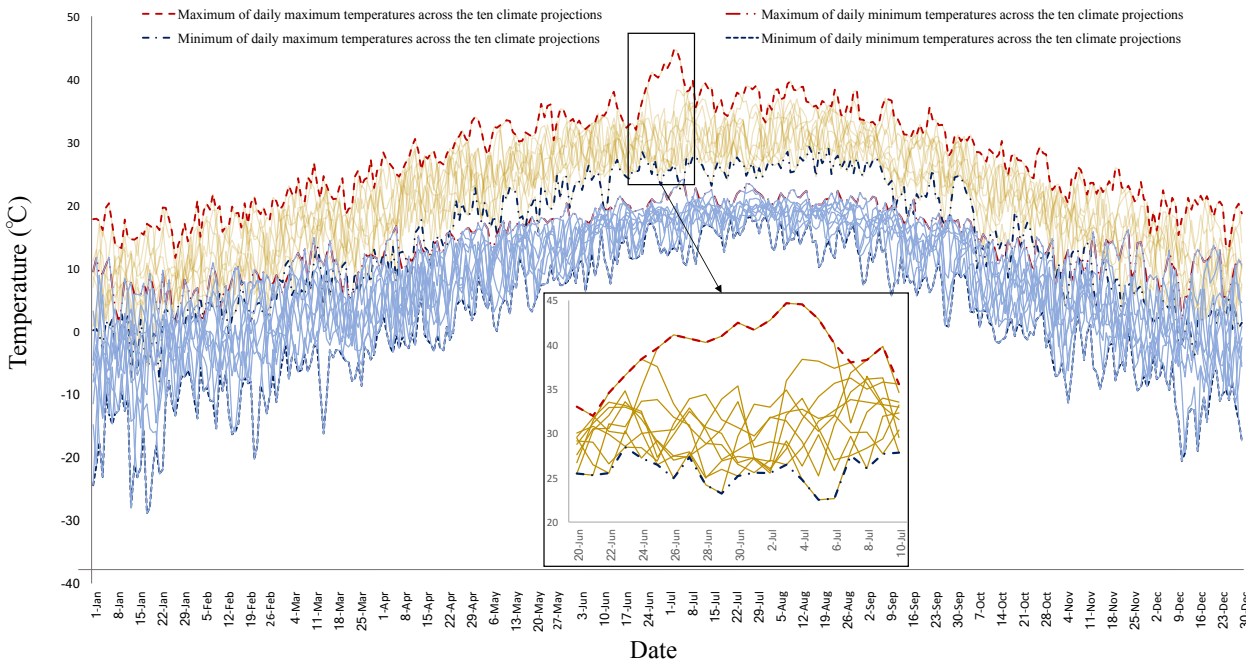


Figure 1.2: The daily maximum and minimum temperatures for the City of Knoxville, Tennessee from ten different climate projections for the year 2030. The dashed lines present the maximum and minimum temperatures across the ten projections over the year. (For details on the climate projections refer to Table 3.5.)

The degree of benefit from PV panels and GRs highly depends on the weather and climate conditions of the location in which they are installed [180, 231]. However, the information on how the weather and/or climate conditions evolve over time in specific regions/locations are limited and often unreliable. Indeed, although the global trend of climate change is consistently reported, in general there is no consensus among current climate projections and their evolution over time in specific regions/locations [118]. For instance, Figure 3.2 presents the daily maximum and minimum temperatures for the City of Knoxville, Tennessee from ten different climate projections for the year 2030, provided by Oak Ridge National Laboratory's Urban Dynamics Institute (UDI) [216] and Oak Ridge National Laboratory's Climate Change Science Institute (CCSI) [35]. As seen in the figure, the projections can differ by up to approximately 25.4 and 37.1 degrees Celsius for daily maximum and minimum temperatures, respectively, in a given day. Hence, using each of these forecasts to guide future benefits of installing PV panels and GRs, either separately or jointly, may result in a different set of recommendations.

PV panels and GRs are relatively expensive and have long lifespans, and hence, they are both considered long-term investments. PV panels can generally retain a high efficiency of 80%-85% up to 20 years after installment [74]. Similarly, GRs are reported to last on the order of 40 years [169, 147], almost twice as long as traditional roofs. Therefore, it is important to carefully plan such investments to maximize their expected return.

In this paper, we present an approach to consolidate a set of future climate projections when making long-term investment decisions on the installation of PV panels and GRs, from the perspective of a regional governing body. Specifically, we develop a two-stage stochastic programming model to determine the optimal placement of PV panels and GRs, either separately or jointly, among a set of candidate rooftops. Our objective is to maximize the profit from the energy generated and saved using these practices, considering the uncertainties in the future evolution of the climate and the positive interaction of PV panels and GRs in increasing PV panels' efficiency. We develop a profit-maximizing model to allow governing bodies and policy makers to carefully evaluate their options before making an investment.

Optimal placement problems are studied in a wide array of domains and applications (e.g., for the placement of distributed generation source [224], phasor measurement units [91], multiple allocation hubs [52], and wind turbines [143], or in facility location problems [4]). In this paper, we formulate an optimal placement problem for joint installation of PV panels and GRs. In the literature, studies involving PV panels mostly focus on underlying PV material or cell technology [215, 43, 119]. Alternatively, there is a body of work that aims to determine the best placement option for individual PV panels. For instance, there are a number of studies that evaluate rooftop characteristics to calculate individual rooftop solar access using geographic information system (GIS) [130, 230, 220, 161], or aim to develop GIS-based models to optimize electricity generation estimation of PV panels installed on rooftops [107].

Additionally, there exist studies whose objectives are to find the optimal installation criteria for PV panels, e.g., size, tilt angle, converter properties. An integrated multi-objective optimization model is developed in [124] to determine rooftop-specific installation criteria for PV panels to maximize their energy production effectiveness and efficiency. Similarly, a particle swarm optimization algorithm is developed in [125] to find the optimal installation details (i.e., number of PV modules, their optimal tilt angle and distribution

among the DC-AC converters) for a grid-connected PV system to maximize the total net profit and environmental benefits of the system. In another study [135], a simulation model is developed to find the optimal size and slope of PV systems under certain climate conditions subject to equipment costs as well as electricity and sale-back tariffs. In a similar vein, in [42], a Bayesian approach is used to optimally size stand-alone PV systems under climate change uncertainty.

There exist only a few large scale studies that attempt to optimize the implementation of PV panels. In [10], the output of large scale renewable energy farms (both wind and solar) is evaluated and compared with that of rooftop PV panels, after minimizing energy generation costs and greenhouse gas emissions. In another study [167], the optimal strategy to implement PV systems to achieve national carbon emission reduction targets is proposed. None of these large scale studies, however, consider future climate scenarios to capture the uncertainty in output of PV panels, nor do they take into account GRs, their energy saving properties, or their interactions with PV panels.

The literature related to GRs mainly focuses on their many potential environmental benefits, e.g., management of runoff water quality and quantity [23], reduction of heat island and improvement of urban comfort [192], contribution to plant and ecological diversity [51], and reduction of urban air pollution [236], to name a few. Also, a major group of studies explore GRs' physical properties, e.g., types of substrate [8], hydrologic performance [133], thermal behavior [155], and vegetation types [199].

There exits a few studies in the literature that attempt to optimize energy savings/cost reductions achieved using GRs. For instance, [87] simulate the thermal behavior of a building covered with GRs in order to optimize the energy savings achieved by installing green media on the rooftop of a building. The results show that the installation of GRs for buildings that meet the most recent insulation regulations leads to moderate levels of energy savings. In another study, [120] investigate the economic and environmental benefits of GRs through an optimal-scenario selection model. The authors preform life-cycle cost analysis for fifteen different types of GRs and conclude that the cost reductions and environmental benefits achieved by GRs are noteworthy. [39] conduct a cost-benefit optimization on GR sizes. Their results show that the amount of energy savings increases in the size of GR. Despite

their contributions, none of these studies, however, examine the optimal placement of GRs in a large scale study.

Stochastic programming has been extensively used in the literature for modeling long-term planning problems under uncertainty [25]. Specifically, two-stage stochastic programming has been widely applied in a variety of studies including but not limited to portfolio selection [1], transportation planning [18], disaster management [157], waste management [141], scheduling [166], and distributed energy systems [245]. Similar to other works in the literature, here we aim to incorporate uncertainty about the future through a set of possible scenarios. However, to the best of our knowledge, this is the first study that uses such approach for incorporating climate change into urban planning over a long planning horizon.

Various cities or states in the U.S. have invested in, or are currently leading, projects to place green infrastructure and/or energy-efficient practices and technologies [79, 211, 80]. Most of these projects, however, are focused on investing in a single geographic region or a small community, and involve a single type of practice alone (e.g., solar panels, LED lights, green infrastructure). In this study, we take a forward-looking view and provide a general model that can account for joint placement of GRs and PV panels across various geographical regions simultaneously. To the best of our knowledge, this is the first model that accounts for multi-region, multi-practice placement, hence allowing policy makers to plan large-scale implementations, while accounting for the potential interactions between the practices.

The remainder of this paper is organized as follows. First we clearly define the scope of the problem and present the model formulation in Section 2.2. Next, in Section 1.3, we calibrate the model using the literature, industry reports and a few datasets. In Section 1.4, we first discuss the solution approach. Next we conduct a case study for a mid-sized city in the U.S., namely, Knoxville, Tennessee, perform sensitivity and robustness analyses, and provide environmental insights. Lastly, we conclude in Section 2.5.

1.2 Model Formulation

In this section, we present a two-stage stochastic programming model with complete recourse to determine the placement of PV panels and GRs to maximize the overall profit. The first stage decisions are to choose a set of candidate sites to install PV panels and GRs, either separately or jointly. After all uncertainties are realized, second stage decisions, i.e., the amount of electricity sold to or purchased from the grid, are made. Note that consistent with the current practice, we assume that excess energy generated by PV panels can be sold to the grid [17]. In the remainder of the paper, the word *energy* refers to electrical energy unless otherwise stated.

Let T denote the planning horizon and K denote the set of regions, where I^κ denotes the set of candidate sites within region $\kappa \in K$. Let the discrete random variable W with probability mass function p_W denote the sample path of the future climate evolution for the regions of interest over the planning horizon. Let η_ω denote the the realization probability of scenario $\omega \in \Omega$, where Ω is a finite discrete set of projected climate scenarios, i.e., $\eta_\omega = p_W(\omega)$.

Let the first stage binary variables x_i^κ and y_i^κ denote whether or not PV panels and GR are installed at candidate site $i \in I^\kappa$, respectively, where each assumes the value 1 if the corresponding practice is installed at site $i \in I^\kappa$ and equals to 0, otherwise. Let k_i^κ denote the total area of PV panel installed at site $i \in I^\kappa$. Let c_i^κ and g_i^κ denote the cost of installing PV system and GR at site $i \in I^\kappa$, respectively.

Let the second stage variables $e_{i\omega}^\kappa$ and $s_{i\omega}^\kappa$ denote the amount of energy generated and saved in kWh at candidate site $i \in I^\kappa$ under scenario $\omega \in \Omega$, respectively. Additionally, let H_i^κ denote the average hourly electricity consumption at each candidate site $i \in I^\kappa$ to maintain the building temperature via air conditioning, and R^κ denote the total required electricity for space conditioning in region $\kappa \in K$ over the planning horizon. Let δ denote the percentage change in energy consumed for space conditioning over the planning horizon, due to an array of technological, sociological, climatic, and economic factors. Lastly, let B denote the initial budget available for investment.

PV panels rely on solar irradiation to generate electricity and their outputs significantly differ depending on the number of hours they are exposed to sunlight. A 'peak sunlight hour'

Table 1.1: Notation used in the two-stage stochastic model.

Name	Description
Sets	
Ω	Set of climate scenarios, where $\omega \in \Omega$
K	Set of regions, where $\kappa \in K$
I^κ	Set of candidate sites in region $\kappa \in K$, where $i \in I^\kappa$
First Stage Variables	
x_i^κ	Equals 1 if PV panels are installed at site i in region κ and 0, otherwise
y_i^κ	Equals 1 if GR is installed at site i in region κ and 0, otherwise
c_i^κ	Installation cost of PV system at site i in region κ (USD)
g_i^κ	Installation cost of GR at site i in region κ (USD)
k_i^κ	Area of PV panel installed at site i in region κ (m^2)
Second Stage Variables	
$e_{i\omega}^\kappa$	Energy generated by PV panels at site i in region κ under scenario ω (kWh)
$s_{i\omega}^\kappa$	Energy saved by GR at site i in region κ under scenario ω (kWh)
r_ω^κ	Energy sold to the grid in region κ under scenario ω (kWh)
ϕ_ω^κ	Energy purchased from the grid in region κ under scenario ω (kWh)
Parameters	
F	PV system fixed cost (USD)
Q	PV panel output (W)
B	Initial budget available for investment (USD)
γ	Cost per kWh purchased from the grid (USD)
μ	Price per kWh sold to the grid (USD)
α	Percentage energy saving in cooling degree-hours due to GR installation
β	Percentage energy saving in heating degree-hours due to GR installation
θ	Percentage efficiency increase in the output of PV panels due to integration with GRs
δ	Percentage change in energy consumed for space conditioning over the planning horizon
V^κ	PV system variable cost in region κ (USD)
$\mathbb{C}^\kappa$	Total maintenance cost per m^2 PV panel installed in region κ (USD)
P^κ	Cost per m^2 for installing GR in region κ (USD)
R^κ	Total energy requirement for space conditioning in region κ over the planning horizon (kWh)
η_ω	The realization probability of scenario ω, where $\sum_\omega \eta_\omega = 1$
A_i^κ	Rooftop surface available at site i in region κ (m^2)
H_i^κ	Average hourly electricity consumption for space conditioning at site i in region κ (kWh)
ι_i^κ	Rooftop radiation potential of site i in region κ
Stochastic Parameters	
L_ω^κ	Total number of peak sunlight hours available in region κ under scenario ω over the planning horizon
λ_ω^κ	Total number of cooling degree-hours in region κ under scenario ω over the planning horizon
τ_ω^κ	Total number of heating degree-hours in region κ under scenario ω over the planning horizon

is typically used to describe the intensity of sunlight in a specific area, where 1 peak sunlight hour is equivalent to 1 kWh/m^2 [13, 201]. Hence, the number of peak sunlight hours for a day represents the accumulative solar irradiation over the course of the day. Additionally, the level of solar radiation received by any rooftop depends on a variety of factors, e.g., aspect of the building, rooftop slope, and the shadowing effect or solar access to buildings. Let ι_i^κ denote the rooftop solar radiation potential at site $i \in I^\kappa$, which quantifies the percentage of daily available sunlight that an average rooftop at site $i \in I^\kappa$ receives. Let the stochastic parameter L_ω^κ denote the total number of peak sunlight hours available over the planning horizon in region $\kappa \in K$ under scenario $\omega \in \Omega$.

Cooling and heating degree-hours are measures of how many degrees and for how long the outside temperature is above or below certain base temperatures, respectively [58]. These metrics are typically used to determine whether or not space heating and cooling are required for buildings. Let λ_ω^κ and τ_ω^κ denote the total number of cooling and heating degree-hours over the planning horizon, during which space cooling and heating are required, respectively, for buildings in region $\kappa \in K$ under scenario $\omega \in \Omega$. Additionally, let α and β denote the percentage of energy saving due to GR installation in cooling and heating degree-hours, respectively. Lastly, recall that the joint installation of PV panels and GRs positively affect the PV panels output. Let θ denote the percentage increase in the output of PV panels as a result of their integration with GRs. Table 2.1 summarizes all the notation used in model formulation.

Recall that our objective is to maximize the profit from energy generated and saved, i.e.,

$$Z = \max \sum_i \sum_\kappa -(Fx_i^\kappa + k_i^\kappa V^\kappa + A_i^\kappa P^\kappa y_i^\kappa) + \sum_\omega \sum_\kappa \eta_\omega (r_\omega^\kappa \mu - \phi_\omega^\kappa \gamma). \tag{1.1}$$

The first term inside the maximization corresponds to the installation cost of PV panels and GRs in a subset of candidate sites across all regions. The second term inside the maximization corresponds to energy generated and saved under all scenarios across all regions. The following equations, i.e., Equations (2.2) - (1.9), present the constraints of the model,

$$g_i^\kappa = A_i^\kappa P^\kappa y_i^\kappa \qquad \forall\, i, \kappa, \tag{1.2}$$

$$c_i^\kappa = Fx_i^\kappa + k_i^\kappa(V^\kappa + \mathbb{C}^\kappa) \qquad \forall i, \kappa, \tag{1.3}$$

$$\sum_i \sum_\kappa (c_i^\kappa + g_i^\kappa) \leq B, \tag{1.4}$$

$$k_i^\kappa \leq A_i^\kappa x_i^\kappa \qquad \forall\, i, \kappa, \tag{1.5}$$

$$e_{i\omega}^\kappa = QL_\omega^\kappa k_i^\kappa \iota_i^\kappa (1 + y_i^\kappa \theta) \qquad \forall\, i, \omega, \kappa, \tag{1.6}$$

$$s_{i\omega}^\kappa = H_i^\kappa y_i^\kappa (\alpha \lambda_\omega^\kappa + \beta \tau_\omega^\kappa) \qquad \forall\, i, \omega, \kappa, \tag{1.7}$$

$$\sum_i (e_{i\omega}^\kappa + s_{i\omega}^\kappa) + \phi_\omega^\kappa - r_\omega^\kappa \geq (1+\delta) R^\kappa \qquad \forall \omega, \kappa, \tag{1.8}$$

$$r_\omega^\kappa \leq \sum_i e_{i\omega}^\kappa \qquad \forall\, \kappa, \omega. \tag{1.9}$$

Consistent with the literature [50, 180, 61], we assume that if the decision is to install GR at site $i \in I^\kappa$, it must be large enough to completely cover the rooftop; hence, Equation (2.2) calculates the GR installation cost at site i in region κ. Equation (2.1) links the PV system cost, c_i^κ, to its two different components, namely, PV system fixed cost, denoted by F, and PV system variable and maintenance costs in region κ, denoted by V^κ and $\mathbb{C}^\kappa$, respectively. Note that PV panels require very little maintenance [31, 228], while extensive GRs are essentially cost-saving compared with conventional roofs when it comes to maintenance [99, 94, 233]. In this study, we assume the property owner is responsible for maintenance costs, whether or not their properties are selected by the model as candidates for placement of the green practices, i.e., $\mathbb{C}^\kappa = 0$. We revisit this assumption in our computational study in Section 2.4.4 to investigate the impact of incorporating maintenance costs directly into the model.

Equation (2.7) limits the total cost of PV systems and GRs to a given budget B. Equation (1.5) guarantees that the area covered with PV panels cannot exceed the available rooftop surface. Note that simultaneous installation of PV panels and GRs on a rooftop is possible as PV panels are generally installed slightly elevated above the roof surface.

Recall that the integration of PV panels and GRs can help cool down the panels, thereby resulting in a higher electricity output. Therefore, Equation (1.6) calculates the energy generated by PV panels at site $i \in I^\kappa$ under scenario $\omega \in \Omega$.

The amount of energy savings from GR at each candidate site is given by Equation (1.7). The amount of electricity sold to or purchased from the grid, r^κ_ω and ϕ^κ_ω, respectively, serve as second stage decisions in the model. We assume that each region has certain energy requirements for space conditioning over the planning horizon. Hence, Equation (1.8) guarantees that for each region the total energy generated, $e^\kappa_{i\omega}$, and saved, $s^\kappa_{i\omega}$, and the total electricity sold to the grid, r^κ_ω, or purchased from the grid, ϕ^κ_ω, is at least equal to the energy requirement for space conditioning of the region. Lastly, Equation (1.9) assures that the electricity sold to the grid cannot exceed the electricity generated by systems.
Note that the placement problem (1.1)-(1.9) has complete recourse. That is, for all the first-stage decisions, regardless of the uncertainties, there exists at least one feasible second-stage decision [25].

1.3 Model Calibration

In this section, we use the literature and a series of datasets to calibrate the model formulated in Section 2.2 to further conduct a case study for the City of Knoxville, Tennessee.

1.3.1 Parameters Estimated From the Literature

In the following, we use the literature and industry reports to estimate model parameters.
Planning horizon, T. In this paper, we use two planning horizons of 10 years and 20 years. These two horizons are chosen based on the availability of future climate projections as well as the lifespan of current commercially available PV panels and GRs.
PV system fixed cost, F, and PV system variable cost in region κ, V^κ. The cost of installing PV system includes the workforce cost, plus the costs of the system components, i.e., solar modules (which is referred to the PV cell circuits sealed in an environmentally protective laminate [84]), mounting device, DC-AC power inverter, and wiring. Note that both workforce and component costs consist of fixed costs and variable costs, i.e., some of

these costs are fixed for any installation, regardless of the size of the PV system, whereas the others are functions of the size of the system. For instance, the workforce cost consists of a fixed cost for engineering design, permit, and contract fees, plus a variable labor cost to install the system. Similarly, the PV system cost consists of a fixed cost for DC-AC power inverter and wiring, plus a variable cost for PV modules and mounting device that is a function of the PV system size. In the following, we first calculate the fixed and variable costs of the workforce. Next, we estimate the fixed and variable costs of the PV system components. We then use these values to estimate PV system fixed cost, F, and PV system variable cost in our region of interest, V^κ.

According to a 2015 report by the National Renewable Energy Laboratory (NREL) [45], installing a 5 kW PV system with a size of 37.5 m^2 (400 ft^2) on a residential rooftop costs \$7,950, which includes the one-time engineering design, permit, and contract fees, plus the labor costs. In contrast, the cost of installing a commercial system of size 743.2 m^2 (8000 ft^2) equals \$92,132, including the one-time fees and labor costs. We assume the labor costs for installing the PV system increase linearly in the system size, and the one-time fees are equivalent. Let $\mathbb{W}$ denote the total workforce cost needed to install PV system and recall that k_i^κ denotes the area of PV panel installed at site $i \in I^\kappa$. Hence, using linear regression, we obtain $\mathbb{W} = 3500 + 120k_i^\kappa$. Consequently, we use the intercept of \$3,500 and the slope of \$120 per m^2 as the fixed and variable costs of workforce required for installing a PV system.

Connecting the PV system to the grid requires inverters to convert the direct current (DC) from PV panels into alternating current (AC). These inverters generally cost between \$1,000 and \$5,000 based on their capacity and quality [204, 229], with relatively limited additional cost for wiring. In this study, we consider the average cost of \$3,500 for the fixed cost of PV system components, which depending on the brand, is sufficient enough for purchasing inverters with a size of 3,000 W to 12,000 W [229]. Hence, the PV system fixed cost, F, equals to \$7,000, which consists of the fixed part of total workforce cost, i.e., \$3,500, plus the inverter and wiring costs, i.e., \$3,500.

As of 2017, PV modules cost between \$0.85 and \$1.5 per W. That is, for a panel with the size of 1 m^2 and 150 W–250 W output on top efficiency, the module cost ranges from \$128 to \$375, while the mounting device (frame) costs an additional \$60 per m^2. Therefore,

the PV system variable cost, V^{κ}, for the City of Knoxville, including the variable part of workforce cost, i.e., \$120 per m^2, plus module and mounting device cost, ranges between \$310 and \$560 per m^2.

PV panel output, Q. Commonly available PV panels have an efficiency ranging from 13.5% to 20% [45]. Therefore, the real output of one m^2 panel during an hour of peak sunlight ranges from 135–200 W.

Total maintenance cost per m^2 PV panel installed in region κ, $\mathbb{C}^{\kappa}$. PV panels are made of tempered glass, making them able to withstand harsh weather conditions. Moreover, PV panels have no moving parts, except for panels with tracking mounts, making them very reliable and able to continue operation with minimal maintenance [31]. Most PV panel manufacturers guarantee their products for 20 to 25 years [228]. Therefore, if PV panels cease working, the PV panel companies will fix the issue at no cost. However, in order to utilize PV panels on their full potential, the surface of PV panels should be cleaned throughout their lifespan, which imposes an annual cleaning cost of \$0.25 to \$1.5 per panel [228], or equivalently \$0.15 to \$0.92 per m^2 of panel [77]. Note that these costs do not consider the positive impact of GRs on reducing air borne pollutants and dust in GR integrated PV panels [97].

Recall that in this study we use two planning horizon lengths, i.e., $T = 10$ and $T = 20$ years. Hence, assuming that the current estimated maintenance costs of \$0.15 to \$0.92 per m^2 of panel increase with inflation, we consider the total maintenance $\mathbb{C}^{\kappa}$, incurring in the beginning of the planning horizon, to range between \$1.5 and \$9.2 when $T = 10$ years and between \$3 and \$18.4 when $T = 20$ years.

Average hourly electricity consumption for space conditioning at site i in region κ, H_i^{κ}. Generally speaking, electricity consumption increases in building size [68]. We use the data available from a 2009 survey by the EIA [68] to characterize the relationship between the average hourly energy consumption for space conditioning and building size. Note that we consider a residential level of energy consumption for all the candidate sites in this study. The data suggests a strong linear relationship between the energy consumption and the building size, where it ranges between 25 m^2 and 400 m^2. Recall that A_i^{κ} denotes the available rooftop surface at candidate site i. We assume that the total size of each building is equal to its available rooftop surface, and each candidate site corresponds to a single unit. Hence, the

relationship can be best approximated as

$$H_i^\kappa = 0.508 + 0.004 A_i^\kappa. \tag{1.10}$$

(For further details about the data and model, please refer to Appendix A.)

Cost per m^2 for installing GR in region κ, P^κ. GRs are typically classified into three main types, namely, extensive, semi-intensive, and intensive, mainly based on their types of vegetation and properties, such as weight, use, and maintenance [111]. In this study, consistent with the existing literature that focuses on energy saving aspect of GRs, we only consider extensive GR, which is the least expensive and most resilient type of GR [50, 180, 61]. According to the U.S. General Services Administration (GSA), the cost per m^2 of extensive GR is approximately \$12 [100] which includes the drainage layer cost as well as labor cost. Consistent with published reports, we do not consider setup costs for GRs [100].

Price per kWh sold to the grid, and cost per kWh purchased from the grid, γ and μ, respectively. Selling excess electricity generated to the grid and being paid in return [81], known as feed-in tariffs, or more specifically export tariffs [81], is not generally offered in the U.S., except in a limited number of states [75]. However, net metering, which allows for sending the extra electricity generated to the grid at normal retail value and receiving credit for it, is supported by most utility providers [197]. Therefore, consistent with these methods, we consider the same value for the electricity sold to and purchased from the grid as we assume the excess electricity that is sent to the grid can be credited and hence, used by any of the candidate sites. According to [65], as of 2017, each kWh of electricity purchased from the grid costs approximately 10.3 cents. Hence, we set μ and γ equal to 10.3 cents.

Total energy requirement for space conditioning in region κ over the planning horizon, R^κ. According to [64], an average household in the state of Tennessee approximately consumes 12,000 kWh annually. Additionally, based on a recent report [121], the number of buildings in the City of Knoxville is 209,183. Hence, the expected annual energy required by the City of Knoxville equals 2,491 GWh. According to [69], in the state of Tennessee, 42% of energy consumed by residential sector is used for space conditioning. Therefore, for $T = 10$ and

$T = 20$ years, the total energy required for space conditioning in the residential sector in the City of Knoxville equals to 10,462 GWh and 20,924 GWh, respectively.

Percentage energy saving in cooling degree-hours due to GR installation, α, and percentage energy saving in heating degree-hours due to GR installation, β. The percentage of energy saving in cooling degree-hours achieved due to the installation of GRs differs across various studies, ranging from 10% to 16.7% [50, 61, 12, 244, 83, 206, 175]. While almost all studies agree on the fact that using GRs results in savings in cooling degree-hours, there is a lack of consensus on the impact of GRs in heating degree-hours. Indeed, a few empirical studies report that using GRs contribute to energy loss in heating degree-hours while others suggest that it results in energy savings. For instance, a recent, long-term study reports that GRs increase the required amount of energy to heat the space to a comfortable level (i.e., 22 degrees Celsius in this study) in heating degree-hours by 6.2% [50]. Consistently, another study performed in different climates throughout Europe reports up to 1% GR-related energy loss in cold seasons in certain climates [12]. In contrast, two empirical studies suggest that the energy savings from GR in heating degree-hours is negligible and can be ignored [83, 206]. However, there exists another group of studies that report reductions of 4% to 10% in energy savings as a result of GRs in heating degree-hours [61, 12, 175, 244]. Therefore, in this study, we let α and β assume a wide range of values to capture the different, and sometimes contradicting, estimates reported in the literature. Specifically, we let α range from 10% to 20% and β range from -10% to 10%.

Percentage efficiency increase in the output of PV panels due to integration with GRs, θ. As the results from the previous studies show, integrating PV panels with GRs results in a higher panel efficiency, mainly due to the cooling effect of GRs. However, these studies report a relatively wide range of values for the percentage efficiency increase, i.e., from 3.33% to 8% [40, 110].

Percentage change in energy consumed for space conditioning over the planning horizon, δ. In general, changes in human behavior with respect to energy consumption is not always easily quantifiable and can be impacted by various technological, sociological, climatic, and economic factors [108, 104]. Over the past few decades, the level of energy consumption for space conditioning in the U.S. residential sector has experienced a steady decline, decreasing

from 58% of overall energy consumption per household in 1993, to 48% in 2009 [70]. The projections for the energy consumption for space conditioning, on the other hand, are mixed [71, 108]. Published studies report various degrees of increase/decrease in the level of energy consumption for space heating and cooling [187, 7, 140, 22, 109, 136, 196, 188, 190, 191]. For instance, [196] project the decrease of 24% in the level of energy consumption for space heating and the increase of 39% in the level of energy consumption for space cooling by year 2020. In other studies, [109] and [7] project the decrease of as much as 33% and 13% in the level of energy consumption for space heating, and the increase of as much as 158% and 40% for space cooling by years 2080 and 2030, respectively. Note that according to [68], only a quarter of the total energy consumed for space conditioning in the U.S. residential sector is used for space cooling, while the remaining three quarters is used for space heating. Hence, in this study to capture a wide array of variability, we use a weighted average of the reported values for space heating and cooling, and consequently, account for up to 60% change in total energy consumption for space conditioning.

Initial budget available for investment, B. The net budget for 2017-2018 for the City of Knoxville is equal to $378.8 million. The City dedicates a fraction of the budget to various long-term urban development projects. For instance, in the 2017-2018 budget, $17.8 million is dedicated to the conversion of approximately 300,000 street lights across the City to the LED technology, for which the payback period is anticipated to be less than a decade [211]. Consistent with the budget allocated to this project and other investments in green technologies, in our case study, we set the initial budget available for investment, B, equal to $20 million.

Table 1.2 summarizes the parameters that are calibrated from the literature and considered in our numerical studies. The table presents the ranges of values obtained from the literature. In our numerical studies, however, we capture a range slightly larger than the reported values to account for additional uncertainty and possible parameter estimation errors. We conduct our numerical studies at the discrete levels provided in the table.

Table 1.2: Parameter values estimated from the literature and industry reports.

Parameter	Ranges	Levels	Sources
PV system variable cost, V^{κ} (USD)	$[210, 435]$	100, 200, 400, 600	Chung et al. [45]
Annual maintenance cost per m^2 PV panel installed in region κ, $\frac{\mathbb{C}^{\kappa}}{T}$ (USD)	$[0.15, 0.92]$	0.15, 0.62, 0.92	[31, 228]
PV panel output, Q (W)	$[135, 200]$	100, 200	Chung et al. [45], Solar Quotes [204]
Percentage energy saving in cooling degree-hours due to GR installation, α	$[10\%, 16.7\%]$	$10\%, 20\%$	Ascione et al. [12], Coma et al. [50], Dunec [61], Feng and Hewage [83], Raji et al. [175], Spala et al. [206], Zhao and Srebric [244]
Percentage energy saving in heating degree-hours due to GR installation, β	$[-6.1\%, 10\%]$	$-10\%, 10\%$	Ascione et al. [12], Coma et al. [50], Dunec [61], Feng and Hewage [83], Raji et al. [175], Spala et al. [206], Zhao and Srebric [244]
Percentage efficiency increase in the output of PV panels due to integration with GRs, θ	$[3.33\%, 8\%]$	$2.5\%, 10\%$	Chemisana and Lamnatou [40], Hui and Chan [110]
Percentage change in energy consumed for space conditioning over the planning horizon, δ	$[-60\%, 60\%]$	$-60\%, -40\%, -20\%, 0\%, 20\%, 40\%, 60\%$	Amato et al. [7], Belzer [22], EIA [71, 70], Huang [109], Loveland and Brown [136], Mansur et al. [140], Rosenthal et al. [187], Ruth and Lin [188], Sailor [190], Sailor and Pavlova [191], Scott et al. [196]

1.3.2 Parameters Estimated From Data

To estimate the remaining parameters, we use a few datasets including climate projections and solar insolation provided by UDI [216] and CCSI [35].

Total number of cooling degree-hours, $\lambda_{\omega}^{\kappa}$, and heating degree-hours, τ_{ω}^{κ}, in region κ under scenario ω over the planning horizon. The climate system evolves as a result of slow changes in boundary conditions, physical parameters, ocean and sea ice, etc. [114]. General circulation models (GCMs) are climate models which exploit the general circulation mathematical model of a planetary atmosphere (atmospheric GCMs) or ocean (oceanic GCMs) to numerically simulate and project changes in Earth's climate system. Coupled GCMs (CGCMs) consist of models that combine atmospheric GCM (AGCM) with oceanic GCM (OGCM) into interactive ocean-atmosphere models [237]. In this study, we use the climate projections from ten CGCMs as listed in Table 3.5.

The available projections consist of daily precipitation as well as minimum and maximum temperatures for 1 km^2 and 4 km^2 grids for the City of Knoxville from January 2011 through December 2050. In this study, we use the data for two planning horizons of length $T = 10$ years and $T = 20$ years, starting from January 2011. In order to reduce the computational effort, we use each climate projection as a scenario in our model, after averaging the daily

Table 1.3: Ten coupled general circulation models (CGCMs) generated at Oak Ridge National Laboratory's Climate Change Science Institute [35] using high-performance computing resources, including Titan, America's fastest supercomputer [35].

Model	Institute of development
Japanese Meteorological Research Institute Coupled Global Climate Model (MRI-CGCM3)	Meteorological Research Institute of the Japan Meteorological Agency [117]
Max-Planck-Institute Earth System Model Mixed Resolution (MPI-ESM-MR)	Max Planck Institute for Meteorology [150]
Geophysical Fluid Dynamics Laboratory Earth System Model (GFDL-ESM2M)	Geophysical Fluid Dynamics Laboratory [173]
The Australian Community Climate and Earth System Simulator (ACCESS)	Commonwealth Scientific and Industrial Research Organization [54]
The NCAR's Community Climate System Model (CCSM4)	Climate and Global Dynamics Laboratory at the National Center for Atmospheric Research [153]
The Institute Pierre Simon Laplace Climate Model (IPSL-CM5A)	Institute Pierre Simon Laplace [115]
The Beijing Climate Center Climate System Model (BCC-CSM)	Beijing Climate Center, China Meteorological Administration [21]
Norwegian Earth System Model (NorESM1-M)	Multi-institutional, Coordinated Climate Research in Norway [63]
The Centro Euro-Mediterraneo sui Cambiamenti Climatici Climate Model (CMCC-CM)	Euro-Mediterranean Center on Climate Change [49]
Flexible Global Ocean Atmosphere Land System (FGOALS)	Institute of Atmospheric Physics, Chinese Academy of Sciences, State Key Laboratory of Numerical Modeling for Atmospheric Sciences and Geophysical Fluid Dynamics [127]

projections for all grids spanning the City of Knoxville. We examine the impact of using the exact projections for each grid on the results in Section 2.4.4.

Note that the ten CGCMs are based on similar empirical or theoretical assumptions, hence they are somewhat correlated [118]. However, as discussed in Section 2.1, the projected daily temperatures and precipitation values vary across the ten CGCMs. Table 3.6 presents the maximum, average and the range of standard deviation for daily pairwise comparisons across the ten projections over the given planning horizon. As seen in Table 3.6, the average value of the pairwise differences for daily maximum and minimum temperatures for both $T = 10$ years and $T = 20$ years are on the order of 5 degrees Celsius, which highlight the existing variations in the projected values. (For detailed plots on daily/monthly/yearly average temperatures for the City of Knoxville, Tennessee for the ten different climate projections, please see Appendix B.)

As discussed, the data generated by CGCMs are on a daily basis. However, to accurately calibrate the model formulated in Section 2.2, we require hourly data. Hence, we use the widely accepted cosine function to disaggregate the temperature data into hourly predictions

[93], i.e.,

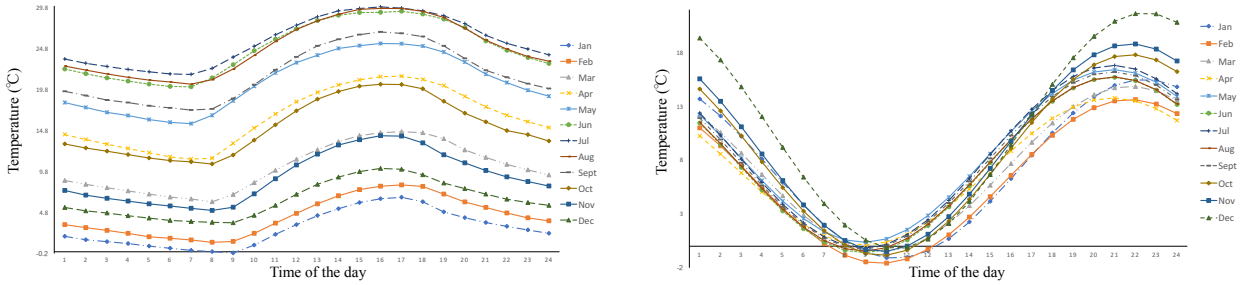
$$Y_t = a\cos\left(\frac{\pi(t+b)}{12}\right) + c + \epsilon. \tag{1.11}$$

Using this function requires daily minimum and maximum temperatures, and the time of the day during which these extreme temperatures occur. Hence, to estimate these data points, we use the hourly historical data from 2010 to 2012 provided by McGhee Tyson Airport weather station in Knoxville [53], to obtain the time at which the daily minimum and maximum temperatures were previously observed. As shown in Figure 3.4a, the daily minimum and maximum temperatures occur at different times during the day dependent on the month of the year. For instance, in the month of May, the daily minimum and maximum temperatures on average occur at 7 A.M. and 4 P.M., respectively, while in January, the daily minimum and the maximum temperatures on average occur at 9 A.M. and 5 P.M., respectively. Figure 3.4b shows the hourly temperatures for ACCESS CGCM obtained from Equation (1.11) and calibrated with the data presented in Figure 3.4a. The same approach is used to obtain the hourly temperatures from the remaining nine CGCMs.

In order to estimate the total number of cooling and heating degree-hours during a given day, we need cut-off values to guide when cooling and heating are required. Recommended comfort human temperatures are often reported as 20-23.3 degrees Celsius in winter and 22.8 to 25.6 degrees Celsius in summer [33]. A 2009 survey conducted by the EIA [71] shows that in the U.S., residential households usually use space conditioning for heating and cooling when the outdoor temperature ranges between 14.4 and 17.8 degrees Celsius, and 17.8 and 19.4 degrees Celsius, respectively. In this study, consistent with the recent published works, we set the cut-off values for heating and cooling degree-hours to 22 and 18 degrees Celsius, respectively [50, 58].

Table 1.4: Maximum, average and the standard deviation range for daily pairwise comparisons across the projections from ten CGCMs, presented in Table 3.5, over two planning horizons of length $T = 10$ years and $T = 20$ years, starting from January 2011.

Parameter	T=10			T=20		
	Maximum	Average	Standard deviation range	Maximum	Average	Standard deviation range
Daily maximum temperature (°C)	30.63	4.71	[0.89,7.95]	31.41	4.72	[0.79,7.95]
Daily minimum temperature (°C)	41.58	4.82	[0.47,11.13]	41.58	4.79	[0.47,11.22]
Daily precipitation (mm)	105.26	5.40	[0.02,38.88]	105.26	5.45	[0.02,38.88]



(a) The hourly temperatures in a day, averaged across month of the year from 2010 to 2012 based on the historical data [53].

(b) The ACCESS CGCM projected hourly temperatures in a day, averaged across month of the year from 2011 to 2021, obtained using Equation (1.11).

Figure 1.3: Example hourly temperature values for the City of Knoxville.

Total number of peak sunlight hours available in region κ under scenario ω over the planning horizon, L_ω^κ. Our datasets report projected temperature and precipitation, but do not include the daily *peak* sunlight hours. Also note that the number of daily peak sunlight hours is different from the readily available number of daily sunlight hours [200]. Hence, we use the amount of daily precipitation to estimate the total number of peak sunlight hours available, L_ω^κ. Specifically, we assume that any day with a precipitation greater than 10 mm is a cloudy day, and hence no peak sunlight hour is considered for such days. We obtain the estimate of 10 mm by comparing the results for the years 2011 and 2012 with the annual average peak sunlight hours [56].

Rooftop radiation potential, ι_i^κ, and rooftop surface available, A_i^κ, at site i in region κ. To obtain rooftop radiation potential, we use the solar insolation dataset provided by UDI [216] and CCSI [35]. This dataset includes the information about the rooftop size and solar insolation for 209,183 buildings in the City of Knoxville for the year 2003. The model that produces the data uses GIS and high-resolution Light Detection And Ranging (LiDAR) data to generate solar radiation intensity values for each building [121]. This high spatial and temporal resolution dataset is depicted in Figure 1.4. As seen in Figure 1.4, large rooftops generally have high solar insolation values mainly due to their flat surface and unobstructed access to the sunlight.

To estimate the values of ι_i^κ, we first obtain the per m^2 solar insolation values by dividing the solar insolation value of each rooftop by the size of the rooftop (in m^2). We then rescale them to range between 0 and 1.

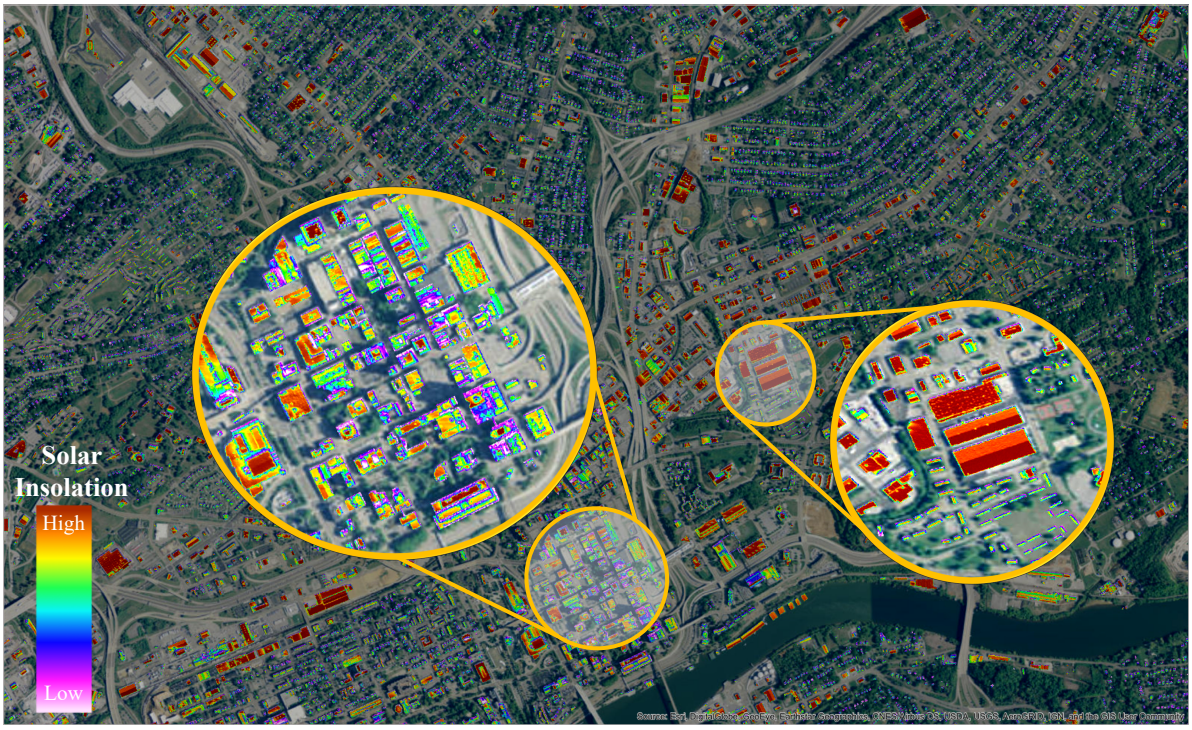
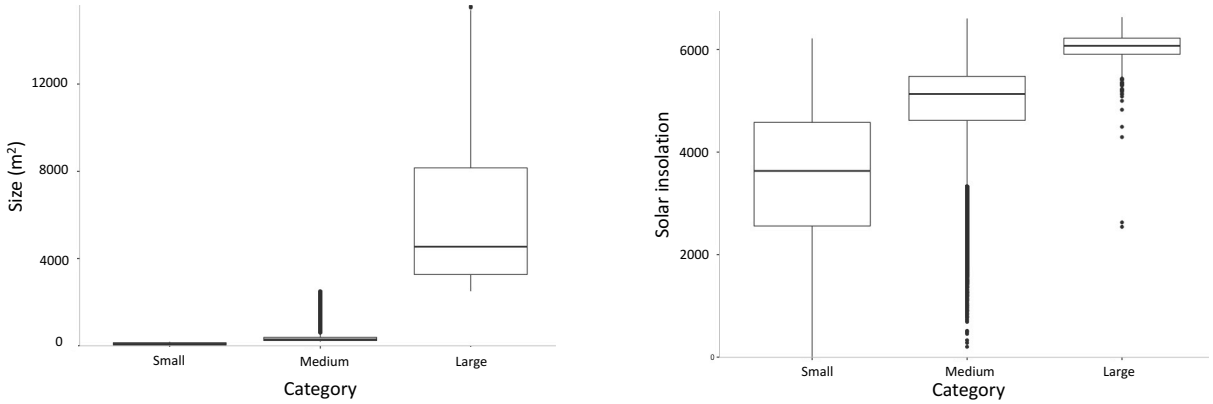


Figure 1.4: Visual-SOLAR radiation map for the City of Knoxville, Tennessee [121].

NREL [86] defines three categories for building sizes, i.e., small (with rooftop sizes less than 185 m^2), medium (with rooftop sizes between 185 m^2 and 2,500 m^2), and large (with rooftop sizes larger than 2,500 m^2). Figures 1.5a and 1.5b respectively show the distribution of rooftop sizes and solar insolation values for the 209,183 buildings in the City of Knoxville. As seen in Figure 1.5b, in general, the larger the building, the larger the solar insolation value. *The realization probability of scenario* ω, η_ω. In this study we use the climate projections discussed earlier in this section as our scenarios. The parameter η_ω gives the likelihood that a scenario is realized. As discussed, climate projections can be correlated [118]. However, due to the lack of information about the exact development process of the CGCMs, here we assume that all scenarios are equally probable, i.e., $\eta_\omega = 0.1 \; \forall \omega \in \Omega$.

1.4 Computational Study

In this section, we provide extensive numerical results. First, we discuss the solution approach and introduce additional metrics in Section 1.4.1. Next, in Section 1.4.2 we provide



(a) Rooftop surface. **(b)** Solar insolation.

Figure 1.5: Rooftop size and solar insolation for the 209,183 buildings in the City of Knoxville, stratified across rooftop size category.

a case study and discuss the results. Next, in Sections 2.4.4 and 1.4.4, we conduct extensive sensitivity and robustness analyses on model parameters, respectively, and provide insights. Finally, in Section 1.4.5 we discuss the environmental implications of the optimal solutions obtained in the case study.

1.4.1 Solution Approach and Additional Metrics

We use the L-shaped decomposition algorithm [221] to efficiently solve the problem. In order to implement this method, we linearize Equation (1.6). To remove the non-linearity caused by $k_i^\kappa y_i^\kappa$, we employ the big M method [98]. We add two new continuous variables $\zeta_i^{1\kappa}$ and $\zeta_i^{2\kappa}$ to the model such that

$$\zeta_i^{1\kappa} + \zeta_i^{2\kappa} = k_i^\kappa, \qquad \zeta_i^{1\kappa} \leq M y_i^\kappa, \qquad \zeta_i^{2\kappa} \leq M(1 - y_i^\kappa) \qquad \forall i, \kappa, \tag{1.12}$$

where M is a sufficiently large number. We add the set of constraints in Equation (1.12) to the model and replace Equation (1.6) with the following set of constraints:

$$e_{i\omega}^\kappa = QL_\omega^\kappa k_i^\kappa \iota_i^\kappa + QL_\omega^\kappa \iota_i^\kappa \zeta_i^{1\kappa} \theta \qquad \forall\, i, \omega, \kappa. \tag{1.13}$$

In the following we introduce two new metrics. These metrics are used to facilitate the comparison of the results.

Return on investment, ROI. Recall that our objective is to maximize the overall profit from energy generated and saved. However, to more easily compare the efficiency of the prescribed investment options, we introduce this new metric. Specifically, return on investment is calculated by dividing the net profit by the cost of investment multiplied by 100, i.e.,

$$\text{ROI} = \frac{\sum_i \sum_\kappa -(Fx_i^\kappa + k_i^\kappa V^\kappa + A_i^\kappa P^\kappa y_i^\kappa) + \sum_\omega \sum_i \sum_\kappa \eta_\omega (e_{i\omega}^\kappa + s_{i\omega}^\kappa)}{\sum_i \sum_\kappa (Fx_i^\kappa + k_i^\kappa V^\kappa + A_i^\kappa P^\kappa y_i^\kappa)} \times 100. \tag{1.14}$$

Sustainability index, SI. As discussed in Section 2.1, one of the major intangible, non-financial benefits associated with using PV panels and GRs is reducing the reliance on fossil fuels. This metric quantifies the percentage of the requisite energy that is saved or generated by using GRs and/or PV panels under the optimal solution, i.e.,

$$\text{SI} = \frac{\sum_\omega \sum_i \sum_\kappa \eta_\omega (e_{i\omega}^\kappa + s_{i\omega}^\kappa)}{\sum_\kappa R^\kappa} \times 100. \tag{1.15}$$

Although our objective is not to maximize SI, such metric can help policy makers to compare intangible benefits of the provided solutions.

1.4.2 Case Study

In this section, we present the results for a case study for the City of Knoxville, Tennessee. Specifically, we examine a set of 209,183 buildings, as candidate sites in one region, given an initial investment budget of $20 million. As discussed in the introduction, we take the perspective of a regional governing body throughout this paper. Nonetheless, the model is versatile and can be easily modified and calibrated to study the problem from other perspectives (e.g., utility companies).

Note that an average residential building in the southern U.S. built by 2010 is of size 220 m^2 [37] and has 1.5 floors [38]. In this study, to capture the energy savings of GRs which

Table 1.5: The parameter values in the three cases considered in the case study for the City of Knoxville.

Case study	PV panel output, Q (kW)	PV system variable cost, V (USD)	Percentage energy saving in cooling degree-hours by GRs, α	Percentage energy saving in heating degree-hours by GRs, β	Percentage efficiency increase in PV panel output, θ
Case 1	0.15	400	10%	0.0%	5%
Case 2	0.2	200	10%	0.0%	5%
Case 3	0.2	200	10%	0.0%	$\theta_t = 0.0013\mathbb{T}_t + 0.091$

typically only provide energy savings for the top floor unit(s), we assume all buildings are single units.

In order to capture the effects of current prices and efficiency of the PV panels, we consider three cases. In this section, we set $\delta = 0$. We later conduct sensitivity analysis on the impact of parameter δ on the solutions. In these cases, we use the values estimated form the literature and summarized in Table 1.2. Specifically, in all three cases, we set the percentage energy saving in cooling and heating degree-hours by GRs, i.e., α and β, respectively, equal to 10% and 0%. In Case 1, we consider the price and efficiency of current commercially available panels. That is, we set the PV panel output, Q, and the PV system variable cost in the City of Knoxville, V^{κ}, equal to 0.15 and 400, respectively. As discussed in Section 2.1 the cost of PV panels is on the decline while their efficiency is increasing. Hence, Case 2 considers efficient PV panels with lower than average cost to capture a likely upcoming scenario. In both Cases 1 and 2 we set the percentage efficiency increase in the output of PV panels due to integration with GRs, θ, equal to 5%. Note that θ is directly related to the ability of GRs to reduce their surrounding environment temperature. In Case 3, we use the range reported in Table 1.2 to approximate a linear relationship between hourly percentage efficiency increase in the output of PV panels due to integration with GRs and hourly temperature. In this case, unlike Cases 1 and 2 in which we consider a fixed value for θ regardless of the outside temperature, we incorporate the effect of the outside temperature in the GR-provided efficiency increase of PV panels. Let θ_t denote hourly percentage efficiency increase in the output of PV panels due to integration with GRs and $\mathbb{T}_t$ denote the hourly temperature. From the linear regression we obtain $\theta_t = 0.0013\mathbb{T}_t + 0.091$. Applying this function to the climate projections results in θ_t values that range from 0.064 to 0.14, which are larger than θ values considered in both Case 1 and Case 2. Table 1.5 summarizes the three cases considered.

Table 1.6: Optimal solution for an initial budget of $20 million available for investment over two planning horizons of length $T = 10$ years and $T = 20$ years for the cases presented in Table 1.5.

	$T = 10$						$T = 20$					
	Stand-alone PV (m^2)	Stand-alone GR (m^2)	PV+GR (m^2)	Budget spent ($)	SI	ROI	Stand-alone PV (m^2)	Stand-alone GR (m^2)	PV+GR (m^2)	Budget spent ($)	SI	ROI
Case 1	0	999	0	11,988	0.0033%	75.82%	0	21,969	0	263,628	0.0283%	37.97%
Case 2	0	999	0	11,988	0.0033%	75.82%	99,612	2,295	0	20,000,000	2.8724%	84.60%
Case 3	0	999	0	11,988	0.0033%	75.82%	0	4,735	93,930	20,000,000	2.8893%	87.72%

We use Gurobi Optimizer version 7.5 [102] on an iMac Pro with an 8-core 3.2 GHz Intel Xeon W processor and 32 GB of RAM to solve the model. The solution time for the three cases ranges between 422.2 seconds and 463.6 seconds. Appendix C provides further details on the solution time, number of variables, and number of constraints for the three cases.

Table 1.6 provides the optimal solutions for the three cases presented in Table 1.5. In all three cases, the total energy generated/saved is not enough to fully compensate the requisite energy needs of the City of Knoxville for space conditioning, either because of non-profitability of PV panels/GRs or the limited available budget for investment. Hence, in all these cases, the value of the objective function is negative. However, as seen in the table, ROIs are positive, suggesting that the income from the total energy generated/saved is higher than the budget spent.

First, note that when $T = 10$ only a small proportion of the available budget is spent under the optimal solution and only GRs are installed in all three cases. This is mainly due to the fact that when $T = 10$, the amount of electricity generated by PV panels is not nearly enough to cover their installation costs. In addition, because only GRs are installed in these three cases and the values for α and β are identical across the cases, the solutions and the metrics are also the same.

Similarly, when $T = 20$ in Case 1 only GRs are installed under the optimal solution and not all available budget is spent. However, in Cases 2 and 3, the optimal solution also prescribes to install PV systems and all available budget is allocated. Specifically, in Case 1, 21,969 m^2 of stand-alone GRs are installed under the optimal solution. Considering the average residential building rooftop size of 145 m^2 in the southern U.S. [37], this is enough to cover to approximately 152 average residential buildings. In Case 2, more than 99% of the available budget is allocated to installing 99,612 m^2 of stand-alone PV panels, and the

rest of the budget is allocated to installing 2,295 m^2 of stand-alone GRs, in total covering an approximately 703 average residential buildings. Note that in this case GRs are not integrated with PV panels; hence, they are mainly installed to provide energy savings. In Case 3, approximately 94% of the budget is allocated to installing PV panels, all of which GR integrated, and the rest is used for installing an additional 4,735 m^2 of stand-alone GRs. In total, under the optimal solution, these practices cover an approximately 680 average residential buildings. Recall that estimated percentage efficiency increase in the output of PV panels due to integration with GRs in Case 3 is overall higher than the two other cases. Hence, in Case 3 more budget is allocated to GRs compared to Case 2 and all panels are GR integrated to achieve a higher electricity output. Note that contrary to Case 2, in Case 3 GRs are mainly used to help improve the output of PV panels.

The model generally prescribes the stand-alone GRs to be installed on small rooftops. Recall that Equation (1.10) presents the relationship between hourly energy consumption for space conditioning and building size. From Equation (1.10), the magnitude of the intercept is much larger than that of the slope. Therefore, for instance, two small buildings would consume more energy than a large building that has a rooftop area equivalent to the total area of the two small rooftops. Note that the energy savings from GRs are a fraction of the total energy consumed by the buildings (based on α and β.) Therefore, because GRs do not have a set up cost, when it is optimal to install stand-alone GRs, the model typically prioritizes small rooftops to generate more profit through their energy savings.

In contrast, the model generally prescribes to install PV panels on large rooftops, partially due to the fact that installing PV systems has a fixed set-up cost. Additionally, as discussed in Section 1.3.2, buildings with large rooftops often have the highest radiation potential, ι_i^κ, as they are mostly flat and unlikely to be completely shaded by their surrounding buildings. Hence, the model prioritizes large rooftops for PV installation to minimize the cost while maximizing the electricity generation.

As shown in Table 1.6, for $T = 10$ years, Cases 1-3 result in the same ROI values as the corresponding solutions are identical. For $T = 20$ years, the solutions vary for the three cases and the highest ROI value is achieved in Case 3 in which the benefit of GRs are

most accurately captured. The SI values in Table 1.6 are generally higher for $T = 20$ years compared to $T = 10$ years, as PV panels are installed for $T = 20$ years.

1.4.3 Sensitivity Analysis

In this section, we conduct extensive sensitivity analysis to evaluate the impact of model parameters on the optimal solution. First, we conduct a sensitivity analysis on an array of parameters related to PV panels, GRs, and their interaction. Second, we examine the impact of possible changes in energy consumed for space conditioning over the planning horizon on optimal solutions. Next, we investigate the impact of incorporating maintenance cost directly into the model as a responsibility of the entity in charge of planning, e.g., the regional governing body. Lastly, we evaluate the impact of using the averages of the daily projections over all grids spanning the City of Knoxville, instead of the true projections for each grid, when calibrating the model, and provide recommendations.

Table 1.7 presents the results from the sensitivity analysis for different levels of PV system variable cost, V^{κ}, PV panel output, Q, percentage efficiency increase in the output of PV panels due to integration with GRs, θ, and percentage energy saving in cooling and heating degree-hours due to GR installation, α and β, respectively, as presented in Table 1.2. In general, when PV systems are expensive but have relatively low output, i.e., high V^{κ} values and low Q values, the optimal solution mainly depends on the energy savings from GRs. In this case, if the percentage energy saving in heating degree-hours due to GR installation, β, is low, no additional profit can be generated from installing GRs or PV panels. Hence, the model chooses to not spend any budget at all. When β is high, the model chooses to spend budget but only for stand-alone GRs, mainly to achieve energy savings, and hence maximize the profit. In this case, the total number of stand-alone GRs depends on and increases in the percentage energy saving in cooling degree-hours due to GR installation, α.

For cost-efficient PV systems, i.e., low V^{κ} values and high Q values, the optimal solution mainly depends on the percentage efficiency increase in the output of PV panels due to integration with GRs, θ. That is, when θ is low, the optimal solution is to install stand-alone PV panels. However, when θ is high, the model takes full advantage of the added efficiency and prescribes to install a large quantity of GR integrated PV panels, with the

Table 1.7: Area covered by stand-alone GRs, stand-alone PV panels, and GR integrated PV panels under different values for PV panel output, PV system variable cost, percentage energy saving in cooling and heating degree-hours due to GR installation, and percentage efficiency increase in the output of PV panels due to integration with GRs for an initial budget of \$20 million available over two planning horizons of length $T = 10$ years and $T = 20$ years.

PV panel output, Q (kW)	PV system variable cost, V^{κ} (USD)	Percentage energy saving in cooling degree-hours by GRs, α	Percentage energy saving in heating degree-hours by GRs, β	Percentage efficiency increase in PV panel output, θ	$T = 10$					$T = 20$				
					Stand-alone PV (m^2)	Stand-alone GR (m^2)	PV+GR (m^2)	SI	ROI	Stand-alone PV (m^2)	Stand-alone GR (m^2)	PV+GR (m^2)	SI	ROI
10%	100	10%	-10%	2.5%	0	0	0	0.000%	0.00%	199,400	0	0	1.283%	82.43%
				10%	0	885	178,030	1.965%	63.13%	0	885	178,030	3.508%	225.45%
			10%	2.5%	0	76,875	0	0.056%	38.76%	187,087	103,443	0	1.356%	87.12%
				10%	0	14,344	176,410	2.031%	65.26%	0	14,344	176,410	3.574%	229.68%
		20%	-10%	2.5%	0	0	0	0.000%	0.00%	199,396	31	0	1.283%	82.43%
				10%	0	885	178,030	1.979%	63.59%	0	885	178,030	3.523%	226.39%
			10%	2.5%	0	192,650	0	0.155%	43.22%	169,430	250,580	0	1.480%	95.14%
				10%	0	34,058	174,386	2.074%	66.65%	0	34,074	174,385	3.618%	232.52%
	200	10%	-10%	2.5%	0	0	0	0.000%	0.00%	0	0	0	0.000%	0.00%
				10%	0	0	0	0.000%	0.00%	0	2,302	94,068	1.145%	73.62%
			10%	2.5%	0	76,875	0	0.056%	38.76%	0	589,660	0	0.270%	49.03%
				10%	0	76,875	0	0.056%	38.76%	0	104,608	88,277	1.251%	80.43%
		20%	-10%	2.5%	0	0	0	0.000%	0.00%	0	137	0	0.000%	23.42%
				10%	0	0	0	0.000%	0.00%	0	2,335	94,066	1.153%	74.12%
			10%	2.5%	0	192,650	0	0.155%	43.22%	0	1,166,725	0	0.641%	58.85%
				10%	0	192,650	0	0.155%	43.22%	0	251,691	79,999	1.394%	89.60%
	400	10%	-10%	2.5%	0	0	0	0.000%	0.00%	0	0	0	0.000%	0.00%
				10%	0	0	0	0.000%	0.00%	0	0	0	0.000%	0.00%
			10%	2.5%	0	76,875	0	0.056%	38.76%	0	589,660	0	0.270%	49.03%
				10%	0	76,875	0	0.056%	38.76%	0	589,660	0	0.270%	49.03%
		20%	-10%	2.5%	0	0	0	0.000%	0.00%	0	137	0	0.000%	23.42%
				10%	0	0	0	0.000%	0.00%	0	137	0	0.000%	23.42%
			10%	2.5%	0	192,650	0	0.155%	43.22%	0	1,166,725	0	0.641%	58.85%
				10%	0	192,650	0	0.155%	43.22%	0	1,166,725	0	0.641%	58.85%
	600	10%	-10%	2.5%	0	0	0	0.000%	0.00%	0	0	0	0.000%	0.00%
				10%	0	0	0	0.000%	0.00%	0	0	0	0.000%	0.00%
			10%	2.5%	0	76,875	0	0.056%	38.76%	0	589,660	0	0.270%	49.03%
				10%	0	76,875	0	0.056%	38.76%	0	589,660	0	0.270%	49.03%
		20%	-10%	2.5%	0	0	0	0.000%	0.00%	0	137	0	0.000%	23.42%
				10%	0	0	0	0.000%	0.00%	0	137	0	0.000%	23.42%
			10%	2.5%	0	192,650	0	0.155%	43.22%	0	1,166,725	0	0.641%	58.85%
				10%	0	192,650	0	0.155%	43.22%	0	1,166,725	0	0.641%	58.85%
20%	100	10%	-10%	2.5%	199,300	0	0	2.580%	82.91%	199,300	0	0	4.122%	264.89%
				10%	0	885	178,030	7.054%	226.66%	0	885	178,030	8.584%	551.67%
			10%	2.5%	198,435	8,039	0	2.593%	83.33%	198,435	8,039	0	4.135%	265.72%
				10%	0	1,589	177,955	7.110%	228.47%	0	1,589	177,955	8.640%	555.27%
		20%	-10%	2.5%	199,300	0	0	2.580%	82.91%	199,300	0	0	4.122%	264.89%
				10%	0	885	178,030	7.068%	227.12%	0	885	178,030	8.598%	552.61%
			10%	2.5%	196,007	28,274	0	2.615%	84.05%	196,007	28,274	0	4.158%	267.20%
				10%	0	3,455	177,755	7.128%	229.05%	0	3,455	177,755	8.658%	556.45%
	200	**10%**	**-10%**	**2.5%**	**0**	**0**	**0**	**0.000%**	**0.00%**	**99,750**	**0**	**0**	**1.315%**	**84.49%**
				10%	0	2,302	94,068	2.311%	74.26%	0	2,302	94,068	3.853%	247.65%
			10%	2.5%	0	76,875	0	0.056%	38.76%	93,643	103,443	0	1.386%	89.09%
				10%	0	10,824	93,585	2.351%	75.56%	0	10,824	93,585	3.893%	250.22%
		20%	-10%	2.5%	0	0	0	0.000%	0.00%	99,748	31	0	1.315%	84.49%
				10%	0	2,302	94,068	2.319%	74.51%	0	2,302	94,068	3.861%	248.16%
			10%	2.5%	0	192,650	0	0.155%	43.22%	84,815	250,580	0	1.508%	96.88%
				10%	0	39,001	91,849	2.381%	76.52%	0	39,001	91,849	3.924%	252.21%
	400	10%	-10%	2.5%	0	0	0	0.000%	0.00%	0	0	0	0.000%	0.00%
				10%	0	0	0	0.000%	0.00%	0	192	48,490	1.256%	80.74%
			10%	2.5%	0	76,875	0	0.056%	38.76%	0	589,660	0	0.270%	49.03%
				10%	0	76,875	0	0.056%	38.76%	0	106,739	45,386	1.340%	86.09%
		20%	-10%	2.5%	0	0	0	0.000%	0.00%	0	137	0	0.000%	23.42%
				10%	0	0	0	0.000%	0.00%	0	224	48,489	1.260%	80.99%
			10%	2.5%	0	192,650	0	0.155%	43.22%	0	1,166,725	0	0.641%	58.85%
				10%	0	192,650	0	0.155%	43.22%	0	251,111	41,181	1.470%	94.49%
	600	10%	-10%	2.5%	0	0	0	0.000%	0.00%	0	0	0	0.000%	0.00%
				10%	0	0	0	0.000%	0.00%	0	774	32,648	0.350%	22.49%
			10%	2.5%	0	76,875	0	0.056%	38.76%	0	589,660	0	0.270%	49.03%
				10%	0	76,875	0	0.056%	38.76%	0	330,878	26,176	0.527%	33.89%
		20%	-10%	2.5%	0	0	0	0.000%	0.00%	0	137	0	0.000%	23.42%
				10%	0	0	0	0.000%	0.00%	0	804	32,648	0.353%	22.66%
			10%	2.5%	0	192,650	0	0.155%	43.22%	0	1,166,725	0	0.641%	58.85%
				10%	0	192,650	0	0.155%	43.22%	0	703,127	18,877	0.788%	50.67%

remaining budget spent on stand-alone GRs. In this case, the proportion of budget spent on stand-alone GRs increases in both α and β.

In general, the length of the planning horizon can significantly impact the optimal solution. For instance, as the highlighted row on Table 1.7 shows, for $T = 10$ years the optimal solution is to not spend any budget, whereas for $T = 20$ years the optimal solution is to allocate all of the budget to install stand-alone PV panels.

Additionally, ROI and SI values are generally higher for $T = 20$ years compared to $T = 10$ years. To eliminate the effect of different planning horizon lengths, we calculate the average annual ROI and SI values for $T = 10$ years and $T = 20$ years by dividing the values in the table by their planning horizon lengths. The results show that for $T = 20$ years the average annual ROI and SI values are at least as large as the average annual values for $T = 10$ years for any combination of parameters. This is mainly due to the higher number of peak sunlight hours and cooling degree-hours during the second decade of the 20-year planning horizon.

Overall, the results from Table 1.7 show that while the optimal solution of the model relies on the values of the key parameters, the length of the planning horizon, T, plays a significant role in the allocation of the initial investment. Moreover, Table 1.7 shows that both the percentage energy saving in cooling and heating degree-hours due to GR installation, α and β, and percentage efficiency increase in the output of PV panels due to integration with GRs, θ, can significantly affect the optimal solution. The values of α and β rely on several different factors, e.g., the type of green media or isolation layer installed, and vary significantly from one climate type to another. Hence, region-specific studies are needed to accurately estimate these parameters before large-scale implementation. In addition, to the best of our knowledge and despite the overwhelming evidence on the benefits of PV-GR integration, these benefits are not completely characterized in the literature. Hence, there is a need to further investigate and quantify this efficiency increase to better justify large-scale investments.

Table 1.8 presents the results of a sensitivity analysis with respect to percentage change in energy consumed for space conditioning over the planning horizon, δ, using its estimated values as presented in Table 1.2, for the three cases presented in Table 1.5. First, note that the optimal solutions presented in Table 1.8 are more or less consistent with those presented in Table 1.6, where $\delta = 0$. That is, when $T = 10$, under the optimal solution, only a small

Table 1.8: Area covered by stand-alone GRs, stand-alone PV panels, and GR integrated PV panels under different values of δ, for an initial budget of \$20 million available over two planning horizons of length $T = 10$ years and $T = 20$ years for the cases presented in Table 1.5.

Case study	The rate of energy consumption, δ	$T = 10$						$T = 20$					
		Stand-alone PV (m^2)	Stand-alone GR (m^2)	PV+GR (m^2)	Budget spent (\$)	SI	ROI	Stand-alone PV (m^2)	Stand-alone GR (m^2)	PV+GR (m^2)	Budget spent (\$)	SI	ROI
Case1	-60%	0	137	0	1,644	0.0009%	40.87%	0	629	0	7,548	0.0025%	69.98%
	-40%	0	389	0	4,668	0.0018%	49.60%	0	3,506	0	42,072	0.0077%	41.02%
	-20%	0	629	0	7,548	0.0025%	67.97%	0	8,039	0	96,468	0.0138%	46.60%
	20%	0	3,506	0	42,072	0.0076%	39.35%	0	45,121	0	541,452	0.0478%	36.14%
	40%	0	5,474	0	65,688	0.0104%	41.99%	0	76,875	0	922,500	0.0705%	37.43%
	60%	0	8,039	0	96,468	0.0136%	44.87%	0	116,127	0	1,393,524	0.0947%	39.74%
Case 2	-60%	0	137	0	1,644	0.0009%	40.87%	99,792	137	0	20,000,000	7.1776%	84.52%
	-40%	0	389	0	4,668	0.0018%	49.60%	99,777	389	0	20,000,000	4.7856%	84.54%
	-20%	0	629	0	7,548	0.0025%	67.97%	99,740	999	0	20,000,000	3.5899%	84.57%
	20%	0	3,506	0	42,072	0.0076%	39.35%	99,422	5,474	0	20,000,000	2.3949%	84.70%
	40%	0	5,474	0	65,688	0.0104%	41.99%	99,268	8,039	0	20,000,000	2.0544%	84.85%
	60%	0	8,039	0	96,468	0.0136%	44.87%	99,051	11,649	0	20,000,000	1.7997%	85.06%
Case 3	-60%	0	137	0	1,644	0.0009%	40.88%	0	2,447	94,060	20,000,000	7.2069%	88.59%
	-40%	0	389	0	4,668	0.0018%	49.60%	0	2,715	94,044	20,000,000	4.8064%	88.63%
	-20%	0	629	0	7,548	0.0025%	67.97%	0	2,969	94,030	20,000,000	3.6064%	85.33%
	20%	0	3,506	0	42,072	0.0076%	39.35%	0	6,019	93,857	20,000,000	2.4116%	87.87%
	40%	0	5,474	0	65,688	0.0104%	41.99%	0	10,824	93,585	20,000,000	2.0694%	86.89%
	60%	0	8,039	0	96,468	0.0136%	44.87%	0	14,650	93,369	20,000,000	1.8130%	87.18%

proportion of the available budget is spent and only stand-alone GRs are installed. Also, when $T = 20$, in Case 1 only a limited number of stand-alone GRs are installed, whereas in Cases 2 and 3, the majority of the available budget is spent to place stand-alone PV panels and GR integrated PV panels, respectively, and the remaining budget is used for stand-alone GRs. In all three cases, the total area of installed GRs (i.e., stand-alone GRs and GR integrated PV panels) increases in δ, whereas the total area of installed PV panels (i.e., stand-alone PV panels and GR integrated PV panels) decreases in δ. Note that a larger δ means a higher amount of energy consumption over the planning horizon. Hence, when δ is large, GRs, which can save a fraction of the total energy consumed, provide additional benefits compared to PV panels. Therefore, as δ increases, the model allocates a larger portion of the budget to GRs.

It is interesting to note the extent to which the value of δ affects the decisions. For instance, when $T = 20$, the increase in δ drastically increases the total area of installed stand-alone GRs in Case 1, whereas this increase is more modest in Case 2 and especially in Case 3. This is mainly because in Case 1, not all of the budget is allocated. Also, only GRs are economically profitable. Hence, as δ increases, additional GRs are installed to provide further benefit. However, in Case 2, in which all of the budget is already allocated, for stand-alone GRs to be further prioritized over stand-alone PV panels, the energy savings

achieved through their installation must be higher than the energy generated by PV panels. Therefore, the increase in δ only modestly increases the area of installed stand-alone GRs. In Case 3, in which again all of the budget is already allocated, PV panels installed enjoy an increase in the output as a result of integration with GRs. Therefore, compared to Case 2, stand-alone GRs face more resistance in being prioritized over GR integrated PV panels, hence a slower growth in the total area of installed stand-alone GRs in this case.

Moreover, for the cases in which all of the budget is spent under the optimal solution, i.e., in Cases 2 and 3 when $T = 20$, SI decreases, whereas ROI increases in δ. Recall that higher levels of δ leads to higher levels of profit through the installation of GRs. Therefore, given the same \$20 million budget, the amount of savings increases in δ, resulting in higher profit and ROI. However, because the amount of increase in GR energy savings is smaller than that of energy consumption, SI decreases in δ.

Lastly, for the cases in which only a small proportion of the budget is spent on installing stand-alone GRs under the optimal solution, i.e., Cases 1-3 when $T = 10$ and Case 1 when $T = 20$, the amount of budget spent and SI both increase in δ. This is mainly because higher δ increases the achievable profit through the installation of GRs, making this practice a viable option for a larger number of candidate sites. As a result, a larger proportion of the budget is used to install a larger area of GRs across the candidate sites, leading to higher values of SI.

Table 1.9 presents the results when maintenance costs are directly incorporated into the model, using the estimated values as presented in Table 1.2, for the three cases presented in Table 1.5. First, note that for in all cases when $T = 10$ and in Case 1 when $T = 20$, the results in Table 1.9 remain the same as those obtained when maintenance costs are assumed to be the property owners' responsibility, presented in Table 1.6. This is because in these cases, it is not optimal to install PV panels even without incorporating their maintenance costs directly into the model and accounting for PV maintenance costs only makes them a more costly, and hence less favorable, option.

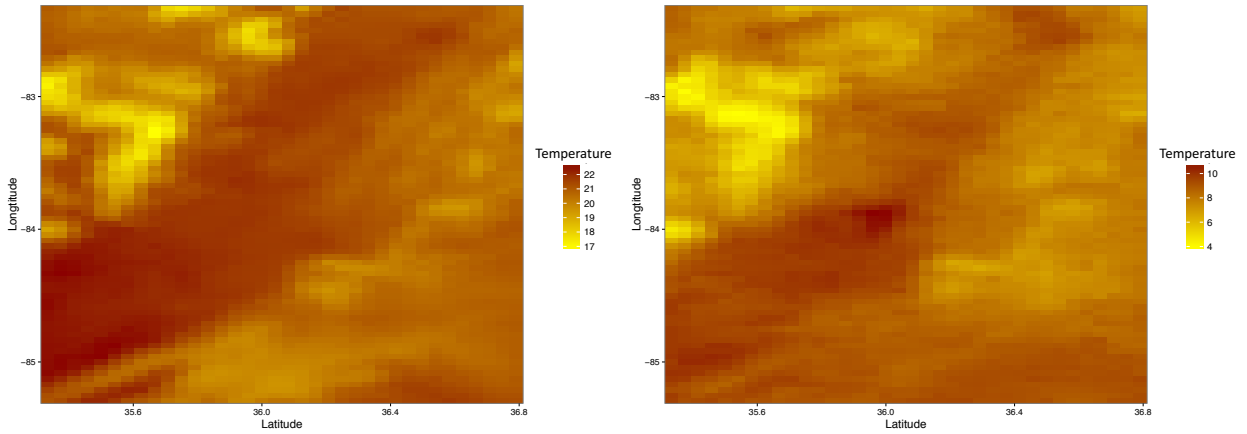
As seen in Table 1.9, for Cases 2 and 3 when $T = 20$, accounting for PV panel maintenance costs impacts the optimal solutions and negatively affects the ROI and SI metrics. In general, consistent with the intuition, the higher the PV maintenance cost, the more costly the PV panels and hence, the lower the the total area of PV panels installed. In particular, in Case

Table 1.9: Area covered by stand-alone GRs, stand-alone PV panels, and GR integrated PV panels under different values of $\mathbb{C}^{\kappa}$, for an initial budget of \$20 million available over two planning horizons of length $T = 10$ years and $T = 20$ years for the cases presented in Table 1.5.

Case study	Annual per m^2 PV panel maintenance cost, $\frac{\mathbb{C}^{\kappa}}{T}$ (\$)	$T = 10$						$T = 20$					
		Stand-alone PV (m^2)	Stand-alone GR (m^2)	PV+GR (m^2)	Budget spent (\$)	SI	ROI	Stand-alone PV (m^2)	Stand-alone GR (m^2)	PV+GR (m^2)	Budget spent (\$)	SI	ROI
Case 1	0.15	0	999	0	11,988	0.0033%	75.82%	0	21,969	0	263,628	0.0283%	37.97%
	0.62	0	999	0	11,988	0.0033%	75.82%	0	21,969	0	263,628	0.0283%	37.97%
	0.92	0	999	0	11,988	0.0033%	75.82%	0	21,969	0	263,628	0.0283%	37.97%
Case 2	0.15	0	999	0	11,988	0.0033%	75.82%	98,122	2,295	0	20,000,000	2.8307%	81.93%
	0.62	0	999	0	11,988	0.0033%	75.82%	94,001	2,295	0	20,000,000	2.7118%	74.28%
	0.92	0	999	0	11,988	0.0033%	75.82%	91,317	3,506	0	20,000,000	2.6372%	69.49%
Case 3	0.15	0	999	0	11,988	0.0033%	75.82%	0	6,140	92,525	20,000,000	2.8476%	84.96%
	0.62	0	999	0	11,988	0.0033%	75.82%	0	4,018	88,876	20,000,000	2.7291%	77.13%
	0.92	0	999	0	11,988	0.0033%	75.82%	0	4,362	86,470	20,000,000	2.6547%	72.41%

2, when the annual per m^2 PV maintenance cost increases from \$0.15 to \$0.62, stand-alone PV panels become more expensive and the portion of spent budget that is allocated to PV panels results in fewer square meters of PV panels. When the annual per m^2 PV maintenance cost increases further from \$0.62 to \$0.92 , stand-alone PV panels become a less favorable option compared to stand-alone GRs and hence, more of the budget is spent on the latter and the total area of stand-alone PVs drops further. A similar trend is observed for Case 3, in which as the per m^2 PV maintenance cost increases, GR integrated PV panels become more expensive and consequently, the portion of spent budget that is allocated to PV panels results in fewer square meters of PV panels. However, in this case, GR integrated PV panels generally remain a favorable option despite the increase in their cost. Hence, as the annual per m^2 PV maintenance cost increases, a larger portion of the budget is allocated to GR integrated PV panels to mitigate the effect of their increased cost. Finally, the remaining portion of the budget that is not spent on installing GR integrated PV panels is allocated to install stand-alone GRs.

Finally, we investigate the impact of using the averages of the daily projections over all grids spanning the City of Knoxville, instead of the true projections for each grid, when calibrating the model. As discussed, the daily temperature projections are generated for grids of sizes 1 km^2 and 4 km^2. The daily maximum and minimum temperature projections of the 10 CGCMs show a variation across grids in the City of Knoxville. For instance, Figures 1.6a and 1.6b depict the heat map of average daily maximum and minimum temperatures over the year 2030 projected by the ACCESS CGCM across 4-kilometer wide grids for the City



(a) Average daily maximum temperature.

(b) Average daily minimum temperature.

Figure 1.6: Heat map for average daily maximum and minimum temperatures over the year 2030 projected by the ACCESS CGCM across 4-kilometer wide grids for the City of Knoxville.

of Knoxville. Other climate models show a similar pattern, indicating the variation in the hourly temperatures over different grids.

Here, we examine the impact of accounting for the exact projections provided for each grid through a grid-based calibration approach. Specifically, we calculate the total number of cooling and heating degree-hours for each 4 km^2 grid separately, assign each candidate site with the parameters of their corresponding grid, and then resolve the model. Table 1.10, which is analogous to Table 1.6, presents the optimal solution for two planning horizons of length $T = 10$ years and $T = 20$ years for the three cases presented in Table 1.5. As seen in the table, more GRs are installed under the grid-based calibration approach. For instance, in Case 1 for $T = 20$ years, the optimal solution prescribes to increase the total area of stand-alone GRs installed by 80%. This is due to the fact that most of the small and medium buildings in the City of Knoxville are located in the warmer grids and they are assigned a higher number of cooling degree-hours under the grid-based calibration approach. Hence, by installing more GRs the model can achieve more energy savings and consequently a higher profit. The increase in energy savings is also reflected in the SI values. The highest percentage of increase in SI values is equal to 2.22% for Case 1 when $T = 20$ years, which translates into 276.5 GWh of energy saved and generated through sustainable resources.

Table 1.10: Optimal solution for an initial budget of $20 million available for investment over two planning horizons of length $T = 10$ years and $T = 20$ years for the cases presented in Table 1.5 under the grid-based calibration approach.

	$T = 10$						$T = 20$					
	Stand-alone PV (m^2)	Stand-alone GR (m^2)	PV+GR (m^2)	Budget spent	SI	ROI	Stand-alone PV (m^2)	Stand-alone GR (m^2)	PV+GR (m^2)	Budget spent	SI	ROI
Case 1	0	2,813	0	33,756	0.0076%	43.98%	0	39,551	0	474,612	0.0505%	36.75%
Case 2	0	2,813	0	33,756	0.0076%	43.98%	99,521	3,818	0	20,000,000	2.8736%	84.68%
Case 3	0	2,813	0	33,756	0.0076%	43.98%	0	5,989	93,859	20,000,000	2.8941%	87.83%

In general, the grid-based calibration approach provides more accurate representation of the problem at hand. However, the solution provided in Table 1.10 is relatively consistent with that of Table 1.6. Hence, considering that the data pre-processing for the grid-based calibration approach is much more computationally expensive, it may or may not be beneficial to use the grid-based calibration approach depending on the specific characteristics of the region of interest.

1.4.4 Robustness Analysis

As discussed earlier, limited data is available for estimating some of the important model parameters. Hence, it is not unlikely that these parameters are wrongly estimated during implementation. In this section, we conduct robustness analysis to investigate the impact of parameter misspecification on the solution. Specifically, we evaluate the robustness of the model with respect to parameters α, β, and θ, for $T = 10$ and $T = 20$ years, and provide the expected loss of profit due to parameter misspecification.

Let Z^* denote the total profit generated in USD given the true parameter settings. Let $\hat{Z}$ denote the total profit generated in USD from executing the model under extreme parameter misspecifications. Recall that Table 1.2 provides the estimated parameter ranges and levels used in the study. Hence, $\hat{Z}$ gives the total profit generated when a subset of parameters have been misspecified in the extreme, i.e., the parameters of interest assume their maximum (minimum) values as reported in Table 1.2, while the true parameter values are at their minimum (maximum). We let $\hat{x_i^\kappa}$, $\hat{y_i^\kappa}$, and $\hat{k_i^\kappa}$ denote the corresponding solution. Now let $\tilde{Z}$ denote the total profit in USD when the solution $\hat{x_i^\kappa}$, $\hat{y_i^\kappa}$, and $\hat{k_i^\kappa}$ is evaluated under the true parameter values. Lastly, let $\tilde{O}$ denote the cost of misspecifying the parameters, i.e., $\tilde{O} = Z^* - \tilde{Z}$.

Table 1.11: Robustness analysis for different parameter combinations for an initial budget of $20 million available over two planning horizons of length $T = 10$ years and $T = 20$ years. Negative values are enclosed in parentheses.

Planning horizon, T	Percentage energy saving in cooling degree-hours by GRs, α	Percentage energy saving in heating degree-hours by GRs, β	Percentage efficiency increase in PV panel output, θ	Z^* (USD)	$\tilde{Z}$ (USD)	$\tilde{O}$ (USD)
10	10%	-10%	2.5%	(642,680,064)	(642,306,584)	373,480
			7.5%	(642,680,064)	(642,306,584)	373,480
		10%	2.5%	(644,895,574)	(642,680,064)	2,215,510
			7.5%	(644,895,574)	(642,680,064)	2,215,510
	20%	-10%	2.5%	(642,680,064)	(642,405,147)	274,917
			7.5%	(642,680,064)	(642,405,147)	274,917
		10%	2.5%	(645,583,951)	(642,680,064)	2,903,887
			7.5%	(645,583,951)	(642,680,064)	2,903,887
20	10%	-10%	2.5%	(2,441,792,744)	(2,437,914,658)	3,878,086
			7.5%	(2,442,331,322)	(2,438,457,551)	3,873,771
		10%	2.5%	(2,446,274,934)	(2,441,402,503)	4,872,431
			7.5%	(2,446,791,546)	(2,441,792,744)	4,998,802
	20%	-10%	2.5%	(2,441,792,744)	(2,439,849,247)	1,943,497
			7.5%	(2,442,412,330)	(2,440,445,560)	1,966,770
		10%	2.5%	(2,453,838,358)	(2,441,483,511)	12,354,847
			7.5%	(2,454,220,178)	(2,441,792,744)	12,427,434

Table 1.11 presents the robustness analysis results on the three parameters of percentage energy saving in cooling degree-hours due to GR installation, α, percentage energy saving in heating degree-hours due to GR installation, β, and percentage efficiency increase in the output of PV panels due to integration with GRs, θ, for an initial budget of $20 million available over two planning horizons of length $T = 10$ years and $T = 20$ years. The parameters α, β, and θ are particularly chosen as they are generally difficult to estimate and are functions of many other factors themselves, such as the type of GR vegetation, the GR isolation layer, and the climate. As seen in Table 1.11, the lost opportunity, $\tilde{O}$, ranges between $275 thousand and $12.4 million. Note that for $T = 10$, the values of $\tilde{O}$ are not impacted by the change in the value of θ as no PV panel is installed in these cases. Overall, despite the significant difference among the values of $\tilde{O}$ in the table, this difference is somewhat small with respect to θ, when all other parameters are held constant. The values of $\tilde{O}$ are in general most sensitive with respect to the parameters α, and especially β, and hence, care needs to be taken when calibrating these parameters for an investment in a particular climatic region.

1.4.5 Environmental Insights

Table 1.12: Total amount of requisite fossil fuels to produce the electricity saved and/or generated under the optimal solution in Cases 1–3 for two planning horizons of length $T = 10$ years and $T = 20$ years.

	$T = 10$			$T = 20$		
	Coal (kg)	Natural gas (m^3)	Oil (m^3)	Coal (kg)	Natural gas (m^3)	Oil (m^3)
Case 1	153,304	11,103,187	3,946	1,310,055	94,881,781	33,721
Case 2	153,304	11,103,187	3,946	104,851,660	9,650,189,247	3,419,991
Case 3	153,304	11,103,187	3,946	108,665,787	9,809,140,900	3,477,032

Recall that the goal of the model is to maximize the overall *profit* from energy generated and/or saved across a set of regions by investing in PV systems and/or GRs. In this section, we discuss the environmental implications of such an investment and provide insights on the benefits achievable by the implementation of the proposed model.

Table 1.12 presents the positive impact of implementing the optimal solutions provided for the three cases introduced in Table 1.5, for $T = 10$ years and $T = 20$ years, from an environmental perspective. Specifically, Table 1.12 presents the amount of fossil fuels needed [66] to produce the amount of electricity that is generated and/or saved through the implementation of the solutions provided in Table 1.6, after accounting for the required energy for manufacturing, distribution, and end-of-life processing of installed PV panels [16, 5, 72, 85]. Note that the corresponding required energy for GRs are negligible [24]. (Please see Appendix D for more detail.)

For instance, consider Case 3 in Table 1.6. When $T = 20$ years, it is optimal to install 4,735 m^2 stand-alone GRs and 93,930 m^2 GR integrated PV panels. As shown in Table 1.12, implementing this solution in the City of Knoxville achieves approximately 108.7 million kg reduction in coal usage, or equivalently, 9.8 billion m^3 or 3.5 million m^3 reduction in natural gas or oil usage, respectively. According to [67], these values translate into approximately 214 million kg, 19 billion kg, and 10 billion kg decrease in CO_2 emissions, respectively.

1.5 Conclusion and Remarks

In this study, we evaluate the overall profit from energy generated and saved through installation of PV panels and GRs, while incorporating future climate uncertainties and the interaction between the practices. We study the model over two different planning horizon lengths, $T = 10$ and $T = 20$ years. The results suggest that a 10-year planning horizon is generally too short to allow for a profitable investment. However, a 20-year planning horizon, which is also more consistent with the lifespans of PV panels and GRs, is a better time frame for evaluating the outcomes of an investment on these green technologies. The results also show the importance of incorporating the PV-GR integration efficiency increase as it can significantly change the optimal solutions. The sensitivity analysis demonstrates that different cost and output of PV panels can significantly change the optimal solution. The sensitivity and robustness analyses show that the model is sensitive with respect to GR-related parameters, suggesting the need for careful calibration of these parameters before large scale implementation in any climate region. Lastly, the results indicate that considering the long-term changes in the rate of energy consumption affects the distribution of budget/rooftop areas between PV panels and GRs.

In this study, we only focus on the energy savings provided by GRs. Future studies may also incorporate other beneficial aspects of utilizing GRs in an urban area (such as run-off reduction, scaling down CO_2 emissions, and heat island mitigation) to more accurately evaluate the overall benefits of installing GRs and their significant role in increasing the urban resiliency. In addition, although the developed model is capable of considering multiple regions, due to limited data availability, especially with regard to future climate projections, in this study we only focus on one region, i.e., Knoxville, Tennessee. Future studies may include using this model to evaluate investment options across multiple regions with different climates.

Chapter 2

Optimizing PV System Integrated Lithium-ion Batteries Return Under Climate Uncertainly

2.1 Introduction

Photovoltaic (PV) panels output cost has reduced noticeably in the past few years, turning them to a favorable renewable energy source. The application of PV panels specially in the residential sector witnessed a noticeable increase during the past years [177]. However, the main challenge in utilizing this source of renewable energy is that the demand for electricity does not always take place when PV panels are able to generate electricity, i.e., during night-time and cloudy days. This can be addressed through the storage of the excess energy generated by PV panels in order to be used when the PV system is not able to function [214].

Various energy storage systems have been developed, studied, and utilized throughout the years (e.g., pumped hydro-power, compressed air energy storage, thermal, flywheels, solid state batteries, and flow batteries) [78]. Each of these methods have their disadvantages which in some cases makes them impractical, technically or economically, specifically for small-scale implementation [170]. For instance, pumped hydro-power (as the most

utilized and matured utility-scale energy storage system) requires specific topographic site specifications and requires significant initial investments which makes them only suitable for large-scale electricity storage systems . Flywheels are mainly fit for applications which require short discharge duration. Thermal storage systems are only used to provide air conditioning, mainly for buildings. Compressed air storage needs specific site locations as well as natural gas combustion to help the compression and expansion process [165, 170, 113].

Battery storage systems (solid state and flow) need high levels of maintenance and generally have low cycling time [170]. Flow batteries have high operating cost, low energy and density and complicated to manage and use [165, 138]. The oldest rechargeable solid state battery technology are lead-acid batteries [160] which generally have short lifespan, need high levels of maintenance, and have poor energy density [59, 212, 165]. [160] state that lead-acid batteries are cost-ineffective for storing large amounts of energy which makes them unfit for grid storage system.

According to the U.S. solar Energy Monitor, the most common energy storage method is through utilization of Lithium-ion (Li-ion) batteries [203]. The high charge and discharge efficiency of Li-ion batteries, low level of requisite maintenance, and low capacity loss during idle time, as well as their capability in delivering a high number of cycles compared to other common types of batteries (e.g., lead-acid batteries) during their lifetime makes them a suitable choice for long-term and frequent residential applications [202]. The main challenge in utilizing Li-ion batteries for the residential sector in the recent years was the fact that they were disproportionately expensive compared to other common types of batteries (e.g., lead-acid batteries), which made them economically impractical [182, 212]. Moreover, to use Li-ion batteries, a battery management system (BMS) is also usually needed, which results in even higher expenses [165]. However, the recent technological advancements in development of Li-ion batteries and their production procedure resulted in more cost-efficient batteries [219]. According to [26, 202], the cost of Li-ion batteries is expected to reduce by more than $500 per kWh by the end of the decade, landing at less than $100 per kWh. As a result of the recent improvements in the Li-ion battery production and the cost reductions, battery connected PV systems are becoming a financially viable alternative to fossil fuels [214, 182].



Figure 2.1: An example of battery integrated PV systems.

Li-on batteries were first developed in 1991 and have been extensively utilized since then [170]. These batteries mainly use lithium as cathode, porous carbon as anode, and an electrolyte as conductor to transition the ions from the anode to the cathode [20]. Low atomic number and high electrode potential of the Li-ion rechargeable cells results in a significantly higher energy density compared to other common types of batteries (e.g., lead-acid and zinc) [238].

Li-ion batteries have been studied from different aspects in the literature. There is a large body of research on the underlying structure of Li-ion batteries. For example, in [241], the authors provide a review over the different stabilization methods for a specific type of anode for Li-ion batteries (Lithium-Sulfur batteries). Another example is the work by [36] which reviews the recent progress in Silicon/Graphine nano-camposites in Li-ion batteries. In addition to the above two sources, a comprehensive review on modeling of the solid electrolyte interphase (a passivation layer which is formed on electrode surfaces from decomposition products of electrolytes) for Li-ion batteries is provided in [223]. Overall, the existing literature demonstrates the significant energy storage potential of Li-ion batteries.

Irrespective of the advancements in the technology of Li-ion batteries, these batteries degrade over time due to various reasons such as aging, use, and environmental impacts [240]. However, by monitoring the health of the battery and conducting prognostics, sudden and unpredicted breakdowns of the Li-ion batteries can be avoided. Health monitoring and prognostics of machinery have been thoroughly studied in the literature. A brief history of the different maintenance techniques is presented in [144]. In another study, [116] present a number of most common algorithms, models, and technologies for condition based maintenance. Li-ion batteries show electro-chemical behaviors, making the developed health monitoring and prognostics algorithms and technologies for machinery unfit for them [240]. That is, the scarcity of the data (due to the inaccessibility of the chemical reactions inside the battery), different data types from monitoring (value-type instead of wave-form data), and the dynamic operation profile of Li-ion batteries (dependency on the demand behavior) make the available technologies and algorithms for diagnostics and prognostics of machinery incompatible with Li-ion batteries [240]. Hence, it is important to understand the underlying structure of these batteries in order to optimize the utilization of them by decreasing the degradation level and preventing catastrophic failures Health monitoring and prognostic models for Li-ion batteries should consider the mentioned properties as well as other factors related to performance and degradation of these batteries (e.g., capacity loss due to aging, capacity imbalance among cells, and self-discharge) [240].

Several studies focused on prognostics and health monitoring of Li-ion batteries. For instance, [240] provide a review on different aspects of research and development in prognostics and health monitoring on Li-ion batteries. More specifically, they provide an overview on different algorithms and models developed to estimate the state-of-charge (SOC), voltage, capacity, and remaining-useful-life in Li-ion batteries. A comparison between different prognostic algorithms for estimating the remaining useful life for Li-ion batteries is conducted in [189]. They provide a comparison between algorithms such as relevance vector machine, kernel-based regression/classification techniques, and Bayesian treatment of support vector machine. In [222], different methods for monitoring the capacity, SOC, state of health, available power, impedance parameters, and remaining useful life are critically evaluated. A review of the health management and battery prognostic techniques of Li-ion

batteries with a focus on the batteries in electric and hybrid vehicles is conducted in [183] in order to provide insights on the cost effective methods to deal with battery life issues.

Batteries in general are non-ideal energy sources. That is, minimizing the level of energy consumption of the system does not translate to maximizing its battery life [178]. Battery optimization studies mainly aim to justify the utilization level of batteries in a way that longevity of the battery is increased while the system that relies on the battery still performs on an acceptable rate. For instance, in [123], the authors model the sensor readings in a wireless network using a dynamic Gaussian Bayesian network to maximize prediction accuracy while maintaining the budgetary constraints on battery consumption. That is, they aim to utilize the correlation between sensors to predict readings from other sensors in order to minimize the prediction error and optimize the battery utilization level. [6] study battery optimization for remote health monitoring applications. In their study, they aim to increase the battery lifetime of the monitoring device in the context of cardiovascular disease. The results from their studies show an increase of 300% in battery lifetime. [176] first propose a high-level model based on electrochemical and diffusion equations for the discharge process of lithium-ion batteries. Moreover, based on the model, they develop a battery cost function to minimize the battery cost for scheduling and voltage scaling algorithms.

In another study, [137] propose a battery-aware scheduling optimization model for battery powered distributed real-time embedded systems. The authors provide 2 static battery-aware scheduling models, where one of them aims to maximize the utilization of the battery capacity through the optimization of the discharge power profile, whereas the other model aims to optimize the distributed systems which contain voltage-scalable processing elements. That is, the second model provides a scheduling scheme through efficient slack time re-allocation in order to reduce the average discharge power consumption as well as flattening the discharge power profile. Further, the authors examine the proposed scheduling models through experimental results and conclude that the proposed models can expand the lifespan of the batteries by up to 76% and 56% using the first and second models, respectively.

In another attempt for providing battery-aware task scheduling models for battery-powered systems, [44] provide a model for task scheduling in single and multiprocessor systems in order to maximize the lifespan of the battery. That is, they propose heuristic

algorithms that are derived from the properties of the battery model which shape the current load profile of the battery. Further, they examine the proposed model through simulation and conclude that their proposed model results in an increase in the battery lifespan.

In [178], the authors expand their proposed model in [176] and develop a battery model by which they relate the battery cost function to charge delivered to the load as well as the level of unavailable charge. They analyze a relationship between the proportion of unavailable charge recovered and its time and define an objective criterion to choose between energy optimization or battery charge optimization policies. Moreover, the authors drive an upper bound on the recovery time of the battery.

[142] propose a technology selection and operation optimization model for distributed energy systems in commercial buildings. In their study, they evaluate different technology options (i.e., 4 PV panel types, and 4 battery technologies) in order to simultaneously optimize the selection, capacity, and operation of integrated PV battery storage systems. They conclude that an integrated system of mono-crystalline PV and Li-ion results in the best outcomes with a payback period of 8 years.

[210] investigate the potential of PV integrated battery storage systems in low-voltage distribution grids. They propose a multi-objective model which aims to study the trade-off between voltage regulation, peak power reduction, and annual cost. They determine the size of the inverter as well as the battery package, concluding that in a number of scenarios, the optimal solution is to only utilize inverters, while batteries are required only for scenarios in which higher technical performance is required.

Integration of retired Electric Vehicle (EV) batteries with PV panels for residential application is studied by [131]. They propose an optimal control theory algorithm to minimize yearly operation cost of the integrated PV battery system, as well as optimizing the size of the PV module in the system through simulations. Their results show that the battery package should be charged when the electricity price is low, so it can be used when the price rates increase. Note that [131] consider dynamic pricing on the electricity throughout the day and do not factor in the degradation of the battery due to charge/discharge of the battery.

[227] develop a non-linear mixed integer scheduling model for the optimal day-ahead management of a battery storage system for a microgrid. They factor in the battery aging costs while studying a case of a hybrid integrated local energy supplier, i.e., a district of customers are supplied by a utility supplier using renewable and/or conventional energy generation practices. They conclude that the results from their model shows a 37% reduction in the energy cycles while increasing the battery lifetime by 74%.

In [172], an iterative method to optimize a hybrid wind/PV power generation system integrated with battery storage is proposed. They attempt to find the optimal size for the PV and wind power generation systems as well as an integrated battery package through a series of simulations while accounting for deficiency of power supply, relative excess power generated, and un-utilized energy. The authors conclude that the model can be applied for both grid connected and stand-alone microgrids.

The implementation of a battery storage integrated PV system in grid-connected residential buildings significantly relies on the cost of the battery storage. This becomes more important as the new net metering rates are being applied throughout U.S. by which the utility companies compensate distributed energy generated PV systems at lower rates compared to the utility electricity rate [162]. This lower rates makes such energy systems less economically attractive. Hence, while a battery system helps greatly to utilize PV panels more efficiently, it is important to use the battery in a way to maximize the cost efficiency of these practices. In this research, we aim to study a Lithium-Ion battery load connected to a PV system to store the excess generated electricity throughout the day. The stored energy is then used when the PV system is not able to generate electricity due to a lack of direct solar radiation. This study is an attempt to minimizing the cost of electricity bill for a medium sized household by maximizing the battery package utilization. We consider the degradation of battery due to calendar aging and cycles. We develop a Markov decision process (MDP) model to capture the stochastic nature of the output of the PV panel. Due to the minute reduction in the Li-ion battery capacity per day, we have to deal with an excessively large state space. Hence, we aim to develop approximate solution methods in order to reduce the solution time while achieving a good approximation of the optimal policy.

In the late 1950's, the pioneers of artificial intelligence [? ?] first used the term "Reinforcement learning" (RL) for the computational processes which led to an increase to the intensity or likelihood of a response [?]. Since then, in order to improve sequential decision makings RL has been implemented in a variety of studies, ranging from designing agents to play computer games to psychology, neuroscience, natural and social sciences , and engineering [? ?].

In RL decision makers learn about the optimal policy through a series of unsupervised trials and errors, i.e., evaluative learning while interacting with the environment [?]. Evaluative learning can immediately provide the decision makers with the feedback, i.e., one-shot feedback, or evaluate the outcomes over a sequence of decisions, i.e., sequential feedback. RL aims to maximize a scoring function and find the optimal policy while facing with weak feedback, i.e., sampled, evaluative, and sequential feedback [?].

The integration of RL and Neural Networks (NN) have long been studied in the literature [? ?]. Deep NNs, i.e., deep learning (DL), is a machine-learning method which is generally used for supervised or unsupervised learning [?]. The recent improvements in DL due to the significant financial investments, availability of big data, and high computational power has led to a wider array of applications in different subjects [? ?], for example its integration with RL, i.e., deep RL (DRL) [?]. The advent of DRL has resulted in numerous implementation of RL in games (e.g., AlphaGo [?], deep Q-network (DQN) [149]), memory-augmented neural networks (e.g., differentiable neural computer [?]), optimization of deep neural network controllers (e.g., asynchronous methods [?]), unsupervised reinforcement and auxiliary learning [? ?], information extraction [?], and guided policy search [?].

One of the most groundbreaking researches in the area of DRL is achieving human level control through the implementation of RDL. [149] develop a DRL algorithm, i.e., "Deep Q-network" (DQN), through end-to-end RL which is able to finish 49 different Atari 2,600 games as effectively as a professional human gamer. The reason why the integration of RL with DL leads to such improvements is the reduction in the reliance on the domain knowledge through the implementation of stochastic gradient decent in automatic feature engineering and end-to-end learning [?]. In this study, we utilize the DQN algorithm order to achieve

approximate optimal policies. Moreover, to improve the accuracy and decrease the solution time, we provide an extension to DQN for a battery package integrated PV system.

2.2 Model Formulation

In this section, we present the MDP model developed to minimize the electricity cost over the finite horizon T, by optimizing the utilization of a Li-ion battery pack integrated with a PV system.

Let $s_t(\ell, h, \phi)$ denote the state of the process for a battery at day t, $0 \leq t \leq T_{Max}$, where T_{Max} is the maximum number of days considered in the model, ℓ, $\underline{\ell} \leq \ell \leq \overline{\ell}$, is maximum available capacity for the Li-ion battery, h, $0 \leq h \leq \overline{h}$, is the remaining available charge, where $\overline{\ell}$ and $\overline{h}$ denote the maximum available capacity and available charge for a brand new Li-ion battery, respectively, and $\underline{\ell}$ is the minimum threshold for maximum available capacity to replace the battery. Note that ℓ is presented as the remaining percentage of initial maximum available capacity, while h is presented as percentage of ℓ, i.e., 0% to 100% regardless of the value of ℓ. We discretize each time step t, i.e., each day, into day-time and night-time, and use ϕ to represent it, where $\phi = 1$ and $\phi = 0$ denote day-time and night-time, respectively. When $\phi = 0$, the decision epoch is night-time at day t and a decision should be made for the level of discharge; when $\phi = 1$, the decision epoch is day-time at day t, and if $\ell \leq \underline{\ell}$ the battery must be replaced, otherwise a decision should be made to whether replace the battery or charge the battery.

For each night-time decision epoch, i.e., $\phi = 0$, a decision should be made to determine the level of discharge. That is, for state s_t, the set of available actions, $A^0_{s_t}$ is defined as the set of all possible levels of discharge. Therefore, for $\phi = 0$,

$$A^0_{s_t} = \{a : 0 \leq a \leq h\}, \tag{2.1}$$

where a in Equation (2.1) denotes the level of discharge in percentage of the remaining available charge, h. For every day-time decision epoch, i.e., $\phi = 1$, for all $\ell \leq \underline{\ell}$, the only possible action is to replace the battery, and for all $\ell > \underline{\ell}$, the possible actions are to replace or to charge the battery, i.e., choose the charge level. If the action is to charge the battery,

the set of possible charge levels is restricted by the remaining maximum available capacity, i.e., $\overline{h} - h$. The output of PV panels rely on the available daily peak sunlight hours, and only certain charge levels are achievable. Therefore, in Equation (2.2), the charge level cannot exceed the maximum electricity output of the PV panels at day t. Hence, for $\phi = 1$,

$$A^1_{s_t} = \{a : a \leq \min\{y(x), \overline{h} - h\}\} \qquad \forall x \in X(t), \tag{2.2}$$

where $y(x)$ in Equation (2.2) denotes the power output of PV panels from receiving x peak sunlight hours during the day in percentage of remaining available capacity, ℓ, and $X(t)$ is the probable set of peak sunlight hours at day t. Note that we assume that the output efficiency of the PV system does not change over time due to aging or other factors.

As mentioned in Section 2.1, the cells in a Li-ion battery package lose capacity over time. The degradation level of a battery depends on its calendar age as well as its cycle age. Cycle age is defined as the number of full cycles that battery has had through its life time [234]. To approximate the capacity loss, we use the function provided by [234]. Equation(2.3) shows the capacity loss in a Li-ion battery cell due to charge, discharge, and aging,

$$g(\ell, h, a, \tau) = 1 - (1 - \ell)e^{-f_d(a,\tau)}, \tag{2.3}$$

where $f_d(a, \tau)$ is a function of charge and discharge levels, as well as the temperature of the battery package (for a more detailed description of the degradation function used in this paper, interested readers are referred to [234]). As mentioned, we discretize each day into two separate decision epochs. Day-time, during which we make decisions on charging or replacing the battery, and night-time, during which we make decisions on discharging. The capacity reduction due to charging for $\phi = 1$, i.e., day-time, is denoted by $g(\ell, h, \theta, \tau)$, and the capacity reduction due to discharging for $\phi = 0$, i.e., night-time, is denoted by $g(\ell, h, a, \tau)$. The temperature of the battery cells, τ, is considered to be constant and equal to 25 for each day.

Each time the battery is replaced, a battery cost, c, is applied, and a brand new battery with a maximum available capacity $\overline{\ell}$, and a remaining charge available h_0 replaces the old battery. Note that when a battery is replaced at a given day t, it is not available for the

entire duration of day-time ($\phi = 1$) for that given day, and the new battery package has the same type, capacity and price of the previous battery package. Also, we consider a salvage value for the replaced battery, denoted by $c_0(\ell) < c$, as a non-decreasing function in ℓ. Let $V_t(\ell, h, \phi)$ denote the total cost starting from day t and state (ℓ, h, ϕ). For $\phi = 1$, i.e., day-time,

$$V_t(\ell, h, 1) = \begin{cases} R_t(\ell), & \text{if } \ell \leq \underline{\ell}, \\ \\ \min\left\{R_t(\ell), K_t(\ell, h)\right\}, & \text{otherwise,} \end{cases} \tag{2.4}$$

where $R_t(\ell)$ is the cost under the action "Replace,"

$$R_t(\ell) = c - c_0(\ell) + \lambda \cdot V_t(\overline{\ell}, h_0, 0), \tag{2.5}$$

which is calculated as the new battery cost, c, minus battery salvage value, $c_0(\ell)$, plus the discounted cost to go from day t for a new battery where $\phi = 0$, $V_t(\overline{\ell}, h_0, 0)$. $K_t(\ell, h)$ is the cost under the action "keep,"

$$K_t(\ell, h) = \min_{\forall a \in A^1_{s_t}} \left\{ \lambda \cdot \sum_{y \in y(x)} V_t(\ell - g(\ell, h, \theta, \tau), h + \theta, 0) P^t_y(y) \right\}, \tag{2.6}$$

which is equal to the total expected discounted cost to go from day t where $\phi = 0$ and $\theta = \min\{a, y\}$. During night-time, i.e., $\phi = 0$, the total cost to go from day t, i.e., $V_t(\ell, h, 0)$, is equal to the expected electricity cost not supported by the battery, $[d-a]^+$, plus the total expected discounted cost to go from day $t+1$ when $\phi = 1$,

$$V_t(\ell, h, 0) = \min_{\forall a \in A^0_{s_t}} \left\{ \sum_{d \in D^t} [d-a]^+ P^t_D(d)\mu + \lambda \cdot V_{t+1}(\ell - g(\ell, h, a, \tau), h - a, 1) \right\}, \tag{2.7}$$

where the only action is to choose the discharge level. In this model, we assume that the cost of electricity does not change during night time ($\phi = 0$), and it follows a fixed rate pricing.

Table 2.1: Notation used in the model.

Notation	Definition
t	Day t, where $t \in T : \{0, 1, 2, ..., T_{max}\}$
ϕ	Daily time stage , where 0 represents night, and 1 represents day
h	Remaining charge available (%)
ℓ	Maximum available capacity (%)
τ	Battery temperature ()
θ	True charge (%)
$X(t)$	Possible set of peak sunlight hours at day t (hours)
$y(x)$	Power output of PV panels from receiving x peak sunlight hours, where $x \in X(t)$ (%)
$\overline{\ell}$	Brand new Li-ion battery capacity (%)
h_0	Brand new Li-ion battery over the shelf charge (%)
$\overline{h}$	Brand new Li-ion battery maximum charge capacity (%)
$\underline{\ell}$	Maximum available capacity replacement threshold (%)
D^t	Demand at day t (kWh)
μ	Electricity unit cost per kWh (USD)
a	The level of charge and discharge for $\phi = 1$ and $\phi = 0$, respectively (%)
$P_y^t(y)$	Probability of generating y kWh of electricity output at day t, where $y \in y(x)$
$P_D^t(d)$	Probability of facing a demand equal to d kWh at day t, where $d \in D^t$
$g(\ell, h, o, \tau)$	Reduction in battery maximum available capacity due to charging and discharging with current maximum available capacity ℓ, true charge θ, and battery temperature τ, where $o = a$ for $\phi = 0$ and $o = \theta$ for $\phi = 1$ (%)
c	Brand new battery cost (USD)
$c_0(\ell)$	Salvage value for a battery with maximum available capacity ℓ (USD)
$V_t(\ell, h, \phi)$	Total expected discounted cost to go starting from day t with maximum available capacity ℓ, and remaining charge available h at time stage ϕ (USD)
$R_t(\ell)$	The expected discounted cost to go from day t when the decision is to replace the battery pack with a maximum available capacity ℓ (USD)
$K_t(\ell, h)$	The expected discounted cost to go from day t when the decision is to keep and charge the battery pack with a maximum available capacity ℓ and remaining charge h (USD)

2.3 Structural Properties

In this section, we provide several intuitive structural properties. We discretize the maximum available capacity dimension of the state space. The capacity increment, $\delta \in \mathbb{R}_{++}$, is defined such that the maximum available capacity, ℓ, and the reduction in maximum available capacity due to aging, charging, and discharging can be set to integer multiples of capacity increment, δ, and we define the capacity increment by

$$\delta = \max\{\delta \in \mathbb{R}_{++} : \frac{\ell}{\delta} \in \mathbb{Z}_{++}, \frac{g(\ell, h, a, \tau)}{\delta} \in \mathbb{Z}_{++}, \frac{g(\ell, h, \theta, \tau)}{\delta} \in \mathbb{Z}_{++}\}. \tag{2.8}$$

In this section, we make the following intuitive assumptions:

A1: The salvage value for a battery for any given values of ℓ is constant.

A2: The battery package degradation level due to charge, discharge, and aging follows Equation (2.3), and the battery package is always operating in an environment with a temperature of 25 , i.e., $\tau = 25$.

In Theorem 1, we establish a simple solution procedure that exploits the underlying structure of the problem. Prior to presenting Theorem 1, however, we present two technical lemmas.

First, Lemma 1 establishes the behavior of the expected discounted cost to go from day t when the decision is to replace the battery pack with a maximum available capacity ℓ, $R_t(\ell)$, due to changes in maximum available capacity $\ell \geq \underline{\ell}$.

Lemma 1. For any given day t, for $\phi = 1$, $R_t(\ell)$ is non-increasing in $\ell \geq \underline{\ell}$.

Next, Lemma 2 establishes the relationship between the total expected discounted cost to go starting from day t with a maximum available capacity ℓ and remaining charge available h during day-time, $V_t(\ell, h, 1)$, and the maximum available capacity, $\ell \geq \underline{\ell}$.

Lemma 2. For any given day t, and remaining available charge h, $V_t(\ell, h, 1)$ is non-increasing in $\ell \geq \underline{\ell}$.

Based on the results from Lemmas 1 and 2, Corollaries 1 and 2 establish that the expected cost to go from day t when the decision is to keep and charge the battery, i.e., $K_t(\ell, h)$, is non-increasing in ℓ and h.

Corollary 1. For any given day t, and remaining available charge h, $K_t(\ell, h)$ is non-increasing in $\ell \geq \underline{\ell}$.

Corollary 2. For any given day t, and maximum available capacity ℓ, $K_t(\ell, h)$ is non-increasing in h.

Theorem 1 establishes that based on Lemmas 1 and 2, the total expected discounted cost to go starting from day t with maximum available capacity ℓ, and remaining charge available h during day-time, $V_t(\ell, h, 1)$, follows the threshold type policy behavior.

Theorem 1. For any given day t, and remaining battery capacity h, $V_t(\ell, h, 1)$ is of threshold type policy. That is, there exists a maximum available capacity ℓ^* such that

$$V_t(\ell, h, 1) = \begin{cases} K_t(\ell, h), & \text{if} \quad \ell \geq \ell^*, \\ \\ R_t(\ell), & \text{otherwise}, \end{cases} \tag{2.9}$$

2.4 Computational Experiments

In this section, first we study the optimal policies under different assumptions for the parameters of the model. Next, we compare the results from the optimal policy from the model with the currently common battery utilization practice. Finally, we provide a description over the solution approaches developed in this study, and compare their results.

2.4.1 Example Optimal Policies

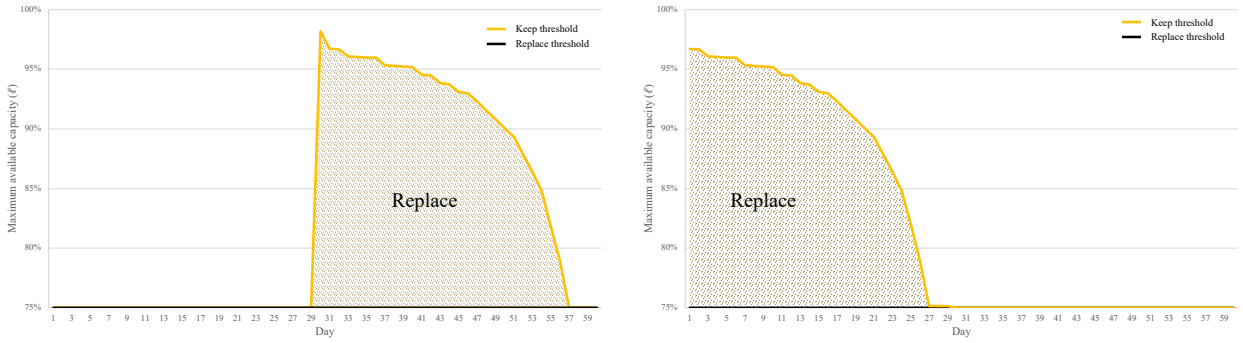
In order to study the optimal policy and observe the changes in the results of the model due to the changes in the assumptions, we conduct a number of experiments through changes in the values of the input parameters to observe their effects on the results of the model. We assume a lower price for the battery package (10% of the actual price), and a higher electricity cost (100 times of the actual price) to be able to observe the results of the model in a shorter span of time, i.e., two months. Table 2.2 shows two different cases designed to capture the effect of changes in the possible set of peak sunlight hours at day t, $X(t)$, on the results of the model.

Table 2.2: Case studies to investigate the effects of changes in possible set of peak sunlight hours at day t, $X(t)$, on the results of the model.

Case study	Possible set of peak sunlight hours at day t, $X(t)$	
	$t \in \{1-30\}$	$t \in \{31-60\}$
Case 1	2	4
Case 2	4	2

Figures 3.4a and 3.4b depict the optimal policy for Cases 1 and 2 with a maximum available capacity replacement threshold, $\underline{\ell}$, equal to 75%, and fully charge/discharge policy, respectively. The fully charge/discharge policy means that for $\phi = 1$ if the decision is to keep the battery package and charge, it is charged as much as possible, and for $\phi = 0$ the battery package is discharged completely. Figure 3.4a (Figure 3.4b) presents a scenario in which each day of the first month, i.e., day 1 to day 30, has 2 hours (4 hours) of peak sunlight hours available, while the second month, i.e., day 31 to day 60, has 4 hours (2 hours) of peak sunlight hours. The figures show that when $X(t) = 2$, the optimal policy is to use the battery as much as possible, and hence not to replace the battery package except when it is restricted by the assumptions of the model to do so, i.e., when $\ell \leq \underline{\ell}$.

However, for $X(t) = 4$, the optimal policy is to replace the battery for values of $\ell \geq \underline{\ell}$, i.e., $\ell^* \geq \underline{\ell}$, which means the replacement of the battery is not due to the restrictions of the model but to maximize the profitability. The figures also show that for the situations under which $\ell^* \geq \underline{\ell}$, the value of ℓ^* reduces in t, and as we progress into the time horizon, or toward the days that less peak sunlight hours are available, the reduction in the level of ℓ^* occurs more drastically. Figure 3.4a shows that for $t = 29$, the value for ℓ^* is at its highest level. Note that the number of peak sunlight hours for $t = 29$, i.e., $X(29)$ is equal to 2, and yet ℓ^* for $t = 29$ is the highest throughout the horizon. This can be explained through the structure of the model. That is, if the decision is to replace the battery package, the day-time t is dedicated to replacing the battery, and the peak sunlight hours during that given day are lost. Therefore, under the optimal policy, it is optimal to replace the battery package a day prior to the days with high peak sunlight hours in order to maximize the income through utilization of the battery package.



(a) Optimal policy for Case 1, for $\underline{\ell} = 75\%$.

(b) Optimal policy for Case 2, for $\underline{\ell} = 75\%$.

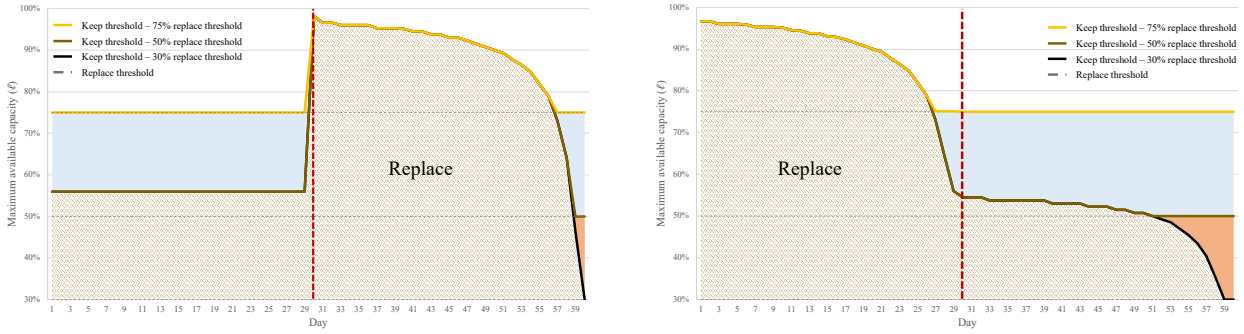
Figure 2.2: Example optimal policy for two different cases shown in Table 2.2, with maximum available capacity replacement threshold, i.e., $\underline{\ell}$, equal to 75%.

Figures 2.3a and 2.3b show the optimal policy under the assumptions of Cases 1 and 2 for different levels of maximum available capacity replacement threshold, i.e., $\underline{\ell}$ equal to 30%, 50%, and 75%.

The figures show that the optimal replace threshold, i.e., ℓ^*, follows the same pattern for all the three different values of $\underline{\ell}$, and it only changes where the values for the maximum available capacity, i.e., ℓ, reaches $\underline{\ell}$. This shows an interesting property of the model that where $\ell \geq \underline{\ell}$, the values for ℓ^* is the same for all levels of $\underline{\ell}$, which means we can get an understanding of the pattern of ℓ^* for lower levels of $\underline{\ell}$ by running the model for higher values of $\underline{\ell}$. The figures also show that for a given day t, when there is a higher potential for the output of the PV system in the future (higher values of possible set of peak sunlight hours, $X(t)$), the values of ℓ^* are higher than the scenarios with smaller values of $X(t)$ in the future. This is reflected in the results shown in Figure 2.3a as for $\underline{\ell} = 30\%$, the values for ℓ^* never go below 55% regardless of the value of $\underline{\ell}$.

2.4.2 Current Practices and Policies

Currently, there are a number of common practices that are used while charging/discharging the batteries. One of the most common practices while utilizing battery storage integrated PV systems is to charge the battery package as much as possible, regardless of the demand, or degradation level of the battery package, and discharge it until the demand is met or the battery is empty, while replacing it only when the replacement threshold $\underline{\ell}$ is met [9]. We



(a) Optimal policy for three different levels of $\underline{\ell}$under the assumptions of Case 1.

(b) Optimal policy for three different levels of $\underline{\ell}$ under the assumptions of Case 2.

Figure 2.3: Example optimal policy for two different cases shown in Table 2.2, with maximum available capacity replacement threshold, i.e., $\underline{\ell}$, ranging between 30% and 75%. The red dashed line shows the day from which possible set of peak sunlight hours at day t, $X(t)$, changes.

Table 2.3: Mean, maximum, minimum, and standard deviation for the results from the comparison between the optimal policy from the model versus the benchmark, i.e., charge as much as possible and discharge until the demand is met or the battery is empty, and replace when maximum available capacity is equal to $\underline{\ell}$, for to two cases presented in Table 2.2.

Cases	Mean	Max	Variance
Case 1	16.38%	27.54%	4.94%
Case 2	46.25%	59.78%	9.24%

compare the outputs from the proposed model in this study with this common benchmark policy over 2 months for Cases 1 and 2 shown in Table 2.2, for a $\underline{\ell} = 75\%$. We set two available charge/discharge levels for day-time and night-time, i.e., 50% and 100% of the remaining charge available h for our model. The price for each kWh of electricity from the grid is multiplied by 100 and set equal to \$10.3, and the price for a battery package is set equal to 10% of the actual battery cost, i.e. \$620 with a capacity of 13.5 kWh, and a night-time demand equal to 15 kWh. Table 2.3 shows the values for mean, maximum, minimum, and standard deviation of the differences in the results while comparing the results from our model with the results from the benchmark policy.

As the results from Table 2.3 show, the optimal policy from the proposed model can reduce the electricity cost compared to when we follow the benchmark. We can see that under the assumptions for Case 1, the value of the mean difference in the value of objective

function is smaller than that of Case 2. This is due to the fact that, one of the main differences between the proposed model and the benchmark is to find the most profitable replacement threshold under the optimal policy while in benchmark, we only replace when we reach the maximum available capacity replacement threshold, $\underline{\ell}$. Under the assumptions of Case 2, the days with high levels of possible set of peak sunlight hours at day t, $X(t)$, take place earlier in the time horizon. Note that from the results shown in Figures 2.3a and 2.3b, the replace threshold is higher during the days with high levels of $X(t)$ compared to the days with lower levels of it. Since we are calculating the value of the total expected discounted cost, the earlier a profit is made, the more valuable it is. As a result, due to the selection of higher optimal replace threshold in early stages in order to maximize the income from the utilization of the battery, the difference between the outcomes from the implementation of the model versus the benchmark policy for Case 2 is higher compared to that of Case 1.

2.4.3 Solution Approach

In this section, we describe the exact and approximate solution approaches developed in the study to solve the proposed model.

Exact Approach

In order to solve the problem, we first implement backward induction method. To reduce the solution time, we exploit the mathematical properties of the model that we have either observed from the results or mathematically proved in Section 2.3. We incorporate the threshold type policy property of our model in the solution method through conducting the following steps. First, we use a heuristic approach to calculate the replace threshold for each day, i.e., ℓ_t^*. If we are not in the last two time steps, and if the next two days have the same number of expected peak sunlight hours, we set the initial value of ℓ_t^* equal to ℓ_{t+1}^*, otherwise we set $\ell_t^* = \underline{\ell}$. Next, we examine this initial value to find the actual value for ℓ_t^* . That is, we set $\ell = \ell_t^*$ and calculate the discounted cost to go from day t given ℓ for the smallest level of remaining charge possible in the battery, i.e., $h = 0\%$, and the fully charged battery, i.e., i.e., $h = 100\%$. This results in three scenarios, i.e., *Scenario 1* where for $h = 0\%$ the

optimal policy is to keep, *Scenario 2* where for $h = 100\%$ the optimal policy is to replace, and *Scenario 3* where for $h = 0\%$, and for $h = 100\%$, the optimal policies are to replace and keep, respectively. According to Corollary 2 of Section 2.3, for *Scenario 1*, the optimal policy is keep for all levels of h, whereas for *Scenario 2*, the optimal policy is to replace for all levels of h. Note that under *Scenario 3*, we need to calculate the value of $V_t(\ell, h, 1)\ \forall h \in [0\%, 100\%]$. Next, we use properties of Theorem 1 of Section 2.3 to reduce the required computation. That is, for *Scenario 1*, we set $V_t(\ell, h, 1) = K_t(\ell, h)\ \forall \ell \geq \ell_t^*,\ h \in [0\%, 100\%]$, and for *Scenario 2*, we set $V_t(\ell, h, 1) = R_t(\ell)\ \forall \ell \leq \ell_t^*,\ h \in [0\%, 100\%]$. Note that for *Scenario 3*, we cannot exploit the properties of Theorem 1. The next step is to determine the search direction. For *Scenario 1* (*Scenario 2*), we reduce (increase) ℓ_t^* by 1 unit and re-evaluate the Scenarios for each step until we observe *Scenario 2* (*Scenario 1*), utilize the properties of Theorem 1, set $t = t - 1$, and redo the previous steps until we reach $t = 0$. Note that under *Scenario 3*, we need to move in both directions (increasing and decreasing) for ℓ^* until we observe other scenarios.

Incorporating the mentioned structural properties and heuristics allows us to drastically reduce the computational intensity and the solution time for the problem. However, this approach requires a considerable amount of time to solve for long planning horizons and we need to recalculate everything if the value of $\underline{\ell}$ is changed. Hence, we develop approximate solution approaches to tackle the mentioned problems.

Approximate Approach

In order to provide an approximate solution approach for the proposed problem, we utilize RL and NN through the implementation of DQNs. We develop a DQN algorithm to provide approximate optimal policies for our model for any point in the state space considering any levels of $\underline{\ell}$. First, we develop a DQN algorithm, and then we propose an extension to DQN algorithm which aims to improve to the accuracy of the DQN while reducing the computation time.

Deep Q-Network (DQN): This algorithm approximates the value of the objective function by learning from random observations from the state space and training a NN model on the outcomes.

Algorithm 1 Deep Q-Nework (DQN) algorithm developed in this study, based on the DQN algorithm introduced by [149].

initialize the replay memory D
initialize action-value function Q with random weight ζ
initialize target action-value function $\hat{Q}$ with weights $\zeta = \zeta^{-}$
set $K = 2T$
for *episode* $= 1$ to M **do**
  initialize sequence $s_1 = \{x_1\}$
  for $k = 1$ to K **do**
    following ϵ-greedy policy, select $a_k = \begin{cases} \text{a random action a}, & \text{with probability } \epsilon \\ \arg\max_a Q(s_k, a; \theta), & \text{otherwise} \end{cases}$
    execute action a_k in emulator and observe reward r_k and next stage x_{k+1}
    set $s_{k+1} = s_k,\ a_t^e,\ x_{k+1}$
    store transition (s_k, a_k, r_k, s_{k+1}) in D
    sample random minibatch of transitions (s_j, a_j, r_j, s_{j+1}) from D
    set $a_k = \begin{cases} r_j, & \text{if episode terminates at step } j+1, \\ r_j + \lambda \cdot \max_{a'} \hat{Q}(\phi_{j+1}, a'; \zeta^{-}), & \text{otherwise} \end{cases}$
    perform a gradient decent on $(y_j - Q(s_j, a_j; \zeta))^2$ w.r.t. the network parameter ζ
    in every C steps, reset $\hat{Q} = Q$, i.e., set $\zeta^{-} = \zeta$
  end for
end for

Augmented DQN (ADQN): In this algorithm, we aim to improve the developed DQN algorithm for this study through utilization of the exact approach. The main idea behind this approach is to gradually train the NN component of DQN over the episodes through the implementation of the exact solution. In this method we replace the target action-value function $\hat{Q}$ by a table containing the results from the exact solutions. That is, we generate V^* values using a higher maximum available capacity replacement threshold, $\underline{\ell}$. This process will reduce the overall training time for DQN as we only need to train one NN model while it helps improving the accuracy of the generated results from DQN. Algorithm 2 shows the pseudo-code for the ADQN algorithm.

Stochastic Augmented DQN (SADQN): This method uses the same concept as ADQN while exploiting different levels of maximum available capacity replacement threshold, i.e., $\underline{\ell}$. This results in a better ability of the resulting algorithm to capture the underlying trend in the results from the exact solution, V^* in order to improve the adaptability of the DQN in estimating the Q values for different levels of $\underline{\ell}$. This method provides us with all the benefits from the ADQN, while enhancing the prediction power of the DQN during estimating the

Algorithm 2 Augmented Deep Q-Network (ADQN) algorithm developed in this study. This algorithm exploits the results from the exact solution method in order to improve the prediction capability of DQN and reduce the training time.

initialize the replay memory D
initialize action-value function Q with random weight ζ
initialize true value matrix $\hat{Q}$
for $t = 1$ to T **do**
  for ϕ in $\{0, 1\}$ **do**
    for ℓ in $[\underline{\ell}, 1]$ **do**
      for h in $[0, 1]$ **do**
        set $\hat{Q}(t, \ell, h, \phi) = V_t^*(\ell, h, \phi)$ using Equations (2.1)-(2.7)
      end for
    end for
  end for
end for
set $K = 2T$
for *episode* $= 1$ to M **do**
  initialize sequence $s_1 = \{x_1\}$
  for $k = 1$ to K **do**
    following ϵ-greedy policy, select $a_k = \begin{cases} \text{a random action a}, & \text{with probability } \epsilon \\ \arg\max_a Q(s_k, a; \theta), & \text{otherwise} \end{cases}$
    execute action a_k in emulator and observe reward r_k and next stage x_{k+1}
    set $s_{k+1} = s_k,\ a_t^e,\ x_{k+1}$
    store transition (s_k, a_k, r_k, s_{k+1}) in D
    sample random minibatch of transitions (s_j, a_j, r_j, s_{j+1}) from D
    set $a_k = \begin{cases} r_j, & \text{if episode terminates at step } j+1, \\ r_j + \lambda \cdot \hat{Q}(\phi_{j+1}), & \text{otherwise} \end{cases}$
    perform a gradient decent on $(y_j - Q(s_j, a_j))^2$ w.r.t. the network parameter ζ
  end for
end for

Table 2.4: Eight different case studies designed to evaluate the performance of the developed approximate algorithms, where $X(t)$ denotes the possible set of peak sunlight hours at day t.

Cases	Days	$X(t)$	Days	$X(t)$	Cases	Days	$X(t)$	Days	$X(t)$
Case 1	15	2	15	4	Case 5	7	2	23	4
Case 2	15	4	15	2	Case 6	7	4	23	2
Case 3	15	2	15	2	Case 7	23	2	7	4
Case 4	15	4	15	4	Case 8	23	4	7	2

results for thresholds that have not been used in the training process of the model. Algorithm 3 shows the pseudo-code for the SADQN algorithm.

2.4.4 Computational Analyses

In this section, we evaluate the accuracy of the algorithms developed in Section 2.4.3 and compare the results with the exact solution method developed in Section 2.4.3. We solve the model for 8 different settings for peak sunlight hours using DQN, ADQN, and SADQN, report the average Mean Absolute Percentage Error (MAPE), preparation time (Prep time) which is the time spent to generate the result using the exact solution model for ADQN and SADQN, and the time spent on the training of the DRL model (Train time). We run each algorithm for 10,000 episode (iterations), with 100 times the actual electricity cost, and 10% of the actual price of the battery. Table 2.5 shows MAPE, Prep time and Train time for the three developed algorithms under 8 different cases, shown in Table 2.4.

Note that we train DQN for $\underline{\ell} = 75\%$, while we use higher $\underline{\ell}$ values for ADQN and SADQN. That is, we set $\underline{\ell} = 95\%$ for ADQN, and $\underline{\ell} \in \{97\%, 98\%, 99\%\}$ for SADQN.

The results from Table 2.5 show that for 10,000 episodes, the overall training time for ADQN and SADQN are considerably lower than DQN, with an average of 233.64 minutes (57% reduction) for ADQN and 222.28 minutes (54% reduction) for SADQN compared to DQN. The highest reduction in total preparation and training time is for Case 8 with 288.7 minutes reduction in the total solution time for ADQN compared to DQN, i.e., 69.5% reduction in solution time. The values for the average MAPE show that while ADQN generally has more error compared to DQN for 10,000 episodes, SADQN often manages to decrease average MAPE compared to DQN. That is, the differences of the average MAPE for

Algorithm 3 Stochastic Augmented Deep Q-Nework (SADQN) algorithm developed in this study. In this algorithm, we use the results from the exact solution method for multiple different $\underline{\ell}$ values in order to improve the prediction capability of DQN for different levels of $\underline{\ell}$ while reducing the training time.

initialize the replay memory D
initialize action-value function Q with random weight ζ
initialize true value matrix $\hat{Q}$
for all $\underline{\ell}$ in L **do**
  for $t = 1$ to T **do**
    for ϕ in $\{0, 1\}$ **do**
      for ℓ in $[\underline{\ell}, 1]$ **do**
        for h in $[0, 1]$ **do**
          set $\hat{Q}(t, \ell, h, \phi) = V_t^*(\ell, h, \phi)$ using Equations (2.1)-(2.7)
        end for
      end for
    end for
  end for
  set $K = 2T$
  for *episode* $= 1$ to M **do**
    choose a random $\underline{\ell} \in L$
    initialize sequence $s_1 = \{x_1\}$
    for $k = 1$ to K **do**
      following ϵ-greedy policy, select $a_k = \begin{cases} \text{a random action a}, & \text{with probability } \epsilon \\ \arg\max_a Q(s_k, a; \theta), & \text{otherwise} \end{cases}$
      execute action a_k in emulator and observe reward r_k and next stage x_{k+1}
      set $s_{k+1} = s_k, a_t^e, x_{k+1}$
      store transition (s_k, a_k, r_k, s_{k+1}) in D
      sample random minibatch of transitions (s_j, a_j, r_j, s_{j+1}) from D
      set $a_k = \begin{cases} r_j, & \text{if episode terminates at step } j+1, \\ r_j + \lambda \cdot \hat{Q}(\phi_{j+1}), & \text{otherwise} \end{cases}$
      perform a gradient decent on $(y_j - Q(s_j, a_j))^2$ w.r.t. the network parameter ζ
    end for
  end for
end for

Table 2.5: Average Mean Absolute Percentage Error (MAPE), preparation time and train time for DQN, ADQN, and SADQN for 10,000 episodes (iterations) over a time span of 30 days, i.e., $T_{Max} = 30$. Average MAPE shows the average value of MAPE from the results of following the optimal policies under each DRL algorithm compared to the exact solution method over the time horizon. Prep time is the time to generate the data using the exact solution method for each algorithm, which is equal to 0 for DQN as we do not generate any data for DQN before starting the algorithm. The Train time denotes the time in minutes that is spent on training the DRL algorithm.

	Case 1			Case 2			Case 3			Case 4		
Algorithm	DQN	ADQN	SADQN	DQN	ADQN	SADQN	DQN	ADQN	SADQN	DQN	ADQN	SADQN
Average MAPE (%)	14.67%	15.17%	8.08%	1.17%	7.16%	1.26%	7.20%	22.00%	0.02%	37.80%	86.40%	20.14%
Prep time (minutes)	0.0	13.5	16.4	0.0	13.6	16.3	0.0	12.3	15.8	0.0	12.5	16.8
Train time (minutes)	442.1	198.1	170.9	440.2	197.2	170.8	372.3	194.0	193.4	370.6	195.2	151.7
	Case 5			Case 6			Case 7			Case 8		
Algorithm	DQN	ADQN	SADQN	DQN	ADQN	SADQN	DQN	ADQN	SADQN	DQN	ADQN	SADQN
Average MAPE (%)	28.45%	25.82%	9.71%	0.04%	25.34%	0.04%	6.95%	14.81%	3.74%	8.97%	19.05%	9.58%
Prep time (minutes)	0.0	11.3	13.5	0.0	11.3	13.4	0.0	9.4	20.8	0.0	9.3	20.5
Train time (minutes)	416.4	153.3	161.4	416.7	154.0	166.0	415.3	117.4	181.5	415.6	117.6	181.9

ADQN compared to DQN ranges between [-2.63%,48.60%], while for SADQN compared to DQN, they range between [-18.74%,0.08%]. Note that the accuracy of the models can change by increasing the training time, i.e., increasing the number of episodes. We conduct a paired T-test on MAPE and solution times for DQN and ADQN as well as DQN and SADQN to check whether or not the differences in the observed values are statistically significant. The results show that while the differences are statistically significant for all tests for solution time, the differences in MAPE values for some cases are not statistically significant. That is, for ADQN and DQN the differences for MAPE for Cases 1 and 5 have P-values equal to 0.86 and 0.49, and for SADQN and DQN, the P-values for Cases 2, 6, and 8 are equal to 0.88, 0.99, and 0.82, respectively.

2.5 Conclusion and Remarks

In this study we develop a MDP model in order to maximize the profitably of a battery package integrated PV system. In our model, we consider the degradation of the battery due to cycles and aging and find the optimal replacement threshold under which the income from the system is maximized. We study the mathematical properties of the model, and incorporate them in the exact solution method in order to reduce the computational intensity as well as solution time. Moreover, due to the large state space of the problem, we develop

different approximate methods through the implementation of DRL, and evaluate their accuracy and solution time.

Chapter 3

An Agent Based Approach to Study the Diffusion Rate and the Effect of Policies on Joint Placement of Photovoltaic Panels and Green Roof under Climate Change Uncertainty

3.1 Introduction

The utilization of renewable energy (RE) sources and implementation of energy efficient (EE) practices have been a key factor in developing more sustainable economies and societies, reducing the pollution, and mitigating the inverse effects of climate change.

The adoption of new, cleaner technologies is still a major challenge to policymakers [11], proven to be a time-consuming task even with the technologies being commercially available [27]. Such issues led governments throughout the world to take different measures in order to increase the adoption rate of RE and EE practices, either through regulations or incentives. In the past few years, policymakers have passed several laws and regulations to foster the rate of implementation of REs and EE practices throughout the world. For example, the

French parliament have made the installation of green roofs (GR) and photovoltaic (PV) panels mandatory for all the new building in commercial zones across the country [101]. San Francisco's legislation require that between 15% to 30% of the rooftop of the new buildings on most new construction projects to be covered by PV panels, GRs, or a combination of both [88]. A similar law has passed by the City of Denver which requires all the buildings over 25,000 square feet to include GR, PV panels, or their combination [171]. And as of 2019, the most recent regulation (and most comprehensive) to make the installation of PV panels mandatory on every newly built home effective from 2020 [112] has passed in California.

While such regulations help the diffusion and adoption rate of REs and EE practices increase, they are considered to be slow or not comprehensive enough as many of them only effect commercial buildings and none of them effects currently existing buildings. Moreover, some claim that such regulations can negatively impact the competitiveness of a society [48]. This makes studying the diffusion rate of green technologies and the effect of promotional policies on their diffusion rate increasingly important. To that aim, in this section, we first provide some information on two of the most popular green technologies, i.e., PV panels for REs and GRs for EE practices. Then we emphasize on the role of the climate change on the outcomes of mentioned green technologies. Lastly, we provide a literature review on currently available diffusion models.

3.1.1 Photovoltaic Panels and Green Roofs

PV panels, considered as the fastest growing renewable energy [73], and GRs, i.e., rooftops covered with a vegetative layer, have gained increasing attention over the past few years as two of the most important green technologies toward development of sustainable societies [132].

PV panels harness solar radiation and turn it into electricity, through which affordable electricity can be generated in both utility and residential levels. Over the past few years, the installation rate of PV panels has been steadily increasing due to the decrease in their cost, increase in their output, and state and federal incentives [73]. There is an abundant body of literature which focuses on PV panels from different aspects (e.g., technological aspect such



Figure 3.1: A GR integrated PV system on a rooftop in a house in Seattle [62].

as underlying material or cell technology [215, 43, 119], best placement options of PV arrays [130, 230, 220, 161], and Optimal placement of PV systems [10, 167].

GRs can provide numerous benefits to the environment in which they are installed (namely, heat island mitigation, energy savings, and storm-water runoff reduction [23, 192, 51]). Different studies assessed achievable benefits through installation of GRs, discussing that savings of $7 to $10 billion can be obtained by widespread installation of GRs throughout the U.S. [61]. GRs have been thoroughly studied for their energy saving properties, proving that savings of up to 10% of the energy consumed for space conditioning can be achieved through installation of GRs [7, 22, 71, 70, 109, 136, 140, 187, 188, 190, 191, 196].

PV panels rely on the solar radiation to generate electricity, which adversely affects the output of PV panels due to increasing the surface temperature of the panels. The output efficiency of PV panels decreases by approximately 1% for every 2 increase in the surface temperature of the PV panels [231]. This issue can be mitigated through the integration of PV panels and GRs, as GRs reduce the temperature of their surrounding environment, hence reducing the surface temperature of the PV panels and increasing the output efficiency of them. Several empirical studies focused on integration of PV panels and GRs to evaluate

the level PV panels' output efficiency benefiting from GRs as a direct result of cooling effect of GRs on their surrounding environment [40].

3.1.2 Climate Change

The current increasing trend in the world temperature and climate change is widely believed to be a direct result of human activity [151]. Studies claim that at the current pace, by the end of the century the average global temperature will rise by up to 5.8 [30, 181]. This fact becomes more important when the output from PV panels and GRs are directly affected by the changes in temperature and the level of precipitation. That is, while various studies agree upon the fact that GRs reduce the level of energy consumption for the buildings underneath them in cooling degree hours, some studies claim that they lead to a higher level of energy consumption during heating degree hours [177]. Moreover, the output electricity of PV panels directly relies on the level of solar radiation to which they are exposed. This lead to the fact that higher level of precipitation, which can roughly be considered as more frequent rain, results in lower level of electricity output from the panels.

3.1.3 Agent Based Modeling and Diffusion Models

Studies about technology diffusion and the effects of policies, social interactions, and economic factors started from the pioneer papers of [103] and [185], and have been carried out for various new products [19, 32, 226] to the present [145]. In the literature, diffusion models are often studied via agent-based modeling (ABM), defined as a system of agents (autonomous elements) (agents). Agents can be defined as identifiable discrete goal oriented autonomous entities which hold a certain set of characteristics [139]. Agents are capable of interacting with other agents inside their environment, and making individual decisions based on their current state and the interactions considering a set of rules set by the environment in which they exist and interact with one another [132]. ABMs have been studied to a wide range of different problems such as social sciences [198], marketing [154] energy [41], and economics [29]. ABMs are well-designed to study systems formed up of individual decision makers to evaluate and forecast the outcomes of problems that rely on the interactions

between agents as well as their individual traits [14] namely the diffusion rate of green technologies. In the following, we present a number of recent studies in which diffusion models are studied and developed.

In [28], the authors propose the foundation and the steps taken to develop a diffusion model for adoption of PV systems. This diffusion model studies the agents and their social network by segregating them based on their zip codes, and also considers the delay between the social media effects on the agents and adoption stage (as developing renewable energies and new technologies is a time consuming procedure) and consider the total number of completed installations as their installed base of PV systems.

An ABM model is developed in [92] to study and calculate the diffusion rate of rooftop PV panels in Connecticut, while focusing on the effect of social media on the diffusion rate. The results from this study show that distance and visibility have the most significant effect on the rate of diffusion of rooftop PV panels, smaller centers contribute to adoption more than larger urban areas, and a strong relationship exists between the number of previously installed PV panels and adoption. Moreover, the results show that peer effect diminishes over time and space, and built environment variables, i.e., housing density, share of renter occupied dwellings, are more influential that household income or political affiliation.

In [148], the authors provide an ABM that evaluates the incorporation of consumer-adoption of distributed PV panels in utility companys expansion plan. The proposed ABM includes three sub models, i.e., Consumer Agent Attitude Assessment, Consumer Agent Financial Assessment, and Consumer Agent Decision, and is designed to help utility companies to identify the trade-offs of various policies to achieve their goals.

In [179] an ABM is proposed to study the behavior of households regarding the installation of water conservation technologies, and conducted a case study for the city of Miami Beach. The results from the ABM show the effects of different factors on the adoption of water conservation technologies.

An empirical geographic information system (GIS) integrated with ABM for adoption of PV panels is proposed in [184]. In this study, authors aim to identify the most critical features to a more precise prediction of the temporal, spatial and demographic patterns for PV panels adoption. Their results show that considering financial aspects of PV panel

adoption results to a good prediction of adoption, agent behavior and agent-level attitude and their interaction are of great importance to predict spatial and demographic patterns of adoption. They develop four different ABMs for the adoption of PV panels and then use these ABMs to simulate the adoption of PV panels in the city of Austin, Texas.

The authors in [174] present an empirically driven agent based model with an approach to utilize empirical data into initialization of agent states for technology adoption with an application on residential PV panels. The focus of their paper is mostly on design, setup, initialization, and validation. They apply their framework to real-world data between 2004-2013 for a residential solar program. Moreover, they develop an ABM of the adoption of residential PV systems in the City of Austin using the data sets from 2004 to 2013.

In [163], the authors study the effect of peer effects in residential PV diffusion through surveying among Swedish PV adopters. Their results show that the peer effect plays an important role; those effected by peer effect, however, already considered to adopt PV panels, and the peer effect mainly plays a role in confirming the fact that PV panels yield the results adopters seek. Their results also show that peer effect mainly effects people through their social relationships, and not between the neighbors that did not had a social relationship with one another. Moreover, their results show that passive peer effect are less important compared to active effects when it comes to adopting PV panels.

Authors, in [2], design an ABM towards capturing the adoption of integrated PV module and battery systems for the city of Ontario, Canada. They run surveys to study the responsiveness of residents to potential energy policies, and incorporate the results as different parameters and factors in the ABM. The results show that the implementation of integrated PV panels and battery systems are incremental rather than exponential in the city of Ontario, and the best policy to encourage the households to develop PV systems is to reduce the implementation cost.

In [89], the authors conducted a series of experiments through which they examined the novel approaches to reduce the soft cost of PV panels installation. They aim to elevate the installation of residential PV panels by two main strategies, i.e., intensive marketing through local social networks, and time-limited discounts and group pricings. They report that in the 3 years of duration of the activity of the Solarize project, the number of household

which adopted PV panels increased from 800 to 12,500, 20 percent of which are as a direct result of their project. The results show that PV installation has a contagious nature and social connections play as the most powerful levers in fostering diffusion of the technology. Moreover, the visibility of PV panels from the street positively affect the peer influence.

In [60], authors deploy different methods to forecast residual PV panel installation in California via different methods, i.e., time-series forecasting model, threshold heterogeneity diffusion model, bass diffusion model, dSolar (National Renewable Energy Laboratorys model). They study the effect of the recent policies such as federal investment tax credit and California net energy metering policy. Their results show that these policies have the potential to increase the annual PV installation by 12%-18%.

In [239], authors present a data-driven ABM framework to forecast individual and aggregate residential rooftop PV panel adoption in San Diego county, California, and then study two different policies to foster PV panel adoption, and optimize their implementation.

In [186], authors present a model for diffusion of innovation which describes the way through which a social system works in popularizing an innovation over time.

Later, [34] utilize the diffusion model proposed by [186] to analyze the peer effect and personality trait link. In this paper, authors investigate the effect of a geographical concentration of a trait of personality on peer effect for PV panel adoption in the UK, across 2600 postcodes, using a first-difference fixed effect regression model. They conclude that peer effect has a stronger role in districts with spatial concentrations of Openness to Experience and Conscientiousness.

In [243], the authors develop a decision support tool to evaluate the effectiveness of different policies (i.e., incentives and regulations) on the growth rate of PV systems while aiming to avoid the instability of transition system or steep rising of the electricity price. The ABM is a hybrid two-level framework, with the lower-level model calculating the PV system payback for each individual household, and the higher-level model considers a broader time-step and studies the household adoption behaviors. This study considers Investment Tax Credit (ITC) and Feed in Tariffs (FiT). Low-level model calculates the income from the on a weekly basis, and then the data is fed into the high-level model where the payback period,

and the desire to install PV systems are calculated based on the output from the low-level model.

In [242], authors study the integration of Plug-in Hybrid Electric Vehicles (PHEV) and PV generation and storage system. They develop an ABM do analyze the demand response programs with high penetration of PHEV and PVs from residential and utility company perspectives.

The mentioned diffusion models are generally studied based on two main aspects, i.e., attitudinal and financial aspects. For the attitudinal aspect, studies often rely on available historical data of adoption rates for the green technologies in the region for which they have conducted the study. The financial aspect of the aforementioned studies, however, has been taken into account differently throughout different studies. That is, while studies consider the diffusion rate of these green technologies based on the behavior of the agents in the system as well as accounting for the financial returns from developing such technologies, the integration of these two approaches are different and are in a direct form. That is, these studies mainly include both behavioral and financial aspects studies these two different aspects simultaneously [28] (mainly in forms of a constraint which is added to the behavioral model), whereas some models include two parallel models where one studies the behavioral aspect, and the other focuses on the financial output of the green technologies [174]. While both approaches account for the financial aspect of the studies, the parallel incorporation of two different models provides more opportunities to study each aspect in a more detailed and comprehensive fashion.

In this study, we aim to develop an agent-based framework which integrates two parallel models, i.e., behavioral and financial, for the city of Knoxville, Tennessee. As mentioned before, the behavioral models mainly rely on historical data for adopters over the region of the study. According to [90],there are approximately 78 installed PV systems over the city of Knoxville, including systems installed by the University of Knoxville for solar studies. Moreover, according to [90], 83% of buildings in city of Knoxville (from approximately 200,000 buildings [121]) are solar viable (they receive a minimum of 75% of maximum solar radiation for the county). These numbers show that there is a great potential for PV development throughout the city of Knoxville. Due to limited number of installed PV

systems and lack of historical data, it is not possible to develop a behavioral model based on historical behavior and diffusion of PV systems (a similar study over the city of Knoxville for personal hybrid electrical vehicles (PHEVs) resorted to synthetic data generation due to this problem [55]). Hence, we aim to develop a model while borrowing the behavioral aspect of our model from currently existing literature.

While all the aforementioned studies have incorporated the profit gained by green technologies or their costs in some fashion, none of them accounts for the uncertainty due to nature of the input parameters, namely, climate change and its effects on the performance and output of these technologies. We aim to develop an optimization model in order to study the changes in the adoption rate of PV panels and/or GRs as a result of promotional policies while incorporating different climate scenarios (in which climate change has been accounted for) to calculate the potentially achievable income from installation of green infrastructures throughout their lifespan. In order to do so, we develop a stochastic mathematical optimization model to find the best setup through which candidate sites can maximize their income from installation of the green technologies (i.e., PV, GR, GR integrated PV, or nothing). In Section 3.2, we thoroughly describe the models that we developed to cover the financial aspect of our diffusion model. Moreover, we provide a description over different behavioral models and the model that we borrow from the existing literature, and finally, we develop an agent-based framework entailing the mathematical and diffusion model to study the effect of promotional policies on the adoption rate of the green technologies.

3.2 Methods

In this section, we introduce the structure of our ABM framework as well as its underlying components. We aim to develop two separate models, i.e., financial and attitudinal, in which we account for both financial and behavioral aspects of the model. In the following, we first introduce the mathematical model developed to calculate the potential outcome from installation of green technologies in Section 3.2.1. Then, in Section 3.2.2 we introduce

the attitudinal model that we borrow from the existing literature. Finally, we discuss the structure of the ABM framework.

3.2.1 Financial Model

In the introduction, we introduced a number of studies which contain models to calculate the payback and financial profitability of green technologies. However, they do not assume any uncertainty in the outcome of the green technologies as a result of uncertain nature of such technologies. For example, [174] assume the level of generated electricity through installation of PV Panels is given for each agent and those model do not account for any sort of uncertainty (e.g., climate change), consider the availability of different packages for each agent, multiple green technologies (PV panels, GR, and GR integrated PV panels), nor changes in the cost efficiency of the PV systems. In order to tackle these shortcomings, we develop a mathematical model in which we incorporate the climate change uncertainty as well as the other mentioned factors into our calculations through the implementation of stochastic programming.

Stochastic programming is well-established in the literature for mathematical modeling while dealing with stochasticity which provides the ability to contain the uncertain nature of parameters through consideration of the probability for different future events [25]. Stochastic programming has been widely applied in a wide array of different problems including but not limited to renewable energies [177], transportation and logistics [18], supply chain management and network design [193], resource allocation problems [134], and unit commitment problem [209].

We develop a mathematical model, through which we calculate the direct potential income from installation of PV panels and/or GRs for a single building, while accounting for climate change and interaction between PV panels and GRs. In this model, we account for shading, solar irradiation, and aspect of the building through calculation of potential level of total electricity output through installation of different packages. We aim to find the optimal settings for which the profit gained by the household from installation of PV panels and/or GRs is maximized. Therefore, we develop an integer programming model (binary programming) with a maximization objective function which aims to maximize the potential

Table 3.1: Model notation for financial sub-model.

Index	Description
Sets	
t	Indicator of day where $t \in T$ and T is the planning horizon
p	Green technology package, where $p \in P$
ω	Climate scenario, where $\omega \in \Omega$
Variables	
x_p	Binary variable, which equals to 1 if package p is installed
Parameters	
C_p	Installation and maintenance cost of package p (USD)
μ	Cost of 1 kWh of electricity (USD)
π_p	Potential income achieved through installation of package p (USD)
O_p^ω	Potential level of total electricity output through installation of package p (kWh)
S_p^ω	Potential level of total energy saving through installation of package p (kWh)
η^ω	Realization probability of climate scenario ω, where $\sum_\omega \eta_\omega = 1$
$I^{\omega t}$	Daily solar irradiation available during day t in climate scenario ω (kWh/m^2)
A_p	Total area of PV arrays for package p (m^2)
E_p^t	PV output efficiency for package p during day t (%)
α_p	Energy saving percentage from GR installation in cooling degree hours for package p (%)
β_p	Energy saving percentage from GR installation in heating degree hours for package p (%)
$\tau_c^{\omega t}$	Total number of cooling degree hours during day t in climate scenario ω (hours)
$\tau_h^{\omega t}$	Total number of heating degree hours during day t in climate scenario ω (hours)
U^t	Daily energy consumption for space conditioning for the building during day t (kWh)
H	Total area of the household (m^2)
λ	The performance ratio of the PV system, where $\lambda \in [0, 1]$

profit gained from the green technologies. We define a set of available green technologies which are a combination of PV panels and GRs that can be installed over a building, which are further described in Section 3.3. Table 3.1 presents the notations used in the income model.

The objective function of this model is to maximize the level of potential profit achievable through the installation of packages over a building, while accounting for different climate scenarios presented by $\omega \in \Omega$,

$$\max Z = \sum_{p \in P} (\pi_p - C_p) x_p, \tag{3.1}$$

subject to

$$\sum_{p \in P} x_p \leq 1, \tag{3.2}$$

$$\pi_p = \sum_{\omega \in \Omega} \eta^{\omega} [O_p^{\omega} + S_p^{\omega}] \mu, \qquad \forall p \in P, \tag{3.3}$$

$$x_p \in \{0, 1\}. \tag{3.4}$$

Eq. (3.2) makes sure that at most, only one package is assigned for installation over a building. Eq. (3.3) calculates the achievable income through energy generation and/or saving via installation of each package over all the probable climate scenarios. Eq. (3.4) imposes the binary restriction for variable x_p. In order to assess the achievable level of electricity generation for each package, Eq. (3.5) calculates the potential electricity generation for each package based on the level of solar irradiation available, the size of the package and its output efficiency under each climate scenario,

$$O_p^{\omega} = \sum_{t \in T} I^{\omega t} A_P E_p^t \lambda \qquad \forall p \in P, \omega \in \Omega. \tag{3.5}$$

The level of energy saving achieved by installation of each package due to GR energy reduction properties is calculated by Eq. (3.6),

$$S_p^{\omega} = \sum_{t \in T} (\alpha_p \tau_h^{\omega t} + \beta_p \tau_c^{\omega t}) U^t, \qquad \forall p \in P, \omega \in \Omega. \tag{3.6}$$

Note that different levels of energy saving is considered during heating and cooling degree hours, which are described thoroughly in Section 3.3.

3.2.2 Attitudinal Model

Studies show that while the economical aspect of a model plays a vital role in maintaining the diffusion rate of green technologies, the behavioral aspect of adopters also has a significant impact on the adoption rate of these technologies. In this section, we introduce the behavioral model which is developed based on the models in the existing literature. In order to incorporate behavioral aspect of the agents in our model, due to limitations mentioned in Section 3.1, we opt to adopt the behavioral model from studies that have similar structure

as the framework developed in this study, i.e., attitudinal models which seek to define the underlying structure of an agents' behavior toward the adoption of new technologies based on their characteristics such as demographics, profitability of the technology, social status, and interactions with other agents.

The changes in agents behaviors and its magnitude as a result of interactions between the agents in a system is mainly studied through the implementation of a set of rules and regulations, either developed based on the subject of the study or through the adoption of theories developed from different fields of study [139]. Such theories mainly have their roots in psychology and social sciences, such as the Theory of Planned Behavior [3], Diffusion of Innovation [186], Tit for Tat [15], and Relative Agreement [57]. Nevertheless, there exists a number models that are developed based on other fields of science, namely the Ising model which has emerged from the field of physics [46].

In this study, the main structure of the attitudinal model is based on the Theory of Diffusion of Innovation (TDI) by [186]. This theory emphasizes that the diffusion of a technology while considerably relies on the technology itself, the communication channels, time and social system play a vital role in the diffusion rate as well. While studying the adoption of new technologies, TDI divides agents into three major groups, i.e., non-adopters, potential-adopters, and adopters [129]. The main difference between non-adopters and potential-adopters roots in the fact that potential-adopters are agents who consider adopting green technologies, and are mainly restrained by financial outcome of the technology. Non-adopters, on the other hand, do not consider adoption of green technologies even if they are financially profitable. In order to assess the overall behavior of each agent towards adoption of green technologies, we evaluated three different models by, [179], [128], and [243]. The model defined [179] was mainly designed to study the adoption of new water saving technology, and considered variables such as garden and pool size, which are not key factors while studying technologies such as PV systems. [128] developed a behavioral model mainly to evaluate the output of PV systems, and set a significant focus on the level of solar irradiation received by the household, which makes the model unfit for studying technologies such as green roofs which do not necessarily benefit from such factors. In this study, we focus on the model developed by [243] in which, they use a linear regression model to calculate the probability

of a household adopting solar panels, denoted by ρ in this study. The independent variables in the linear regression include the potential income of the technologies through calculation of the payback period for them, the characteristics of the household through inclusion of the number of residents and the income of the household. Moreover, they incorporate for the visibility of the green technologies through the inclusion of the total number of advertisement received by the residents of the household. The linear regression developed by [243] returns a value of 0 to 1 indicating how likely an agent is to adopt green technologies. This is ideal for our purpose of study as not only this regression model accounts for different aspects of green technologies, but it generates the resulting value in a scale which is easy to interpret while calculating the values for opinion and uncertainty. Note that by considering the profitability of the green technologies through calculating the payback period, this model can evaluate green technologies such as green roofs and PV systems, hence, making it a suitable fit for our scope of study.

3.2.3 ABM Framework

In this section, we discuss the ABM framework which is used to study the adoption rate of the green technologies. Three different agent types are considered in this study, i.e., candidate sites, green technology packages, and zip codes. Each candidate site is assigned to a zip code based on their coordinates, by which a number of candidate sites characteristics are calculated such as property value, average age of the residents, income level, and the total number of installed packages in the agents' zip code. The parameters of the model are set by the environment, and are updated by the model as the time passes or new regulations are introduced into the model. For each agent, the potential profit from implementation of the available green technologies over the next 20 years is calculated using the model presented in Section 3.2.1 for each time-step. Based on the behavioral model in Section 3.2.2, for each agent to adopt a green technology, two main criteria must be met. That is, the green technology should be profitable (including the incentives and tax-cuts), and the opinion of the agent should surpass a certain global threshold (ϕ_{global}). Note that each agent has access to a number of different green technologies, and the optimization model in Section 3.2.1 chooses the package with the highest financial profit for the agent. The attitudinal

Table 3.2: Common social networks utilized in the literature for ABM [126].

Social network	Description
Fully Connected	Homogeneous network in which each agent is connected to all other agents in the network.
Random	Agents are randomly connected to other agents in the network based on a given probability, independent of other agents in the network.
Regular Lattice	Agents are connected to other agents in the network only based on a distance threshold.
Ring Lattice	Distance based connection of the agents within a given distance threshold, forming a ring.
Small World	A Ring Lattice network which also includes a number of long-distance connections. This includes strongly clustered isolated networks that are also connected with other isolated networks based on a given probability.
Scale Free	The majority of the agents have a small number of connections while some agents have a large number of connections (hubs).

sub-model also takes the characteristics of the agent into consideration through calculation of ρ. The attitude of the agents change over time, as well as their demographics. While the demographics change mainly as a result of time progression, the attitude is changed due to interactions that agents have through their network with one another. While some of the changes in demographics over time are easy to calculate, a group of them cannot be tracked without certain assumptions. For example, the average age of the residents in the household cannot be predicted without making the assumption that the resident in the households do not change over time. Hence, consistent with the existing literature [179, 174] we make the assumption that the demographic of the agents remain unchanged over the time of the study, as well as the assumption that when an agent install a green technology, they do not make any decisions over new installations.

Social network structures are mainly used to define the pattern under which agents interact with one another mainly to calculate the changes in the attitudes of the agents over time. In Table 3.2, we provide a number of common network algorithms currently being utilized in the literature.

Algorithm 4 Pseudo-code Small World network algorithm used to connect the agents in the ABM framework.

```
Set the set of agents N
Set the rewiring probability P_sw
Set the node degree K_sw where N ≫ K_sw ≫ logN ≫ 1
for all i ∈ N do
  Connect to the nearest K_sw nodes
end for
for all i ∈ N do
  for all j ∈ (1, K_sw) do
    j_i ← agents connected nodes to j
    r ← Unif(0, 1)
    if r ≤ p then
      Select m ∈ N \ {j, j_i}
      rewire j to node m
    end if
  end for
end for
```

In order to simulate the interaction between agents, we use the Small World network proposed by [225]. The Small World network configuration contains locally clustered network where the average path lengths between nodes in the network are reduced using randomly rewired links. Algorithm 4 shows the pseudo-code for the Small World network algorithm. In this study, P_{sw} and K_{sw} denote the probability and number of connections in the Small World network, respectively.

Using the social network structure, the ABM framework simulates the interactions among agents and calculates attitude and income model for each agent while accounting for over time evolution of the variables in the environment of the simulation. Based on the Small World network, each agent interacts with a number of other agents in the network through their local and global networks. The local network is based on the physical distance of the agents from one another, where the threshold for distance or the number of connections is an input to the environment of the model. Through the interactions with other agents, the opinion of each agent changes. To calculate the level of changes in agents' behavior, we use RA algorithm developed by [57]. In RA, an agent randomly interacts with another agent in its network. Then each agent, based on their opinions and their uncertainty, updates its opinion based on the new information. Hence, each agent holds two characteristics,

opinion, ϕ_i, and uncertainty ζ_i, where opinion ranges between -1 and 1, and uncertainty ranges between 0 to 2 [146]. Hence, RA between two agents i and j is calculated as

$$\text{RA}_{ij} = \frac{h_{ij}}{\zeta_i} - 1, \tag{3.7}$$

where h_{ij} denotes the overlap between the two agents' bounds and is calculated as

$$h_{ij} = min(\phi_i + \zeta_i, \phi_j + \zeta_j) - max(\phi_i - \zeta_i, \phi_j - \zeta_j). \tag{3.8}$$

Then, for positive values of RA between two agents i and j agent's opinion and uncertainty will be updated as follows,

$$\phi_j := \phi_j + \xi \cdot [(\frac{h_{ij}}{\zeta_i}) - 1](\phi_i - \phi_j), \tag{3.9}$$

and

$$\zeta_j := \zeta_j + \xi \cdot [\frac{h_{ij}}{\zeta_i} - 1](\zeta_i - \zeta_j), \tag{3.10}$$

where ξ is a parameter defined by the environment of the ABM that is responsible for controlling the speed of population convergence. Note that in this way, agents with vastly different opinions are unlikely to effect one another. It is important to consider the fact that agents' opinions evolve over time based on the changes in their behaviors due to interactions with other agents, and hence, two agents with vastly different opinions have the possibility to effect one another as the time progresses and their opinions evolve. If an agents opinion surpasses a global threshold, i.e., ϕ_{global}, the agent turns into a potential adopter, and the installation of the green technologies takes place if only they are profitable.

In this study, we utilize result the Logistic regression model, ρ, of each agent to calculate their opinion, ϕ, and uncertainty, ζ. That is, we make the assumption that those who a value of $\rho = 1$ hold an extremely positive opinion towards green technologies, i.e., $\phi = 1$, while those with a ρ value of 0 are extremely negative towards the technologies, i.e., $\phi = -1$, and those with a value of $\rho = 0.5$ are neutral towards the green technologies, i.e., $\phi = 0$. Eq.

(3.11) shows the formulation used to calculate the opinion for each agent, i.e.,

$$\phi = 2(\rho - 0.5). \tag{3.11}$$

Studies show that those who hold a more extreme opinion towards a subject have lower levels of uncertainty [174]. In order to calculate the uncertainty for each agent, we use their opinion. That is, we assign the agents who have opinion values of 1 with an uncertainty of 0, while those with an opinion of 0 have uncertainties equal to 2, i.e.,

$$\zeta = 2(1 - |\phi|). \tag{3.12}$$

Figure 3.2 represents the structure of the ABM framework used in this study.

3.3 Model Calibration

In this section, we use the value reported in the literature, along with experts opinion and publicly available data sets as well as data sets provided by Oak Ridge National Lab (ORNL) [216, 35] in order to calibrate the model formulated in Section 3.2.1.

Planning horizon, T. In this paper, we study a planning horizons of 20 years since the currently commercially available PV systems generally have a life span of 20 to 30 years [106] while GRs last about 30-40 years [169, 147].

Green technology packages, P, installation and maintenance cost of package p, C_p, and total area of PV arrays for package p, A_p. The focus of this study is on residential PV systems and small commercial systems which their size generally ranges between 2kW - 10kW [106]. Hence, we define 5 different PV system sizes with 2 different output efficiency levels of 15% and 20%, and each PV system is offered with and without GRs while installing GRs only is also another available option. This results in 21 different packages which is offered to each agent, with their relative costs presented in Table 3.3. The cost for GRs is directly related to their size. That is, GRs approximately cost \$12.5 per m^2, while it costs \$7.5 per m^2 for GRs larger than 929 m^2 [96]. Hence, the cost of GR for each agent is calculated based on its rooftop size. [207] report that for PV systems with output efficiency values of 15% and

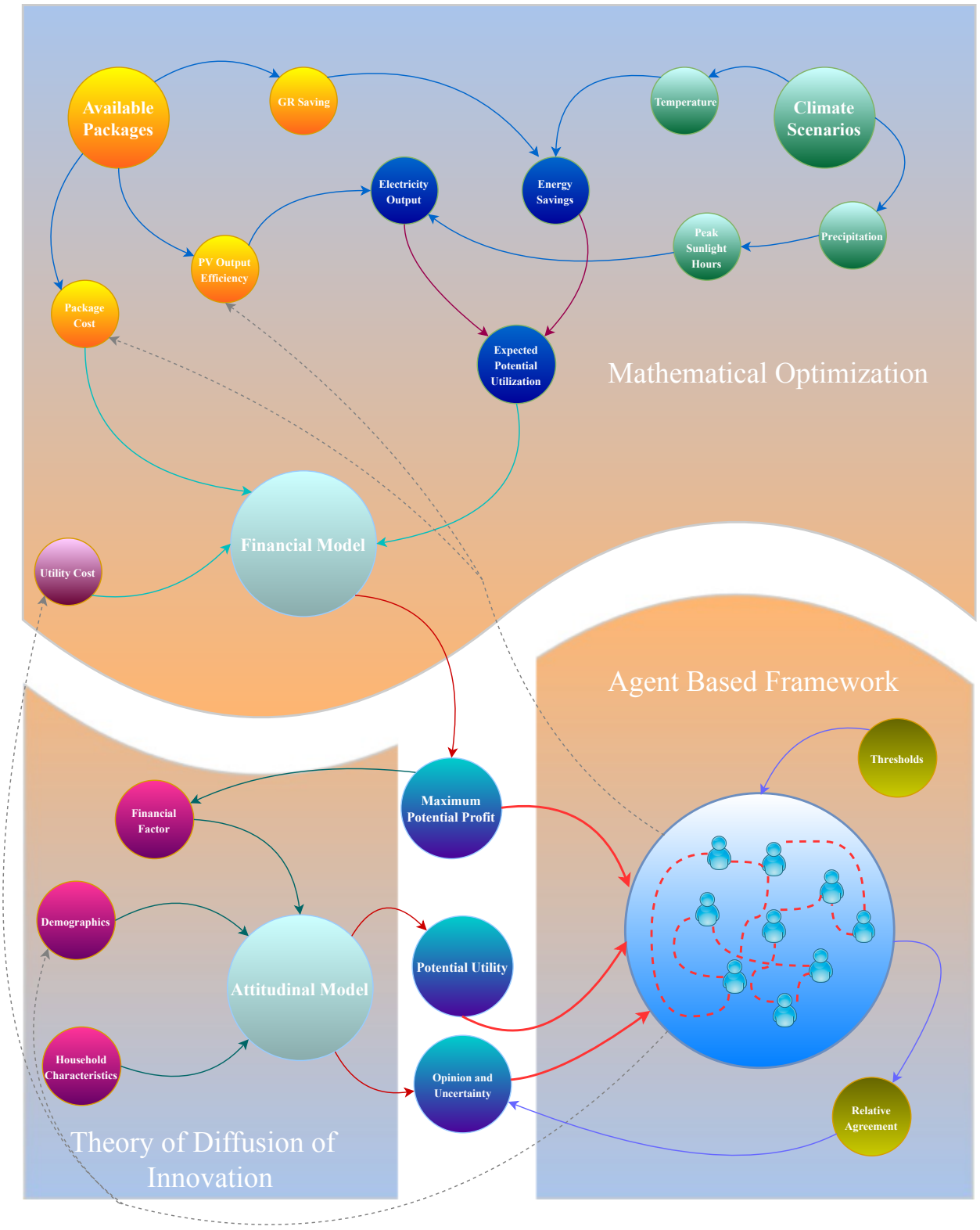


Figure 3.2: The structure of the proposed framework, including Attitudinal and Income model as well as Agent Based Model. The dashed lines indicate the feedback from interactions and time evolution of model variables which originate from the Agent Based Model and is fed to the models.

Table 3.3: The cost per PV system size in USD for southern U.S. for two different panel output efficiency [106].

PV system size (kW)	15% efficiency		20% efficiency	
	Cost (USD)	Area (m^2)	Cost (USD)	Area (m^2)
2	5900	12.39	6800	9.29
3	9000	18.58	10200	13.94
4	12000	24.77	13500	18.58
5	15000	30.97	17000	23.23
10	30000	61.94	34000	46.45

Table 3.4: Price of PV systems per Watts from 2014 to 2018 reported by [76].

Year	2014		2015		2016		2017		2018	
	H1	H2	H1	H2	H1	H2	H1	H2	H1	H2
Cost (USD/Watts)	-	3.86	3.79	3.69	3.57	3.36	3.17	3.13	3.12	3.05

20%, each 15 Watts and 20 Watts have an area of 0.093 m^2, respectively, which results in the total area of PV arrays for package, A_p, shown in Table 3.3. [177] state that the annual maintenance cost for PV panels range between 15 to 90 cents per m^2, while extensive GRs maintenance cost is negligible. Hence, we consider the annual cost for each package equal to 90 cents per m^2.

Table 3.4 shows the price of PV packages per Watts from 2014 to 2018. In order to include the changes in the price of PV systems, we fit a linear regression model to the cost per Watts of PV systems and include it in the model. That is, we do not offer any new green technology packages, but change their costs as the time progresses to capture the existing trend in the overall cost of PV systems.

Climate scenarios, Ω, total number of cooling degree hours during day t in climate scenario ω, $\tau_c^{\omega t}$, total number of heating degree hours during day t in climate scenario ω, $\tau_h^{\omega t}$, and realization probability of climate scenario ω. We use the climate forecasts provided by ORNL [216, 35] as the climate scenarios for this model. The climate forecasts are generated using on 10 different coupled general circulation models (GCMS) [237], and include daily values for maximum and minimum daily temperature as well as precipitation level for each day starting from January 2011 up to December 2050 for grids of $1km^2$ and $4km^2$ for city of Knoxville, TN. In this study, we use the climate projections which are generated using ten different CGCMs as listed in Table 3.5, and assign each with an equal realization probability,

Table 3.5: Coupled general circulation climate forecast models (CGCMs) provided by Oak Ridge National Laboratory's Climate Change Science Institute [35]. These ten projection models are generated using high-performance computing resources, including Titan, America's fastest supercomputer [35].

Model	Institute of development
Japanese Meteorological Research Institute Coupled Global Climate Model (MRI-CGCM3)	Meteorological Research Institute of the Japan Meteorological Agency [117]
Max-Planck-Institute Earth System Model Mixed Resolution (MPI-ESM-MR)	Max Planck Institute for Meteorology [150]
Geophysical Fluid Dynamics Laboratory Earth System Model (GFDL-ESM2M)	Geophysical Fluid Dynamics Laboratory [173]
The Australian Community Climate and Earth System Simulator (ACCESS)	Commonwealth Scientific and Industrial Research Organization [54]
The NCAR's Community Climate System Model (CCSM4)	Climate and Global Dynamics Laboratory at the National Center for Atmospheric Research [153]
The Institute Pierre Simon Laplace Climate Model (IPSL-CM5A)	Institute Pierre Simon Laplace [115]
The Beijing Climate Center Climate System Model (BCC-CSM)	Beijing Climate Center, China Meteorological Administration [21]
Norwegian Earth System Model (NorESM1-M)	Multi-institutional, Coordinated Climate Research in Norway [63]
The Centro Euro-Mediterraneo sui Cambiamenti Climatici Climate Model (CMCC-CM)	Euro-Mediterranean Center on Climate Change [49]
Flexible Global Ocean Atmosphere Land System (FGOALS)	Institute of Atmospheric Physics, Chinese Academy of Sciences, State Key Laboratory of Numerical Modeling for Atmospheric Sciences and Geophysical Fluid Dynamics [127]

i.e., 10%. Note that this study considers a planning horizon, T, of 20 years, starting from January 2011.

In order to provide a higher level of detail on the projection models using in this study, Table 3.6 presents the maximum, average and the range of standard deviation for daily pairwise comparisons across the ten projections over the given planning horizon. The results shown in the table highlight the existing variations in the projected values.

We use cut-off values to calculate the total number of cooling and heating degree days during the planning horizon. To do so, we calculate the average daily temperature by calculating the average of maximum and minimum daily temperature and use the recommended temperatures for human comfort in the literature i.e., 17.5 and 14.2 degrees Celsius for heating and cooling degree days, respectively [33, 50, 58].

Cost of 1 kWh electricity, μ. In this study, we make the assumption that net metering is available for the agents. Net metering allows agents to send the extra electricity generated to the grid at normal retail value and receiving credit for it, which is commonly supported by

Table 3.6: The results from the daily pairwise comparison for the ten CGCMs shown in Table 3.5 over the planning horizon of this study, i.e., $T = 20$, starting from January 2011.

Parameter	T=20		
	Maximum	Average	Standard deviation range
Daily maximum temperature ()	31.41	4.72	[0.79,7.95]
Daily minimum temperature ()	41.58	4.79	[0.47,11.22]
Daily precipitation (mm)	105.26	5.45	[0.02,38.88]

most utility providers in the U.S. [197]. Hence, we assume that the excess electricity generated by an agent can be sent to the grid and used later. We set the cost of electricity equal to 10.3 cents per kWh consistent with the price of electricity in the city of Knoxville, TN [65]. *PV output efficiency for package p during day t, E_p^t.* [158] reports show that in the past 40 years, PV cell output efficiency has increased and recently developed PV cells have an efficiency ranging between 11.5% and 46%. However, the currently commercially available PV cells have 13.5% to 20% output efficiency [45]. Hence, in our study, we consider a variety of PV packages that have an efficiency ranging between 13.5% and 20%. However, we later expand our studies by considering the introduction of new packages with a higher output efficiency as the time passes. The daily output efficiency of each package is calculated for each day based on the average temperature during each day t, by Eq. (3.13),

$$E_p^t = \begin{cases} E_p(1.091 + 0.0013\mathbb{T}_t) & \text{if package } p \text{ contains GR} \\ E_p & \text{o.w.,} \end{cases} \tag{3.13}$$

where $\mathbb{T}_t$ denotes the average daily temperature for the grid in which the building is located and E_p represents the output efficiency of the package. In Eq. (3.13), it is shown that the output efficiency of the installed PV package increases if it is integrated with a GR. The level of increase in output efficiency of PV panels due to integration with GRs have been the subject of numerous empirical studies, and the reported values range from 3.33% to 8% [40, 110]. Note that the reason for this output efficiency increase is due to GRs reducing the temperature of their surrounding area. Hence, the higher the temperature, the greater the cooling and, hence, the higher the efficiency increase. Therefore, we fit a linear regression

line to the reported values from the literature and the maximum and minimum temperatures from the climate forecasts, which results in the regression line reported in Eq. (3.13).

Percentage energy saving in cooling degree-hours due to GR installation, α, and percentage energy saving in heating degree-hours due to GR installation, β. The percentage of energy saving in cooling degree-hours achieved due to the installation of GRs differs across various studies, ranging from 10% to 16.7% [50, 61, 12, 244, 83, 206, 175]. While almost all studies agree on the fact that using GRs results in savings in cooling degree-hours, there is a lack of consensus on the impact of GRs in heating degree-hours. Indeed, a few empirical studies report that using GRs contribute to energy loss in heating degree-hours while others suggest that it results in energy savings. For instance, a recent, long-term study reports that GRs increase the required amount of energy to heat the space to a comfortable level (i.e., 22 degrees Celsius in this study) in heating degree-hours by 6.2% [50]. Consistently, another study performed in different climates throughout Europe reports up to 1% GR-related energy loss in cold seasons in certain climates [12]. In contrast, two empirical studies suggest that the energy savings from GR in heating degree-hours is negligible and can be ignored [83, 206]. However, there exists another group of studies that report reductions of 4% to 10% in energy savings as a result of GRs in heating degree-hours [61, 12, 175, 244]. Therefore, in this study, we let α and β assume a wide range of values to capture the different, and sometimes contradicting, estimates reported in the literature. Specifically, we let α range from 10% to 20% and β range from -10% to 10%.

Total amount of solar irradiation available during day t in climate scenario ω, $I^{\omega t}$. Figure 3.3 presents the daily average level of solar irradiation for each household for the City of Knoxville, TN, provided by UDI [216] and CCSI [35].

These levels reflect the level of solar irradiation during a day in which the average number of peak sunlight hours are available in City of Knoxville, i.e., 4.5 hours [159]. In order to calculate the level of solar irradiation available during each day, we need to estimate the number of daily peak sunlight hours. Note that number of peak sunlight hours throughout each day is direct ly related to the level of daily precipitation during that given day. Figures 3.4a and 3.4b show the monthly average peak sunlight hours and precipitation from 1960 to 1990 for City of Knoxville, TN. Therefore, we use the precipitation forecasts provided by

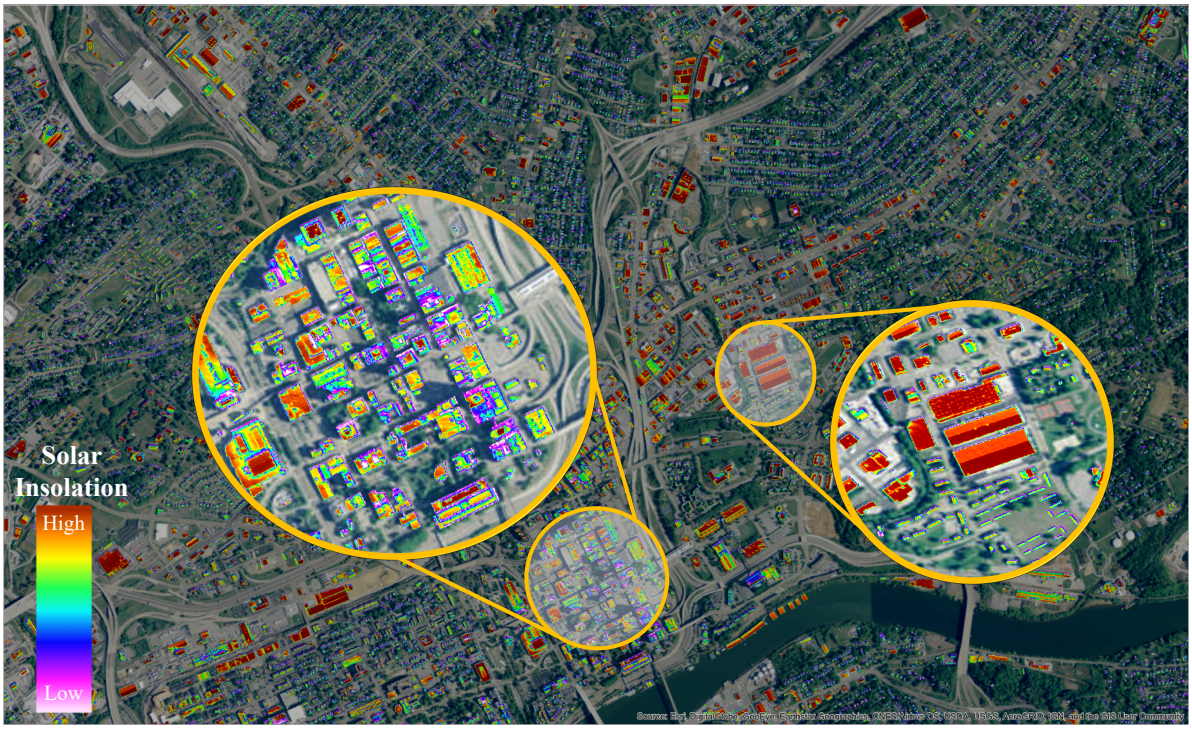


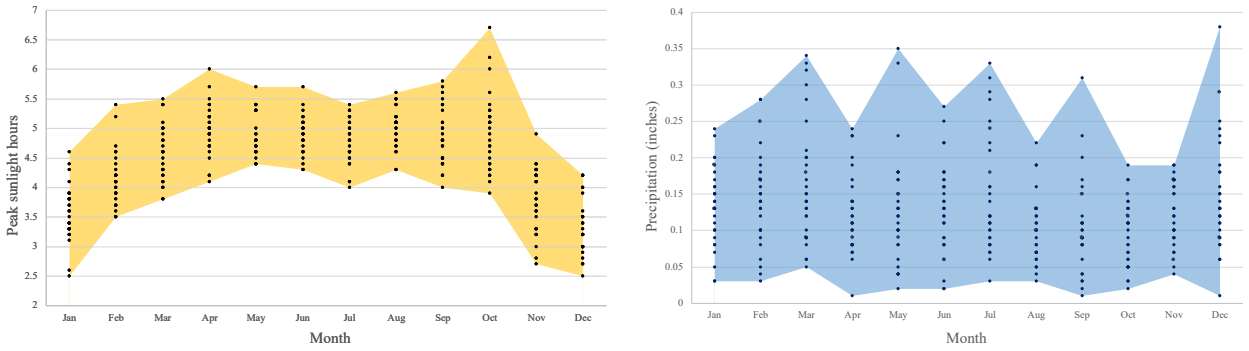
Figure 3.3: Visual-SOLAR radiation map for the City of Knoxville, Tennessee [121].

Table 3.7: Intercept and slope for monthly regression models for peaks sunlight hours versus precipitation level in mm based on historical data for city of Knoxville, TN, based on the data provided by [159] and [156].

Month	Jan	Feb	Mar	Apr	May	Jun	Jul	Aug	Sep	Oct	Nov	Dec
Intercept	4.1973	4.6561	5.0258	5.3702	5.1199	5.2159	5.1398	5.1985	5.2722	5.4577	4.1238	3.6984
Slope	-0.1843	-0.1441	-0.1040	-0.1235	-0.0712	-0.0960	-0.0944	-0.0681	-0.1611	-0.2170	-0.0986	-0.1043

the 10 CGCMS to calculate the level of peak sunlight hours, and hence, solar irradiation. That is, we develop monthly regression models that links the level of peak sunlight hour for each month with the precipitation level, and hence, we can approximate the daily solar irradiation for each grid based on the precipitation forecasts provided by [216] and [35]. Table 3.7 presents the slope and intercept for linear regressions for peak sunlight hours versus precipitation level.

Daily energy consumption for space conditioning for the building during day t, U^t. Electricity consumption usually increases in building size [68]. The data from a 2009 survey by the EIA [68] is used to estimate the relationship between the average daily energy consumption levels for conditioning and the size of the building. The data shows an obvious linear relationship



(a) Monthly average peak sunlight hours for City of Knoxville, TN, from 1960 to 1990 provided by [159].

(b) Monthly average precipitation level for City of Knoxville, TN, from 1960 to 1990 provided by [156].

Figure 3.4: Historical peak sunlight hours and precipitation data for City of Knoxville over 30 years from 1960 to 1990.

Table 3.8: The independent variables and their corresponding normalized coefficients developed by [243].

Factor	Normalized weight	Independent variable	Data source
Payback period	0.319	Payback period	Income model
Household income	0.247	Yearly income in 5 thousand USD Family size	[218]
Advertisement	0.281	Number of advertisements received per family	$Triangular(1, 5, 3.2)$ [243]
Neighborhood	0.153	Number of green technologies installed per neighborhood	1,060 m^2 [217]
ϕ_{Global}	—	adoption threshold	[53.3%-54.5%] [164]

between the size of the building and its energy consumption for conditioning. Eq. (3.14) shows the linear regression used to calculate the average daily energy consumption for each household in this study,

$$U^t = 0.0941H + 11.472 \tag{3.14}$$

The performance ratio of the PV system, λ. According to [168], the quality of PV installation can drastically reduce the output of the PV system due to reasons such as inverter, temperature, DC and AC cable losses, which can result in a decrease in the efficiency of PV system up to 100% of its actual efficiency. We set the value for this parameter equal to 75% consistent with the report by [168].

The probability of a household adopting solar panels, ρ. In order to estimate the value for this variable, we use the linear regression model developed by [243]. Table 3.8 show the parameters used in the linear regression model, their units, corresponding coefficients, and the data source.

In order to calculate the value for each of the factors in the regression model, we follow the formulation proposed by [243]. That is, for payback period we use

$$F_1 = \frac{Max(PP) - PP_i}{Max(PP) - Min(PP)} \tag{3.15}$$

where PP denotes payback period, PP_i denotes the payback period for agent i, and maximum and minimum PP are set to the lifespan of common PV systems plus one, and one, respectively [164]. The household income factor is calculated as

$$F_2 = \frac{(e^{\mathbb{X}-12.4})/n}{1-(e^{\mathbb{X}-12.4})(n)}, \tag{3.16}$$

where V denotes the income of the household in 5 thousand USD. The Advertisement factor that accounts in the total number of advertisement about green technologies received by a family is calculated by using a piece-wise linear function, i.e.,

$$F_3 = \begin{cases} 0.02Adv & \text{if } 0 < Adv \leq 5, \\ 0.04Adv & \text{if } 5 < Adv \leq 10, \\ 0.06Adv & \text{if } 10 < Adv \leq 15, \\ 0.08Adv & \text{if } 15 < Adv \leq 20, \\ 1 & \text{if } Adv > 20, \end{cases} \tag{3.17}$$

where Adv denotes the total number of advertisement received by a family during each time step. In order to calculate the factor of neighborhood, F_4 is calculated as

$$F_4 = \frac{e^{\mathbb{N}-4}}{1-e^{\mathbb{N}-4}} \tag{3.18}$$

where $\mathbb{N}$ denotes the number of neighbors in the neighborhood who adopted green technologies. [217] defines a neighborhood as the area in a radios of 650 m to 1,060 meters around a household. Hence, we set the the neighborhood for each agent as the number of agents in a radios of 1,060 m fro the agents geographical location.

3.4 Computational Studies

In this section, first we conduct a case study on a sample of households in the city of Knoxville, TN. Next,we conduct a sensitivity analysis on the hyper-parameters of the social network. Lastly, we examine different policies and study their effects on the results of the model.

3.4.1 Case Study

In this section, we conduct a case study on a sample of households in the city of Knoxville, TN. This sample is a random subset of the actual households in Knoxville, TN, with a size of 1045 households, i.e., 0.5% of the actual data. We study the diffusion of the green technologies throughout the sample society by only exposing the households with the information form the income model, and study the outcomes of the model. We set the hyper-parameters of the Small World network to 2, 10%, and 60% for N_{sw}, P_{sw}, and ϕ_{Global}, respectively, with 4 interactions per time step. Figure 3.5 shows the results from the model after 20 years of simulation.

As the results from the model shows, after 20 year of simulation, the maximum number of installed packages are in the central Knoxville area, mainly downtown and west town, as well as Northshore and Farragut. Note that buildings in both mentioned neighborhoods generally receive a high level of solar irradiation due the lack of shading/topological properties of the region. Moreover, the daily average temperature values for both of the mentioned areas are higher than their surrounding areas due to the high density of the buildings. Also, these neighborhoods have a higher than average level of income with an average income of approximately 100,000^{+} USD.

3.4.2 Sensitivity Analyses

First, we conduct a number of case studies by running the model for 20 years while accounting for the changes in the price of the green technology packages, as well as interactions among the agents under different network settings. That is, we change the hyper-parameters for the Small World network as well as the decision threshold and number of interactions. A

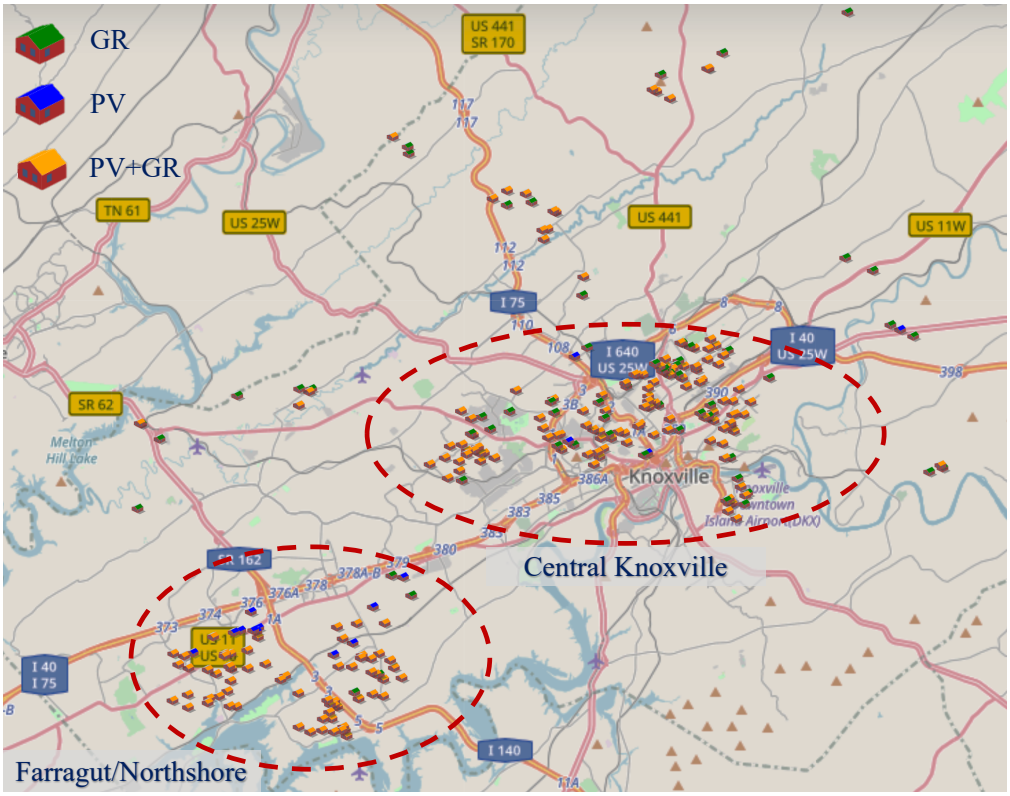


Figure 3.5: The total number of installed packages for a sample of 0.05% of total number of buildings in city of Knoxville, TN, over 20 years. The highlighted areas are the neighborhoods with the most number of installed green technologies. The image only shows the households with installed packages in order to improve the presentation of the results.

Small World network with a high probability value, P_{sw}, resembles a Random Network as the high values for P_{sw} translates to higher probability of randomly connecting to agents which are not neighbors whereas a network with low probability values resembles a Lattice network [225]. Hence, we include three different thresholds of 10%, 50%, and 90% to study the changes in the outcomes of the model under different network structures. The number of interactions indicate the total number of times that each agent interacts with the connections in its networks and updates its opinion, ϕ, and uncertainty, U, values per each time step (during each year).

Table 3.9 shows the results for 27 different setting for parameters of the Small World network as well as the threshold for the opinion threshold over 20 years. In order to reduce the randomness of the model to get a better understanding of the effects of the changes in the networks settings on the results, we set the number of advertisements received per family to a constant value, i.e., 20 during each year. The results from the table show that the total number of installations decreases in decision threshold, ϕ_{Golbal}, which is representative of the fact that in a society, there is a small number of people that hold an extreme opinion towards a subject, whereas the majority of the society have a relatively moderate opinion towards a subject.

We observe that the total number of installations increase in the number of connections, N_{sw} and the number of interactions, where the highest number of installations is for $N_{sw} = 4$ and 8 interactions under a P_{sw} of 90%. From the results, we can observe that generally a higher number of interactions results in a higher number of installations while it generally does not increase the number of agents with an extreme opinion. This means that agents in a more active network tend to have less extreme opinion, as for N_{sw} equal to 4, P_{sw} equal to 90%, and 8 interactions (which roughly translates to a society in which agents have a high number of connections, many of which are spread throughout the society and they actively interact) the total number of agents with an opinion higher than 70% is smaller than the other settings.

The changes in the total number of installed systems show that a more diverse network generally results in an increase in the number of adopters. That is, as the probability of agents connecting to other agents which are not in their geographical neighborhood increases, i.e.,

Table 3.9: The total number of installed PV system, GRs, and GR integrated PV systems, for the agents in the network for different values for network hyper-parameters, decision threshold, and social interactions over twenty years starting from January 2011.

Number of connections (N_{sw})	Probability (P_{sw})	Decision threshold (ϕ_{Global})	Number of interactions = 4				Number of interactions = 8			
			PV only	GR only	PV and GR	Total # of systems	PV only	GR only	PV and GR	Total # of systems
1	10%	50%	35	110	358	503	39	127	434	600
		60%	11	40	128	179	21	51	182	254
		70%	0	5	6	11	0	5	6	11
	50%	50%	43	112	353	508	48	128	440	616
		60%	13	47	130	190	32	83	267	382
		70%	0	5	6	11	0	5	6	11
	90%	50%	34	115	324	473	48	130	441	619
		60%	13	48	148	209	26	86	303	415
		70%	0	5	6	11	0	5	6	11
2	10%	50%	50	121	430	601	55	142	513	710
		60%	12	46	135	193	42	103	419	564
		70%	0	5	6	11	0	5	6	11
	50%	50%	45	124	445	614	51	143	526	720
		60%	12	43	127	182	38	93	396	527
		70%	0	5	6	11	0	5	6	11
	90%	50%	44	118	432	594	52	161	530	743
		60%	13	59	194	266	42	112	406	560
		70%	0	5	6	11	0	5	6	11
4	10%	50%	50	137	495	682	60	167	557	784
		60%	27	75	247	349	53	129	513	695
		70%	0	5	6	11	0	5	6	11
	50%	50%	51	135	496	682	62	169	582	813
		60%	33	83	291	407	50	137	510	697
		70%	0	5	5	10	0	4	0	4
	90%	50%	49	138	505	692	60	171	603	834
		60%	17	39	132	188	52	148	544	744
		70%	0	5	6	11	0	4	0	4

higher values of P_{sw}, the interactions results in a more positive opinion towards the adoption of green technologies. Note that this does not positively effect the number of adopters under high levels of decision threshold as more diverse interactions results in less extreme opinions.

3.4.3 Policy Evaluation

In order to aid in the expansion of residential solar energy adoption, the federal government, state governments, utility companies, and individual organizations provide a variety of programs through which they aim to encourage the installation of green technologies. These programs can be divided into two main categories, i.e., the programs that aim to make green technologies more economical through tax cuts, rebates and incentives [213], and those that aim to increase the diffusion rate of such technologies by increasing their exposure in a society through advertisement, installations, and providing information about the benefits and advantages of such technologies [92]. In this paper, we aim to evaluate the impact of incentives and other programs on the diffusion rate of green technologies in the city of Knoxville, TN. In order to include the programs that increase the financial viability of green technologies, we incorporate the Solar Investment Tax Credit (ITC) into our model. The ITC is provided by the federal government since the Energy Policy Act of 2005 through which a deduction of 30% of the installation cost of a PV system is allocated to the adopters [213]. Moreover, we account for a similar incentives for GRs that reduces provides a tax cut of about 30% for the adopters [47]. Hence, under ITC policy, we account for a 30% reduction in cost of PV systems and GR installation. The role of the visibility and advertisement which encourage the adoption of green technologies have proved significant in the literature [92, 243, 174]. Therefore, we study the impact of increasing the exposure and visibility of green technologies by evaluating the effect of an increase in the number of advertisements towards promoting green technologies through promotional campaigns (PC). That is, we assume that each household receive the maximum number of advertisement assume in the model, i.e., 25 per family, and evaluate its effect on the outcomes of the model. Lastly, we evaluate the joint effect of these policies.

We aim to evaluate the effect of policies on the adoption rate of the green technologies. We study the effects of the ITC incentive under two different scenarios, i.e., ITC exists only

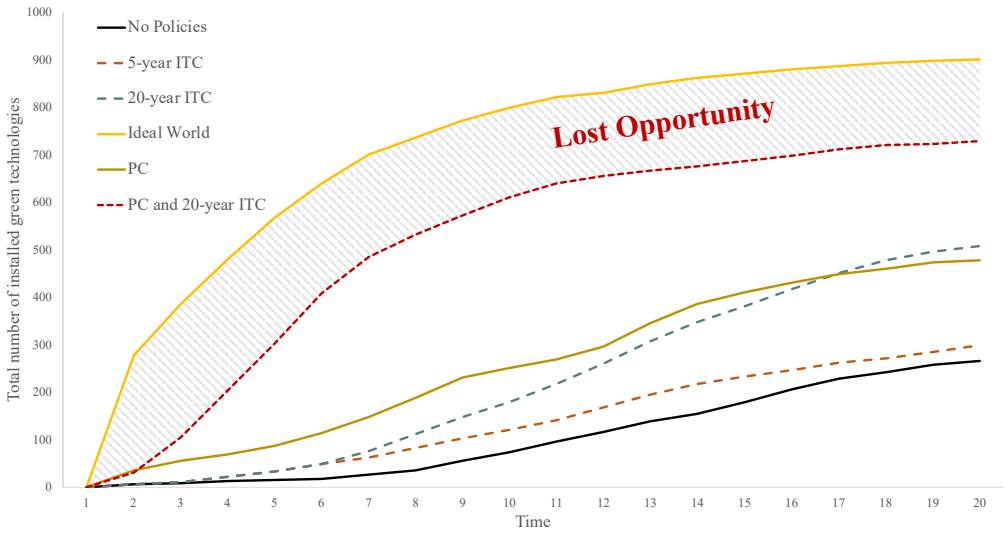


Figure 3.6: The total number of installed packages under 6 different cases, i.e., ideal world, no policies, 5 year and 25 year ITC, PC, and PC and 20-year ITC, where the dashed lines show the cases with ITC policy, and continuous lines represent the cases with no policies. The Lost Opportunity shows the difference between the ideal installation of green technologies and the results form the policy with the most installations.

for the first 5 years of the time horizon, and ITC exists throughout the entire time horizon. Next, we evaluate the effect of the promotions through the implementation of PC for the entire time horizon, with and without the ITC. Lastly, we compare the results with the case where no incentives exist, and the ideal world where the only criterion is whether or not the green technologies are profitable. We set K_{sw}, P_{sw}, and ϕ_{Global} equal to 2, 10%, and 50%, respectively, with four annual interactions between the agents and their connections.

Figure 3.6 shows the total number of installed green technologies under the implementation of different policies. The results show that a 5-year ITC slightly increases the adoption rate when it is being implemented, but for the remaining of the time horizon, the total number of installations is similar with the No Policies case. We observe that while PC performs better than ITC policies for the first 10 years, a 20-year ITC performs better under a long run. This shows the fact that while informing the public about the benefits of green technology helps increase their implementation, a financially beneficial policy outperforms it over the long run. Our results also show that the combination of both PC and ITC results in the most number of installed green technologies. That is, while providing information on the advantages of green

technologies can help the adoption rate, many adopters do not find the payback period short enough to invest in such technologies. Hence, by reducing the payback period through tax cuts and incentives, we can achieve a higher diffusion rate. Note that the Lost Opportunity represents the actual potential of the sample society versus the results from the best policies. We observe that as the price of PV systems reduces over time and more financially profitable systems are introduced, a combination of ITC and PC can reduce the gap significantly. Note that the total number of installed green technologies in the neighborhood of an agent also plays an important role in the adoption rate of green technologies. Hence, by investing in improving the visibility of such technologies, Lost Opportunity can decrease.

3.5 Conclusion

In this paper, we aim to study the diffusion of green technologies under uncertainty. We develop a stochastic optimization model to capture the uncertain nature of the parameters of the model, and find the most profitable package for each individual building. Then, we develop an ABM framework to simulate the interactions of the agents over time. We use a regression model from the existing literature in order to calculate the parameters for the behavioral sub-model, as well as capturing the interactions throughout a society and their effects on the outcome of the model. Next, we conduct a case study over a sample of 1046 households in the city of Knoxville, TN, and evaluate the result. In order to study the effects of the changes in the values of the parameters of the attitudinal model, we conduct a sensitivity analysis over 72 different combinations and provide insights. Lastly, we examine the effect of some of the currently common policies on the outcome of the model and the diffusion rate of the green technologies.

Chapter 4

Conclusions

In Chapter 1, we look at the optimal placement of Photovoltaic (PV) systems and green roofs (GRs) in order to find out whether or not the implementation of green technologies can be financially profitable. To evaluate the financial outcomes of such technologies, we need to take two main factors into account, i.e., the output of PV systems and GRs are directly related to the climate their are installed in, and the fact that climate is changing. One might argue that climate change will not happen fast, and hence, the effects of such phenomenon does not drastically effect the outcome of our investments on green technologies. But, we need to factor in that PV systems and GRs are long-term investments, as they last for 20-25 and 40-50 years, respectively, and are not essentially cheap. Therefore, such evaluations need to be conducted over an acceptable time-span in order to justify the true profitability of PV systems and GRs. This means that we need to focus on the gradual change in the climate as the outcomes of PV systems and GRs need to be evaluated over a moderately long span of time as an investment, and study the profitability of these green practices while accounting for such uncertainties. The long-term nature of these investments, as well as the stochasticity introduced by climate change and various models that forecast these changes differently leads us to the implementation of stochastic programming. The structure of two-stage stochastic programming is perfectly fit for the mentioned problem, as it accounts for the outcome of investments over time as well as the uncertain nature of such outcomes. Then, we study the implementation of the model over the city of Knoxville, TN, over different settings, scenarios, and assumptions. We evaluate the outcomes from the model and discuss

the achievable profits through a city-wide installation of green technologies over the city of Knoxville, TN, as a policy maker.

Next, in Chapter 2, we study another aspect of green technologies in a more granular level. That is, we focus on a single household, who owns a PV system which is integrated with a battery package. We focus on maximizing the profit through minimizing the electricity cost for such household. We aim to find the optimal policy for charging, discharging, and replacing the battery by considering the nature of the battery package, i.e., degradation over time and due to cycles. First, we introduce a Markov decision processes (MDP) optimization model, and evaluate the outcome of the model under different scenarios. Next, we tackle the issue of facing a large state-space due to the minute capacity reduction in batteries over time. This leads us to developing approximate approaches in order to achieve an approximate optimal policy for the utilization of battery integrated PV systems through the utilization of Reinforcement Learning (RL) and Neural Networks (NN) by utilizing Deep Q-Network (DQN) algorithm. We develop extensions on DQN algorithm by exploiting the outcomes of the exact solution in order to reduce the computational intensity and solution time while increasing the accuracy of the model.

Lastly, in Chapter 3 we focus on the role of decision makers and promotional policies on the diffusion rate of the green technologies. In Chapter 1, we made the assumption that a high level decision maker uses the proposed model to find the best optimal installation settings of PV systems and GRs throughout the city of Knoxville, TN. In this chapter, we make this assumption that the decision makers are the households rather than a high level policy maker. This results in higher level of uncertainty as the decision makers do not merely rely on the profitability of the green technologies, but they need to hold a positive opinion against these green practices in order to adopt them. Decision makers' opinion (agents) hold different opinions based on their characteristics as well as their interactions throughout the environment in which they exist. Hence, we utilize an agent based modeling (AMB) framework to study the diffusion rate of the green technologies when the decision makers are presented with the information from an optimization model about their optimal installation settings and their profitability. We account for the behavior of the agents as well as their potential income while their behavior is prune to change due to their social interactions with

other agents in the system. We study the effect of different promotional policies over a 20 year span of time while accounting for the decrease in the cost of the technology and discuss the outcomes.

Bibliography

[1] Abdelaziz, F. B., Aouni, B., and El Fayedh, R. (2007). Multi-objective Stochastic Programming for Portfolio Selection. *European Journal of Operational Research*, 177(3):1811–1823. 7

[2] Adepetu, A. and Keshav, S. (2016). Understanding Solar PV and Battery Adoption in Ontario: An Agent-based Approach. In *Proceedings of the Seventh International Conference on Future Energy Systems*, page 5. ACM. 69

[3] Ajzen, I. (1991). The Theory of Planned Behavior. *Organizational behavior and human decision processes*, 50(2):179–211. 76

[4] Albareda-Sambola, M., Fernández, E., and Saldanha-da Gama, F. (2011). The Facility Location Problem with Bernoulli Demands. *Omega*, 39(3):335–345. 5

[5] Alsema, E. A. and Nieuwlaar, E. (2000). Energy Viability of Photovoltaic Systems. *Energy policy*, 28(14):999–1010. 37, 133

[6] Alshurafa, N., Eastwood, J., Nyamathi, S., Xu, W., Liu, J. J., and Sarrafzadeh, M. (2014). Battery Optimization in Smartphones for Remote Health Monitoring Systems to Enhance User Adherence. In *Proceedings of the 7th international conference on PErvasive Technologies Related to Assistive Environments*, page 8. ACM. 43

[7] Amato, A. D., Ruth, M., Kirshen, P., and Horwitz, J. (2005). Regional Energy Demand Responses to Climate Change: Methodology and Application to the Commonwealth of Massachusetts. *Climatic Change*, 71(1-2):175–201. 17, 18, 66

[8] Ampim, P. A., Sloan, J. J., Cabrera, R. I., Harp, D. A., and Jaber, F. H. (2010). Green Roof Growing Substrates: Types, Ingredients, Composition and Properties. *Journal of Environmental Horticulture*, 28(4):244–252. 6

[9] Angenendt, G., Zurmühlen, S., Mir-Montazeri, R., Magnor, D., and Sauer, D. U. (2016). Enhancing Battery Lifetime in PV Battery Home Storage System Using Forecast Based Operating Strategies. *Energy Procedia*, 99:80–88. 54

[10] Arnette, A. N. (2013). Integrating Rooftop Solar into a Multi-source Energy Planning Optimization Model. *Applied energy*, 111:456–467. 6, 66

[11] Arvanitis, S. and Ley, M. (2013). Factors Determining the Adoption of Energy-saving Technologies in Swiss Firms: An Analysis Based on Micro Data. *Environmental and Resource Economics*, 54(3):389–417. 64

[12] Ascione, F., Bianco, N., deRossi, F., Turni, G., and Vanoli, G. P. (2013). Green Roofs in European Climates. Are Effective Solutions for the Energy Savings in Air-conditioning? *Applied Energy*, 104:845–859. 16, 18, 86

[13] Aurora Energy, a. (2018). Peak Sun Hours. http://www.aurorasolarenergy.com/average-daily-sun-hours/. 10

[14] Axelrod, R. (1997a). Advancing the Art of Simulation in the Social Sciences. In *Simulating social phenomena*, pages 21–40. Springer. 68

[15] Axelrod, R. (1997b). *The Complexity of Cooperation: Agent-based Models of Competition and Collaboration*, volume 3. Princeton University Press. 76

[16] Bankier, C. and Gale, S. (2006). Energy Payback of Roof Mounted Photovoltaic Cells. 37, 133

[17] Banos, R., Manzano-Agugliaro, F., Montoya, F., Gil, C., Alcayde, A., and Gómez, J. (2011). Optimization Methods Applied to Renewable and Sustainable Energy: A Review. *Renewable and Sustainable Energy Reviews*, 15(4):1753–1766. 8

[18] Barbarosolu, G. and Arda, Y. (2004). A Two-stage Stochastic Programming Framework for Transportation Planning in Disaster Response. *Journal of the operational research society*, 55(1):43–53. 7, 73

[19] Bass, F. M. (1969). A New Product Growth for Model Consumer Durables. *Management science*, 15(5):215–227. 67

[20] Battery University, B. (2018). BU-204: How do Lithium Batteries Work? https://batteryuniversity.com/index.php/learn/article/lithium_based_batteries. 41

[21] BCC (2017). Beijing Climate Center, China Meteorological Administration. http://forecast.bcccsm.ncc-cma.net/web/channel-1.htm. 19, 84

[22] Belzer, D. B. (2009). Energy Efficiency Potential in Existing Commercial Buildings: Review of Selected Recent Studies. Technical report, Pacific Northwest National Lab.(PNNL), Richland, WA (United States). 17, 18, 66

[23] Berndtsson, J. C. (2010). Green Roof Performance Towards Management of Runoff Water Quantity and Quality: A Review. *Ecological Engineering*, 36(4):351–360. 6, 66

[24] Bianchini, F. and Hewage, K. (2012). How Green are the Green Roofs? lifecycle analysis of green roof materials. *Building and environment*, 48:57–65. 37

[25] Birge, J. R. and Louveaux, F. (2011). *Introduction to Stochastic Programming*. Springer Science & Business Media. 7, 12, 73

[26] Bloomberg, B. (2017). Were Going to Need More Lithium. https://www.bloomberg.com/graphics/2017-lithium-battery-future/. 40

[27] Bollinger, B. (2015). Green Technology Adoption: An Empirical Study of the Southern California Garment Cleaning Industry. *Quantitative Marketing and Economics*, 13(4):319–358. 64

[28] Bollinger, B. and Gillingham, K. (2012). Peer Effects in the Diffusion of Solar Photovoltaic Panels. *Marketing Science*, 31(6):900–912. 68, 71

[29] Bookstaber, R. M. (2012). Using Agent-based Models for Analyzing Threats to Financial Stability. 67

[30] Bose, B. K. (2010). Global Warming: Energy, Environmental Pollution, and the Impact of Power Electronics. *Industrial Electronics Magazine, IEEE*, 4(1):6–17. 2, 67

[31] Boston Solar, b. (2018). Solar Panels - Lifetime Productivity and Maintenance Costs. http://www.bostonsolar.us/solar-blog-resource-center/blog/solar-panels-lifetime-productivity-and-maintenance-costs/. 11, 14, 18

[32] Brown, L. A. (1981). *Innovation Diffusion; A New Perspective*. Number INVES-ET E14d B878. Methuen. 67

[33] Burroughs, H. and Hansen, S. J. (2013). *Managing Indoor Air Quality Fifth Edition*, volume 1. CRC Press. 20, 84

[34] Busic, A. and Fuerst, F. (2018). Does Your Personality Shape Your Reaction to Your Neighbours' Behaviour? A Spatial Study of the Diffusion of Solar Panels. 70

[35] CCSI (2017). Oak Ridge National Laboratorys Climate Change Science Institute. https://ccsi.ornl.gov. ix, xi, 4, 18, 19, 21, 81, 83, 84, 86, 87

[36] Cen, Y., Sisson, R. D., Qin, Q., and Liang, J. (2018). Current Progress of Si/Graphene Nanocomposites for Lithium-Ion Batteries. *C*, 4(1):18. 41

[37] Census Bureau, U. S. (2018a). Median and Average Square Feet of Floor Area in New Single-Family Houses Completed by Location. https://www.census.gov/const/C25Ann/sftotalmedavgsqft.pdf. 24, 26

[38] Census Bureau, U. S. (2018b). Number of Stories in New Single-Family Houses Completed. https://www.census.gov/construction/chars/pdf/stories.pdf. 24

[39] Chang, N.-B., Rivera, B. J., and Wanielista, M. (2010). Cost Benefit Optimization of Cistern Volume and Green Roof Area in the Florida Showcase Green Envirohome (FSGE). In *Sustainable Systems and Technology (ISSST), 2010 IEEE International Symposium on*, pages 1–6. IEEE. 6

[40] Chemisana, D. and Lamnatou, C. (2014). Photovoltaic-green Roofs: An Experimental Evaluation of System Performance. *Applied Energy*, 119:246–256. 3, 16, 18, 67, 85

[41] Chen, J., Taylor, J. E., and Wei, H.-H. (2012). Modeling Building Occupant Network Energy Consumption Decision-making: The interplay Between Network Structure and Conservation. *Energy and Buildings*, 47:515–524. 67

[42] Chen, S.-G. (2013). Bayesian Approach for Optimal PV System Sizing under Climate Change. *Omega*, 41(2):176–185. 6

[43] Chow, T. T. (2010). A Review on Photovoltaic/Thermal Hybrid Solar Technology. *Applied energy*, 87(2):365–379. 5, 66

[44] Chowdhury, P. and Chakrabarti, C. (2002). Battery Aware Task Scheduling for a System-on-a-chip Using Voltage/Clock Scaling. In *Signal Processing Systems, 2002.(SIPS'02). IEEE Workshop on*, pages 201–206. IEEE. 43

[45] Chung, D., Davidson, C., Fu, R., Ardani, K., and Margolis, R. (2015). US Photovoltaic Prices and Cost Breakdowns: Q1 2015 Benchmarks for Residential, Commercial, and Utility-scale Systems. Technical report, NREL Technical Report, In Preparation. 13, 14, 18, 85

[46] Cipra, B. A. (1987). An Introduction to the Ising Model. *The American Mathematical Monthly*, 94(10):937–959. 76

[47] City of Philadelphia Department of Revenue, p. (2007). Business Income and Receipts Tax Green Roof Tax Credit. https://www.phila.gov/media/20160925174047/Green-Roof-Tax-Credit-Overview-Revised-July-20-2016.pdf. 94

[48] Clarke, R. A. (1994). The Challenge of Going Green. *Reader In Business And The Environment*, page 45. 65

[49] CMCC (2017). Euro-Mediterranean Center On Climate Change. http://www.cmcc.it/models/cmcc-cm. 19, 84

[50] Coma, J., Pérez, G., Solé, C., Castell, A., and Cabeza, L. F. (2016). Thermal Assessment of Extensive Green Roofs as Passive Tool for Energy Savings in Buildings. *Renewable Energy*, 85:1106–1115. 3, 11, 15, 16, 18, 20, 84, 86

[51] Cook-Patton, S. C. and Bauerle, T. L. (2012). Potential Benefits of Plant Diversity on Vegetated Roofs: A Literature Review. *Journal of Environmental Management*, 106:85–92. 6, 66

[52] Correia, I., Nickel, S., and Saldanha-da Gama, F. (2018). A Stochastic Multi-period Capacitated Multiple Allocation Hub Location Problem: Formulation and Inequalities. *Omega*, 74:122–134. 5

[53] CRONOS (2017). Mc Ghee Tyson Airport (KTYS). http://climate.ncsu.edu/cronos/?station=KTYS. 20, 21

[54] CSIRO (2017). ACCESS Climate Model. http://www.csiro.au/en/Research/OandA/Areas/Assessing-our-climate/CAWCR/ACCESS/. 19, 84

[55] Cui, X., Liu, C., Kim, H. K., Kao, S.-C., Tuttle, M. A., and Bhaduri, B. L. (2010). A Multi Agent-based Framework for Simulating Household PHEV Distribution and Electric Distribution Network Impact. *TRB Comittee on Transportation Energy (ADC70)*, 1250:21. 72

[56] Current Results Weather and Science Facts (2017). Average Annual Sunshine by State. https://www.currentresults.com/Weather/US/average-annual-state-sunshine.php. 21

[57] Deffuant, G., Neau, D., Amblard, F., and Weisbuch, G. (2000). Mixing Beliefs Among Interacting Agents. *Advances in Complex Systems*, 3(01n04):87–98. 76, 79

[58] Degree Days Weather Data (2017). Custom Degree Day Data. http://www.degreedays.net. 10, 20, 84

[59] Diouf, B. and Pode, R. (2015). Potential of Lithium-ion Batteries in Renewable Energy. *Renewable Energy*, 76:375–380. 40

[60] Dong, C., Sigrin, B., and Brinkman, G. (2017). Forecasting Residential Solar Photovoltaic Deployment in California. *Technological Forecasting and Social Change*, 117:251–265. 70

[61] Dunec, J. L. (2012). Banking on Green: A look at How Green Infrastructure Can Save Municipalities Money and Provide Economic Benefits Community-Wide. 3, 11, 15, 16, 18, 66, 86

[62] Dwell Development, D. (2015). Solar Panels And A Green Roof Were Included On Top Of This New House In Seattle. https://www.dwelldevelopment.com/

solar-panels-and-a-green-roof-were-included-on-top-of-this-new-house-in-seattle/. xiii, 66

[63] EarthClim (2017). Multi-institutional, Coordinated Climate Research in Norway. http://folk.uib.no/ngfhd/EarthClim/. 19, 84

[64] EIA (2017a). Average Monthly Residential Electricity Consumption, Prices, and Bills by State. http://www.eia.gov/electricity/sales_revenue_price/xls/table5_a.xlsx. 15

[65] EIA (2017b). Average Price of Electricity to Ultimate Customers by End-use Sector. https://www.eia.gov/electricity/monthly/epm_table_grapher.cfm?t=epmt_5_6_a. 15, 85

[66] EIA (2017a). Average Quality of Fossil Fuel Receipts for the Electric Power Industry. https://www.eia.gov/electricity/annual/html/epa_07_03.html. 37

[67] EIA (2017b). Carbon Dioxide Uncontrolled Emission Factors. https://www.eia.gov/electricity/annual/html/epa_a_03.html. 37

[68] EIA (2017c). Residential Energy Consumption Survey (RECS). https://www.eia.gov/consumption/residential/. xii, xiv, 14, 17, 87, 127, 128

[69] EIA (2018a). Fuel Used and End Uses in Northeast Region, Divisions, and States (HC1.8). https://www.eia.gov/consumption/residential/data/2009/hc/hc1.8.xls. 15

[70] EIA (2018b). Heating and Cooling No Longer Majority of U.S. Home Energy Use. https://www.eia.gov/todayinenergy/detail.php?id=10271&src=. 17, 18, 66

[71] EIA (2018c). Today in Energy. https://www.eia.gov/todayinenergy/detail.php?id=14771. 17, 18, 20, 66

[72] EIA, E. (2018d). U.S. Imports of Solar Photovoltaic Modules Mainly Come from Asia. https://www.eia.gov/todayinenergy/detail.php?id=34952. 37, 133

[73] EIA, E. I. A. (2015). Annual Energy Outlook 2015 with Projections to 2040. *Department of Energy*. 2, 3, 65

[74] Energy Informative (2017). The Real Lifespan of Solar Panels. http://energyinformative.org/lifespan-solar-panels/. 5

[75] Energy Informative, E. (2014). What's the Difference Between Net Metering and Feed-In Tariffs? http://energyinformative.org/net-metering-feed-in-tariffs-difference. 15

[76] Energy Sage, E. (2019). How Much Do Solar Panels Cost in the U.S. in 2019? https://news.energysage.com/how-much-does-the-average-solar-panel-installation-cost-in-the-u-s/. xi, 83

[77] Energy Saving Trust, E. (2015). Solar Energy Calculator Sizing Guide. http://www.pvfitcalculator.energysavingtrust.org.uk/Documents/150224_SolarEnergy_Calculator_Sizing_Guide_v1.pdf. 14

[78] Energy Storage Association, E. (2018). Energy Storage Technologies. http://energystorage.org/energy-storage/energy-storage-technologies. 39

[79] EPA, E. (2009). Incorporating Low Impact Development into Municipal Stormwater Programs. https://www3.epa.gov/region1/npdes/stormwater/assets/pdfs/IncorporatingLID.pdf. 7

[80] EPA, E. (2017). Wind Energy Development in Region 8. https://www.epa.gov/sites/production/files/documents/WindEnergyDevelopmentInReg8Draft19Dec07.pdf. 7

[81] Feed-in Tariffs, f. (2018). What Is the Export Tariff? http://www.fitariffs.co.uk/fits/principles/export/. 15

[82] Feldman, D., Barbose, G., Margolis, R., James, T., Weaver, S., Darghouth, N., Fu, R., Davidson, C., and Wiser, R. (2014). Photovoltaic System Pricing Trends: Historical, Recent, and Near-term Projections. 2014 Edition. *Presentation by SunShot, US Department of Energy, NREL/PR-6A20-62558*. 2

[83] Feng, H. and Hewage, K. (2014). Energy Saving Performance of Green Vegetation on LEED Certified Buildings. *Energy and Buildings*, 75:281–289. 16, 18, 86

[84] Florida Solar Energy Center, F. (2018). Cell, Modules, and Arrays. http://www.fsec.ucf.edu/en/consumer/solar_electricity/basics/cells_modules_arrays.htm. 12

[85] Frischknecht, R., Itten, R., Sinha, P., de Wild-Scholten, M., Zhang, J., Fthenakis, V., Kim, H., Raugei, M., and Stucki, M. (2015). Life Cycle Inventories and Life Cycle Assessment of Photovoltaic Systems. *International Energy Agency (IEA) PVPS Task*, 12(9). 37, 133

[86] Gagnon, P., Margolis, R., Melius, J., Phillips, C., and Elmore, R. (2016). Rooftop Solar Photovoltaic Technical Potential in the United States: A Detailed Assessment. *Rep. No. NREL/TP-6A20-65298). Retrieved March*, 30:2016. 22

[87] Gargari, C., Bibbiani, C., Fantozzi, F., and Campiotti, C. A. (2016). Simulation of the Thermal Behaviour of a building retrofitted with a green roof: optimization of energy efficiency with reference to italian climatic zones. *Agriculture and agricultural science procedia*, 8:628–636. 6

[88] Geographic, N. (2016). Green Roofs Take Root Around the World. https://news.nationalgeographic.com/2016/10/san-francisco-green-roof-law/. 65

[89] Gillingham, K. and Bollinger, B. (2017). The Influence of Novel Behavioral Strategies in Promoting the Diffusion of Solar Energy. Technical report, Yale Univ., New Haven, CT (United States). 69

[90] Google Project Sunroof (2019). Estimated Rooftop Solar Potential of Knoxville, TN. https://www.google.com/get/sunroof/data-explorer/place/ChIJqULORiIWXIgRxTT1xNqS6ns/. 71

[91] Gou, B. (2008). Generalized Integer Linear Programming Formulation for Optimal PMU Placement. *IEEE Transactions on Power Systems*, 23(3):1099–1104. 5

[92] Graziano, M. and Gillingham, K. (2014). Spatial Patterns of Solar Photovoltaic System Adoption: The Influence of Neighbors and the Built Environment. *Journal of Economic Geography*, 15(4):815–839. 68, 94

[93] Green, H. M. and Kozek, A. S. (2003). Modelling Weather Data by Approximate Regression Quantiles. *ANZIAM Journal*, 44:229–248. 20

[94] Green Infrastructure Foundation, g. (2017). Making Informed Decisions: A Green Roof Cost and Benefit Study for Denver. https://static1.squarespace.com/static/588221e420099e47b8fe06d8/t/59e0e8d0017db2106c37d7b5/1507911889792/Denver_Cost_Benefit_Report_Final.pdf. 11

[95] Green Match, G. (2017). The Opportunities of Solar Panel Recycling. https://www.greenmatch.co.uk/blog/2017/10/the-opportunities-of-solar-panel-recycling. 133

[96] Green Roof Technology, g. (2017). How Much a Green Roof Costs? https://www.ornl.gov/content/solving-big-problems. 81

[97] Green Roof Technology, g. (2018). Solar Garden Roof – First, Fully Integrated Solar and Extensive Green Roof. http://www.greenrooftechnology.com/Solar_PV_Greenroofs. 14

[98] Griva, I., Nash, S. G., and Sofer, A. (2009). Linear and Nonlinear Programming. *Society for Industrial and Applied Mathematics, Philadelphia*. 23

[99] GSA, U. (2011). The Benefits and Challenges of Green Roofs on Public and Commercial Buildings. *A Report of the United States General Service Administration*. 11

[100] GSA, U. G. S. A. (2011). The Benefits and Challenges of Green Roofs on Public and Commercial Buildings. 15

[101] Guardian, T. (2015). France Decrees New Rooftops Must be Covered in Plants or Solar Panels. https://www.theguardian.com/world/2015/mar/20/france-decrees-new-rooftops-must-be-covered-in-plants-or-solar-panels. 65

[102] Gurobi, O. (2014). Inc.,Gurobi Optimizer Reference Manual, 2015. *Google Scholar*. 26

[103] Hagerstrand, T. (1952). *The Propagation of Innovation Waves*. 67

[104] Hand, M. M. (2012). *Renewable Electricity Futures Study*. National Renewable Energy Laboratory. 16

[105] Hoffert, M. I., Caldeira, K., Jain, A. K., Haites, E. F., Harvey, L. D., Potter, S. D., Schlesinger, M. E., Schneider, S. H., Watts, R. G., Wigley, T. M., et al. (1998). Energy Implications of Future Stabilization of Atmospheric CO2 Content. *Nature*, 395(6705):881–884. 2

[106] Home Advisor, h. (2019). How Much Solar Panels Cost. https://www.homeadvisor.com/cost/heating-and-cooling/install-solar-panels/. xi, 81, 83

[107] Hong, T., Koo, C., Park, J., and Park, H. S. (2014). A GIS (Geographic Information System)-based Optimization Model for Estimating the Electricity Generation of the Rooftop PV (Photovoltaic) System. *Energy*, 65:190–199. 5

[108] Hostick, D. J., Belzer, D. B., Hadley, S. W., Markel, T., Marnay, C., and Kintner-Meyer, M. C. (2014). Projecting Electricity Demand in 2050. Technical report, Pacific Northwest National Laboratory (PNNL), Richland, WA (United States). 16, 17

[109] Huang, Y. (2006). The Impact of Climate Change on the Energy Use of the US Residential and Commercial Building Sectors. *Lawrence Berkeley National Laboratory, Report No. LBNL-60754*. 17, 18, 66

[110] Hui, S. C. and Chan, S. (2011). Integration of Green Roof and Solar Photovoltaic Systems. In *Joint symposium*, pages 1–12. 3, 16, 18, 85

[111] IGRA (2017). International Green Roof Association. http://www.igra-world.com/types_of_green_roofs/. 15

[112] Independent, T. (2018). California Set to Become First US State Requiring Solar Panels on New Homes. https://www.independent.co.uk/news/world/americas/

california-solar-power-panels-homes-renewable-green-energy-climate-change-a8337626.html. 65

[113] International Renewable Energy Agency, I. (2013). Thermal Energy Storage Technology Brief. *IEA-ETSAP and IRENA© Technology Brief E17-January*. 40

[114] IPCC (2017). Intergovermental Panel on Climate Change Data Distribution Centre. http://www.ipcc-data.org/guidelines/pages/gcm_guide.html. 18

[115] IPSL (2017). Institut Pierre Simon Laplace Climate Modeling Center. http://icmc.ipsl.fr/. 19, 84

[116] Jardine, A. K., Lin, D., and Banjevic, D. (2006). A Review on Machinery Diagnostics and Prognostics Implementing Condition-based Maintenance. *Mechanical systems and signal processing*, 20(7):1483–1510. 42

[117] JMA (2017). Japan Meteorological Agency. http://ds.data.jma.go.jp/tcc/tcc/products/gwp/gwp7/html_e/model.html. 19, 84

[118] Jun, M., Knutti, R., and Nychka, D. W. (2008). Spatial Analysis to Quantify Numerical Model Bias and Dependence: How Many Climate Models Are There? *Journal of the American Statistical Association*, 103(483):934–947. 4, 19, 22

[119] Kasper, M., Bortis, D., and Kolar, J. W. (2014). Classification and Comparative Evaluation of PV Panel-integrated DC–DC Converter Concepts. *IEEE Transactions on Power Electronics*, 29(5):2511–2526. 5, 66

[120] Kim, J., Hong, T., and Koo, C.-W. (2012). Economic and Environmental Evaluation Model for Selecting the Optimum Design of Green Roof Systems in Elementary Schools. *Environmental science & technology*, 46(15):8475–8483. 6

[121] Kodysh, J. B., Omitaomu, O. A., Bhaduri, B. L., and Neish, B. S. (2013). Methodology for Estimating Solar Potential on Multiple Building Rooftops for Photovoltaic Systems. *Sustainable Cities and Society*, 8:31–41. xiii, xiv, 15, 21, 22, 71, 87

[122] Köhler, M., Wiartalla, W., and Feige, R. (2007). Interaction Between PV-Systems and Extensive Green Roofs. In *Proceedings of the Fifth Annual Greening Rooftops for Sustainable Communities Conference, Awards and Trade Show*. 3

[123] Komurlu, C. and Bilgic, M. (2016). Active Inference and Dynamic Gaussian Bayesian Networks for Battery Optimization in Wireless Sensor Networks. In *AAAI Workshop: AI for Smart Grids and Smart Buildings*. 43

[124] Koo, C., Hong, T., Lee, M., and Kim, J. (2016). An Integrated Multi-objective Optimization Model for Determining the Optimal Solution in Implementing the Rooftop Photovoltaic System. *Renewable and Sustainable Energy Reviews*, 57:822–837. 5

[125] Kornelakis, A. (2010). Multiobjective Particle Swarm Optimization for the Optimal Design of Photovoltaic Grid-connected Systems. *Solar Energy*, 84(12):2022–2033. 5

[126] Kremers, E. A. (2013). *Modelling and Simulation of Electrical Energy Systems Through a Complex Systems Approach Using Agent-based Models*. KIT scientific publishing. xi, 78

[127] LASG (2017). Institute of Atmospheric Physics, State Key Laboratory of Numerical Modeling for Atmospheric Sciences and Geophysical Fluid Dynamics. http://www.lasg.ac.cn/. 19, 84

[128] Lee, M. and Hong, T. (2019). Hybrid Agent-based Modeling of Rooftop Solar Photovoltaic adoption by integrating the geographic information system and data mining technique. *Energy Conversion and Management*, 183:266–279. 76

[129] Lee, Y.-H., Hsieh, Y.-C., and Hsu, C.-N. (2011). Adding Innovation Diffusion Theory to the Technology Acceptance Model: Supporting Employees' Intentions to Use E-learning Systems. *Journal of Educational Technology & Society*, 14(4):124–137. 76

[130] Levinson, R., Akbari, H., Pomerantz, M., and Gupta, S. (2009). Solar Access of Residential Rooftops in Four California Cities. *Solar Energy*, 83(12):2120–2135. 5, 66

[131] Li, S., He, H., Chen, Y., Huang, M., and Hu, C. (2015). Optimization Between the PV and the Retired EV Battery for the Residential Microgrid Application. *Energy Procedia*, 75:1138–1146. 44

[132] Li, X., Ramshani, M., Khojandi, A., Omitaomu, O., and Hathaway, J. M. (2017). An Agent Based Model for Joint Placement of PV Panels and Green Roofs. In *Simulation Conference (WSC), 2017 Winter*, pages 1133–1144. IEEE. 65, 67

[133] Li, Y. and Babcock, R. W. (2014). Green Roof Hydrologic Performance and Modeling: A Review. *Water Science and Technology*, 69(4):727–738. 6

[134] Li, Y., Huang, G., and Chen, X. (2009). Multistage Scenario-based Interval-stochastic Programming for Planning Water Resources Allocation. *Stochastic Environmental Research and Risk Assessment*, 23(6):781–792. 73

[135] Liu, G., Rasul, M., Amanullah, M., and Khan, M. M. K. (2012). Techno-economic Simulation and Optimization of Residential Grid-connected PV System for the Queensland Climate. *Renewable Energy*, 45:146–155. 6

[136] Loveland, J. and Brown, G. (1996). Impacts of climate change on the energy performance of buildings in the united states. 17, 18, 66

[137] Luo, J. and Jha, N. K. (2001). Battery-aware Static Scheduling for Distributed Real-time Embedded Systems. In *Proceedings of the 38th annual Design Automation Conference*, pages 444–449. ACM. 43

[138] Luo, X., Wang, J., Dooner, M., and Clarke, J. (2015). Overview of Current Development in Electrical Energy Storage Technologies and the Application Potential in Power System Operation. *Applied energy*, 137:511–536. 40

[139] Macal, C. M. and North, M. J. (2005). Tutorial on Agent-based Modeling and Simulation. In *Proceedings of the Winter Simulation Conference, 2005.*, pages 14–pp. IEEE. 67, 76

[140] Mansur, E., Mendelsohn, R., and Morrison, W. (2005). A Discrete-continuous Choice Model of Climate Change Impacts on Energy. 17, 18, 66

[141] Maqsood, I. and Huang, G. H. (2003). A Two-stage Interval-stochastic Programming Model for Waste Management Under Uncertainty. *Journal of the Air & Waste Management Association*, 53(5):540–552. 7

[142] Mariaud, A., Acha, S., Ekins-Daukes, N., Shah, N., and Markides, C. N. (2017). Integrated Optimisation of Photovoltaic and Battery Storage Systems for UK Commercial Buildings. *Applied energy*, 199:466–478. 44

[143] Marmidis, G., Lazarou, S., and Pyrgioti, E. (2008). Optimal Placement of Wind Turbines in a Wind Park Using Monte Carlo Simulation. *Renewable energy*, 33(7):1455–1460. 5

[144] Martin, K. (1994). A Teview by Discussion of Condition Monitoring and Fault Diagnosis in Machine Tools. *International Journal of Machine Tools and Manufacture*, 34(4):527–551. 42

[145] Masuda, Y. J., Liu, Y., Reddy, S. M., Frank, K. A., Burford, K., Fisher, J. R., and Montambault, J. (2018). Innovation Diffusion within Large Environmental NGOs Through Informal Network Agents. *Nature Sustainability*, 1(4):190. 67

[146] Meadows, M. and Cliff, D. (2012). Reexamining the Relative Agreement Model of Opinion Dynamics. *Journal of Artificial Societies and Social Simulation*, 15(4):4. 80

[147] Minnesota Stormwater Manual, m. (2018). Cost-benefit Considerations for Green Roofs. https://stormwater.pca.state.mn.us/index.php?title=Cost-benefit_considerations_for_green_roofs. 5, 81

[148] Mittal, A., Huang, W., and Krejci, C. C. (2017). Consumer-adoption Modeling of Distributed Solar Using an Agent-based Approach. In *Proceedings of the 2017 International Conference of The Computational Social Science Society of the Americas*, page 22. ACM. 68

[149] Mnih, V., Kavukcuoglu, K., Silver, D., Rusu, A. A., Veness, J., Bellemare, M. G., Graves, A., Riedmiller, M., Fidjeland, A. K., Ostrovski, G., et al. (2015). Human-level Control Through Deep Reinforcement Learning. *Nature*, 518(7540):529. 46, 58

[150] MPI (2017). New Earth System Model Of Max Planck Institute For Meteorology. http://www.mpimet.mpg.de/en/science/models/mpi-esm.html. 19, 84

[151] NASA (2018). Climate Change: How Do We Know? https://climate.nasa.gov/evidence/. 67

[152] Nate Burg, E. (2018). What Will We Do with All Those Solar Panels when Their Useful Life Is Over? http://www.eco-business.com/news/what-will-we-do-with-all-those-solar-panels-when-their-useful-life-is-over/. 133

[153] NCAR (2017). CESM Models. http://www.cesm.ucar.edu/models/ccsm4.0//. 19, 84

[154] Negahban, A. and Yilmaz, L. (2014). Agent-based Simulation Applications in Marketing Research: An Integrated Review. *Journal of Simulation*, 8(2):129–142. 67

[155] Niachou, A., Papakonstantinou, K., Santamouris, M., Tsangrassoulis, A., and Mihalakakou, G. (2001). Analysis of the Green Roof Thermal Properties and Investigation of Its Energy Performance. *Energy and Buildings*, 33(7):719–729. 3, 6

[156] NOAA (2018). National Weather Service Forecast Office. https://w2.weather.gov/climate/xmacis.php?wfo=mrx. xi, 87, 88

[157] Noyan, N. (2012). Risk-averse Two-stage Stochastic Programming with an Application to Disaster Management. *Computers & Operations Research*, 39(3):541–559. 7

[158] NREL (2018a). Best Research-Cell Efficiencies. https://www.nrel.gov/pv/assets/pdfs/pv-efficiencies-07-17-2018.pdf. 85

[159] NREL (2018b). U.S. Solar Radiation Resource Maps. https://rredc.nrel.gov/solar/old_data/nsrdb/1961-1990/redbook/atlas/. xi, 86, 87, 88

[160] Oberhofer, A. and Meisen, P. (2012). Energy Storage Technologies & Their Role in Renewable Integration. *Global Energy Network Institute*, 1. 40

[161] Ordóñez, J., Jadraque, E., Alegre, J., and Martínez, G. (2010). Analysis of the Photovoltaic Solar Energy Capacity of Residential Rooftops in Andalusia (Spain). *Renewable and Sustainable Energy Reviews*, 14(7):2122–2130. 5, 66

[162] OShaughnessy, E. J., Ardani, K. B., Cutler, D. S., and Margolis, R. M. (2017). Solar Plus: A Holistic Approach to Distributed Solar PV. Technical report, National Renewable Energy Lab.(NREL), Golden, CO (United States). 45

[163] Palm, A. (2017). Peer Effects in Residential Solar Photovoltaics AdoptionA Mixed Methods Study of Swedish Users. *Energy research & social science*, 26:1–10. 69

[164] Palmer, J., Sorda, G., and Madlener, R. (2015). Modeling the Diffusion of Residential Photovoltaic Systems in Italy: An Agent-based Simulation. *Technological Forecasting and Social Change*, 99:106–131. 88, 89

[165] Parfomak, P. W. (2012). Energy Storage for Power Grids and Electric Transportation: A Technology Assessment. *Congressional Research Service*, 42455. 40

[166] Parisio, A. and Jones, C. N. (2015). A Two-stage Stochastic Programming Approach to Employee Scheduling in Retail Outlets with Uncertain Demand. *Omega*, 53:97–103. 7

[167] Park, H. S., Jeong, K., Hong, T., Ban, C., Koo, C., and Kim, J. (2016). The Optimal Photovoltaic System Implementation Strategy to Achieve the National Carbon Emissions Reduction Target in 2030: Focused on Educational Facilities. *Energy and Buildings*, 119:101–110. 6, 66

[168] Photovoltaic Software, p. (2017). How to Calculate the Annual Solar Energy Output of A Photovoltaic System? https://photovoltaic-software.com/principle-ressources/how-calculate-solar-energy-power-pv-systems. 88

[169] Porsche, U. and Köhler, M. (2013). Life Cycle Costs of Green Roofs. *World Climate & Energy Event*. 5, 81

[170] Port of Long Beach, P. (2016). Energy Storage Technologies White Paper. http://www.polb.com/civica/filebank/blobdload.asp?BlobID=13596. 39, 40, 41

[171] Post, T. D. (2018). As Nations Strictest Green Roof Law Takes Effect in Denver, Plenty of Uncertainty Swirls Around Voter-passed Requirements. https://www.denverpost.com/2017/12/31/denver-green-roof-law/. 65

[172] Prasad, A. R. and Natarajan, E. (2006). Optimization of Integrated Photovoltaic–wind Power Generation Systems with Battery Storage. *Energy*, 31(12):1943–1954. 45

[173] Princeton University (2017). Geophysical Fluid Dynamics Laboratory. https://www.gfdl.noaa.gov/earth-system-model/. 19, 84

[174] Rai, V. and Robinson, S. A. (2015). Agent-based Modeling of Energy Technology Adoption: Empirical Integration of Social, Behavioral, Economic, and Environmental Factors. *Environmental Modelling & Software*, 70:163–177. 69, 71, 73, 78, 81, 94

[175] Raji, B., Tenpierik, M. J., and van den Dobbelsteen, A. (2015). The Impact of Greening Systems on Building Energy Performance: A Literature Review. *Renewable and Sustainable Energy Reviews*, 45:610–623. 16, 18, 86

[176] Rakhmatov, D. and Vrudhula, S. (2003). Energy Management for Battery-powered Embedded Systems. *ACM Transactions on Embedded Computing Systems (TECS)*, 2(3):277–324. 43, 44

[177] Ramshani, M., Khojandi, A., Li, X., and Omitaomu, O. (2018). Optimal Planning of the Joint placement of Photovoltaic Panels and Green Roofs Under Climate Change Uncertainty. *Omega*. 39, 67, 73, 83

[178] Rao, R. and Vrudhula, S. (2005). Battery Optimization vs Energy Optimization: Which to Choose and When? In *Proceedings of the 2005 IEEE/ACM International conference on Computer-aided design*, pages 439–445. IEEE Computer Society. 43, 44

[179] Rasoulkhani, K., Logasa, B., Reyes, M. P., and Mostafavi, A. (2017). Agent-based Modeling Framework for Simulation of Complex Adaptive Mechanisms Underlying Household Water Conservation Technology Adoption. In *Simulation Conference (WSC), 2017 Winter*, pages 1109–1120. IEEE. 68, 76, 78

[180] Refahi, A. H. and Talkhabi, H. (2015). Investigating the Effective Factors on the Reduction of Energy Consumption in Residential Buildings with Green Roofs. *Renewable Energy*, 80:595–603. 3, 4, 11, 15

[181] Rehman, S., Bader, M. A., and Al-Moallem, S. A. (2007). Cost of Solar Energy Generated Using PV Panels. *Renewable and Sustainable Energy Reviews*, 11(8):1843–1857. 2, 67

[182] Revision Energy, R. (2016). Why Go Solar? https://www.revisionenergy.com/why-go-solar/solar-power-can-be-stored-for-later-use/. 40

[183] Rezvanizaniani, S. M., Liu, Z., Chen, Y., and Lee, J. (2014). Review and Recent Advances in Battery Health Monitoring and Prognostics Technologies for Electric Vehicle (EV) Safety and Mobility. *Journal of Power Sources*, 256:110–124. 43

[184] Robinson, S. A. and Rai, V. (2015). Determinants of Spatio-temporal Patterns of Energy Technology Adoption: An Agent-based Modeling Approach. *Applied Energy*, 151:273–284. 68

[185] Rogers, E. M. (1962). Diffusion of Innovations. *New York, NY: Free Press of Glencoe*. 67

[186] Rogers, E. M. (2010). *Diffusion of Innovations*. Simon and Schuster. 70, 76

[187] Rosenthal, D. H., Gruenspecht, H. K., and Moran, E. A. (1995). Effects of Global Warming on Energy Use for Space Heating and Cooling in the United States. *The Energy Journal*, pages 77–96. 17, 18, 66

[188] Ruth, M. and Lin, A.-C. (2006). Regional Energy Demand and Adaptations to Climate Change: Methodology and Application to the State of Maryland, USA. *Energy policy*, 34(17):2820–2833. 17, 18, 66

[189] Saha, B., Goebel, K., and Christophersen, J. (2009). Comparison of Prognostic Algorithms for Estimating Remaining Useful Life of Batteries. *Transactions of the Institute of Measurement and Control*, 31(3-4):293–308. 42

[190] Sailor, D. J. (2001). Relating Residential and Commercial Sector Electricity Loads to Climateevaluating State Level Sensitivities and Vulnerabilities. *Energy*, 26(7):645–657. 17, 18, 66

[191] Sailor, D. J. and Pavlova, A. (2003). Air Conditioning Market Saturation and Long-term Response of Residential Cooling Energy Demand to Climate Change. *Energy*, 28(9):941–951. 17, 18, 66

[192] Santamouris, M. (2014). Cooling the Cities–A Review of Reflective and Green Roof Mitigation Technologies to Fight Heat Island and Improve Comfort in Urban Environments. *Solar energy*, 103:682–703. 6, 66

[193] Santoso, T., Ahmed, S., Goetschalckx, M., and Shapiro, A. (2005). A Stochastic Programming Approach for Supply Chain Network Design under Uncertainty. *European Journal of Operational Research*, 167(1):96–115. 73

[194] Scherba, A., Sailor, D. J., Rosenstiel, T. N., and Wamser, C. C. (2011). Modeling Impacts of Roof Reflectivity, Integrated Photovoltaic Panels and Green Roof Systems on Sensible Heat Flux into the Urban Environment. *Building and Environment*, 46(12):2542–2551. 2

[195] Schneising, O., Reuter, M., Buchwitz, M., Heymann, J., Bovensmann, H., and Burrows, J. (2014). Terrestrial Carbon Sink Observed from Space: Variation of Growth Rates and Seasonal Cycle Amplitudes in Response to Interannual Surface Temperature Variability. *Atmospheric Chemistry and Physics*, 14(1):133–141. 2

[196] Scott, M. J., Dirks, J. A., and Cort, K. A. (2005). The Adaptive Value of Energy Efficiency Programs in a Warmer World. Technical report, Pacific Northwest National Lab.(PNNL), Richland, WA (United States). 17, 18, 66

[197] SEIA, S. E. I. A. (2018). Net Metering. https://www.seia.org/initiatives/net-metering. 15, 85

[198] Smith, E. R. and Conrey, F. R. (2007). Agent-based Modeling: A New Approach for Theory Building in Social Psychology. *Personality and social psychology review*, 11(1):87–104. 67

[199] Snodgrass, E. C. and Snodgrass, L. L. (2006). *Green Roof Plants: A Resource and Planting Guide*. Number 04; SB419. 5, S5. Timber Press Portland. 6

[200] Solar Direct (2017). Solar Electric System Sizing. http://www.solardirect.com/pv/systems/gts/gts-sizing-sun-hours.html. 21

[201] Solar Power Authority, s. (2018). How to Calculate Your Peak Sun-Hours. https://www.solarpowerauthority.com/how-to-calculate-your-peak-sun-hours/. 10

[202] Solar Power World, S. (2015a). Batteries: Which is Best for Solar Storage? https://www.solarpowerworldonline.com/2015/08/what-is-the-best-type-of-battery-for-solar-storage/. 40

[203] Solar Power World, S. (2015b). Solar Storage Charging Up. https://www.solarpowerworldonline.com/2015/06/solar-storage-charging-up/. 40

[204] Solar Quotes (2017). Inverters. https://www.solarquotes.com.au/inverters/. 13, 18

[205] Sonne, J. (2006). Evaluating Green Roof Energy Performance. *Ashrae Journal*, 48(2):59. 3

[206] Spala, A., Bagiorgas, H., Assimakopoulos, M., Kalavrouziotis, J., Matthopoulos, D., and Mihalakakou, G. (2008). On the Green Roof System. Selection, State of the Art and Energy Potential Investigation of a System Installed in an Office Building in Athens, Greece. *Renewable Energy*, 33(1):173–177. 16, 18, 86

[207] SPR (2019). How Much Electricity Does A Solar Panel Produce? https://www.solarpowerrocks.com/solar-basics/how-much-electricity-does-a-solar-panel-produce/. 81

[208] SVS (2017). Renewable Solutions. http://www.svsolar.com/projects/harned.htm. xiii, 3

[209] Takriti, S., Birge, J. R., and Long, E. (1996). A Stochastic Model for the Unit Commitment Problem. *IEEE Transactions on Power Systems*, 11(3):1497–1508. 73

[210] Tant, J., Geth, F., Six, D., Tant, P., and Driesen, J. (2013). Multiobjective Battery Storage to Improve PV Integration in Residential Distribution Grids. *IEEE Transactions on Sustainable Energy*, 4(1):182–191. 44

[211] The City of Knoxville, C. (2018). 2017-2018 Budget. http://www.knoxvilletn.gov/government/city_departments_offices/Finance/budget/budget_archive/2017-2018_budget/. 7, 17

[212] The Daily Caller, T. (2015). Top 11 Problems Plaguing Solar and Wind Power. http://dailycaller.com/2015/12/25/top-11-problems-plaguing-solar-and-wind-power. 40

[213] The Department of Energy, d. (2019). Business Energy Investment Tax Credit (ITC). https://www.energy.gov/savings/business-energy-investment-tax-credit-itc. 94

[214] The Week, T. (2014). Does Solar Energy Have a Battery Problem? http://theweek.com/articles/444064/does-solar-energy-have-battery-problem. 39, 40

[215] Tyagi, V., Rahim, N. A., Rahim, N., Jeyraj, A., and Selvaraj, L. (2013). Progress in Solar PV Technology: Research and Achievement. *Renewable and sustainable energy reviews*, 20:443–461. 5, 66

[216] UDI (2017). Oak Ridge National Laboratorys Urban Dynamics Institute. https://udi.ornl.gov. 4, 18, 21, 81, 83, 86, 87

[217] U.S Census Bureau, p. (2013). How Big is Your Neighborhood? Using the AHS and GIS to Determine the Extent of Your Community. https://www.census.gov/content/dam/Census/programs-surveys/ahs/working-papers/how_big_is_your_neighborhood.pdf. 88, 89

[218] U.S Census Bureau, p. (2019). 2013 - 2017 American Community Survey 5-year Estimates. https://www.census.gov/programs-surveys/acs/news/data-releases.html?#. 88

[219] U.S. Department of Energy, D. (2016). Advanced Batteries 2016 Annual Progress Report. https://www.energy.gov/eere/vehicles/downloads/advanced-batteries-2016-annual-progress-report. 40

[220] Van Hoesen, J. and Letendre, S. (2010). Evaluating Potential Renewable Energy Resources in Poultney, Vermont: A GIS-based Approach to Supporting Rural Community Energy Planning. *Renewable Energy*, 35(9):2114–2122. 5, 66

[221] Van Slyke, R. M. and Wets, R. (1969). L-shaped Linear Programs with Applications to Optimal Control and Stochastic Programming. *SIAM Journal on Applied Mathematics*, 17(4):638–663. 23

[222] Waag, W., Fleischer, C., and Sauer, D. U. (2014). Critical Review of the Methods for Monitoring of Lithium-ion Batteries in Electric and Hybrid Vehicles. *Journal of Power Sources*, 258:321–339. 42

[223] Wang, A., Kadam, S., Li, H., Shi, S., and Qi, Y. (2018). Review on Modeling of the Anode Solid Electrolyte Interphase (SEI) for Lithium-ion Batteries. *npj Computational Materials*, 4(1):15. 41

[224] Wang, C. and Nehrir, M. H. (2004). Analytical Approaches for Optimal Placement of Distributed Generation Sources in Power Systems. *IEEE Transactions on Power systems*, 19(4):2068–2076. 5

[225] Watts, D. J. and Strogatz, S. H. (1998). Collective Dynamics of Small-world Networks. *nature*, 393(6684):440. 79, 92

[226] Webber, M. (2006). Innovation Diffusion: A New Perspective. *Progress in Human Geography*, 30(4):487–489. 67

[227] Weitzel, T., Schneider, M., Glock, C. H., Löber, F., and Rinderknecht, S. (2018). Operating a Storage-augmented Hybrid Microgrid Considering Battery Aging Costs. *Journal of Cleaner Production*, 188:638–654. 45

[228] Whaley, C. (2016). Best Practices in Photovoltaic System Operations and Maintenance. Technical report, National Renewable Energy Lab.(NREL), Golden, CO (United States). 11, 14, 18

[229] Wholesale Solar, W. (2018). Power Inverters. https://www.wholesalesolar.com/power-inverters. 13

[230] Wiese, S., Libby, L., Energy, A., Long, E., and Ryan, B. (2010). A Solar Rooftop Assessment for Austin. In *SOLAR 2010 conference proceedings*. Phoenix AZ. 5, 66

[231] Witmer, L. (2010). *Quantification of the Passive Cooling of Photovoltaics Using*. PhD thesis, The Pennsylvania State University. 2, 4, 66

[232] Witmer, L. and Brownson, J. (2011). An Energy Balance Model of Green Roof Integrated Photovoltaics: A Detailed Energy Balance Including Microclimatic Effects. In *ASES*, pages 17–21. 3

[233] Wong, E., Akbari, H., Bell, R., and Cole, D. (2011). Reducing Urban Heat Islands: Compendium of Strategies. *Environmental Protection Agency, retrieved May*, 12:2011. 11

[234] Xu, B., Oudalov, A., Ulbig, A., Andersson, G., and Kirschen, D. (2016). Modeling of Lithium-ion Battery Degradation for Cell Life Assessment. *IEEE Transactions on Smart Grid*. 48, 134

[235] Yang, C.-J. (2010). Reconsidering Solar Grid Parity. *Energy Policy*, 38(7):3270–3273. 2

[236] Yang, J., Yu, Q., and Gong, P. (2008). Quantifying Air Pollution Removal by Green Roofs in Chicago. *Atmospheric environment*, 42(31):7266–7273. 6

[237] Yongqiang, Y., Xuehong, Z., and Yufu, G. (2004). Global Coupled Ocean-atmosphere General Circulation Models in LASG/IAP. *Advances in Atmospheric sciences*, 21(3):444–455. 18, 83

[238] Yoshio, M., Brodd, R., and Kozawa, A. (2009). *Lithium-ion Batteries: Science and Technologies*. Springer. 41

[239] Zhang, H., Vorobeychik, Y., Letchford, J., and Lakkaraju, K. (2016). Data-driven Agent-based Modeling, with Application to Rooftop Solar Adoption. *Autonomous Agents and Multi-Agent Systems*, 30(6):1023–1049. 70

[240] Zhang, J. and Lee, J. (2011). A Review on Prognostics and Health Monitoring of Li-ion Battery. *Journal of Power Sources*, 196(15):6007–6014. 42

[241] Zhao, H., Deng, N., Yan, J., Kang, W., Ju, J., Ruan, Y., Wang, X., Zhuang, X., Li, Q., and Cheng, B. (2018). A Review on node for Lithium-sulfur Batteries: Progress and Prospects. *Chemical Engineering Journal*. 41

[242] Zhao, J., Kucuksari, S., Mazhari, E., and Son, Y.-J. (2013). Integrated Analysis of High-penetration PV and PHEV with Energy Storage and Demand Response. *Applied energy*, 112:35–51. 71

[243] Zhao, J., Mazhari, E., Celik, N., and Son, Y.-J. (2011). Hybrid Agent-based Simulation for Policy Evaluation of Solar Power Generation Systems. *Simulation Modelling Practice and Theory*, 19(10):2189–2205. xi, 70, 76, 77, 88, 89, 94

[244] Zhao, M. and Srebric, J. (2012). Assessment of Green Roof Performance for Sustainable Buildings Under Winter Weather Conditions. *Journal of Central South University*, 19(3):639–644. 16, 18, 86

[245] Zhou, Z., Zhang, J., Liu, P., Li, Z., Georgiadis, M. C., and Pistikopoulos, E. N. (2013). A Two-stage Stochastic Programming Model for the Optimal Design of Distributed Energy Systems. *Applied Energy*, 103:135–144. 7

Appendices

Table A.1: The energy consumption for different sizes of residential buildings in the U.S. and the state of Tennessee, based on the report by EIA [68].

Size		Average U.S. (kWh)			Average TN (kWh)		
		Total	Space conditioning		Total	Space conditioning	
ft^2	m^2	Annual	Annual	Hourly	Annual	Annual	Hourly
250	23	12,192	5,852	0.67	10,729	4,560	0.52
500	46	16,090	7,723	0.88	14,159	6,018	0.69
1,000	93	21,248	10,199	1.16	18,698	7,947	0.91
1,500	139	26,318	12,633	1.44	23,160	9,843	1.12
2,000	186	29,864	14,335	1.64	26,280	11,169	1.28
2,500	232	33,527	16,093	1.84	29,504	12,539	1.43
3,000	279	36,077	17,317	1.98	31,748	13,493	1.54
3,500	325	38,568	18,513	2.11	33,940	14,424	1.65
4,000	372	46,159	22,156	2.53	40,620	17,263	1.97

Appendix A:

We use the data set *Fuel consumption: Totals and averages, U.S. homes* [68] from the 2009 survey by the EIA[68] in order to develop a regression model of the hourly energy consumption for space conditioning in the state of Tennessee as a function of residential building size. The average level of energy consumption in the residential sector in the state of Tennessee is 12% lower than that of the U.S. [68]. Moreover, in the U.S., 48% of the energy consumption in the residential sector is for space conditioning [68], while in TN this value equals to 42% [68]. Table A.1 presents the total annual energy consumption and the annual and hourly energy consumption for space conditioning for different sizes of residential buildings in the U.S. and TN, as reported by EIA [68]. Consequently, Figure A.1 presents our regression model of the hourly energy consumption for space conditioning in the state of Tennessee as a function of residential building size. The coefficient of determination, R^2, equals to 0.9816, suggesting that the model explains well the variation in the dependent variable.

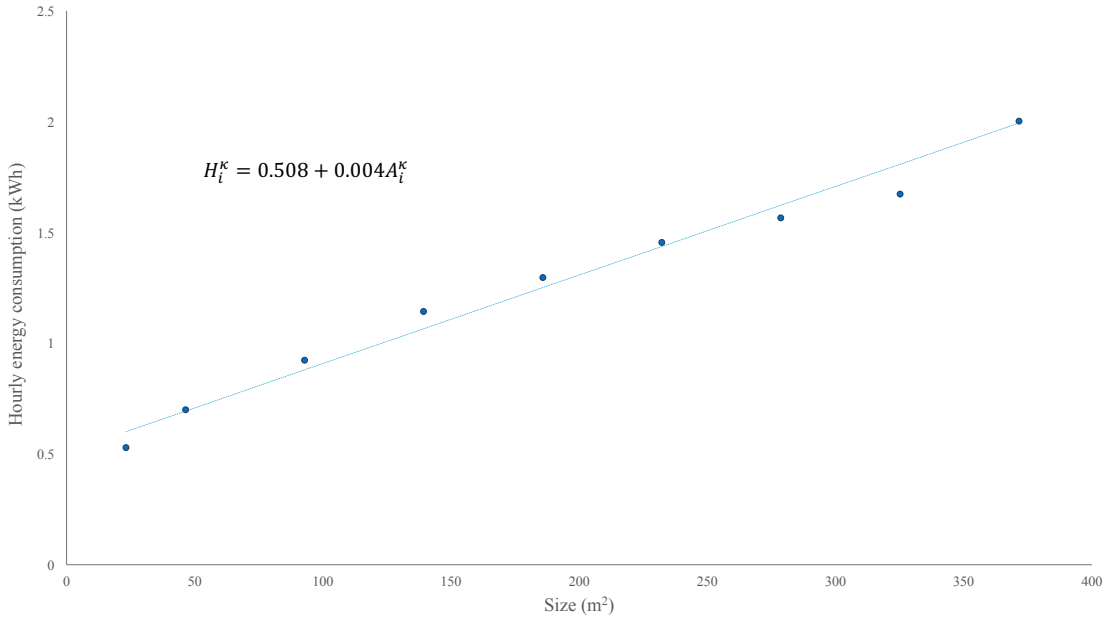


Figure A.1: Average hourly electricity consumption for space conditioning in the state of Tennessee versus building size, based on the data from [68]. The black line represents the regression line for the hourly energy consumption for space conditioning as a function of building size ($R^2 = 0.9816$).

Appendix B:

Figure B.1 depicts the monthly (and seasonal) changes in temperature up to year 2030 for the City of Knoxville, TN. Specifically, this figure presents the monthly average temperatures for the 10 projections, starting from January 2018 to December 2030. As seen in this figure, the monthly average temperatures are projected to slightly increase over the next decade or so.

Figure B.2 presents the yearly average temperatures for the ten projections up to year 2050 for the City of Knoxville, TN. Figure B.3 provides a detailed presentation of the daily average temperatures for these ten projections over the same period. As seen in these figure, although there is a variation across the projections, overall they all show an increasing pattern in the yearly and daily average temperatures over the next few decades.

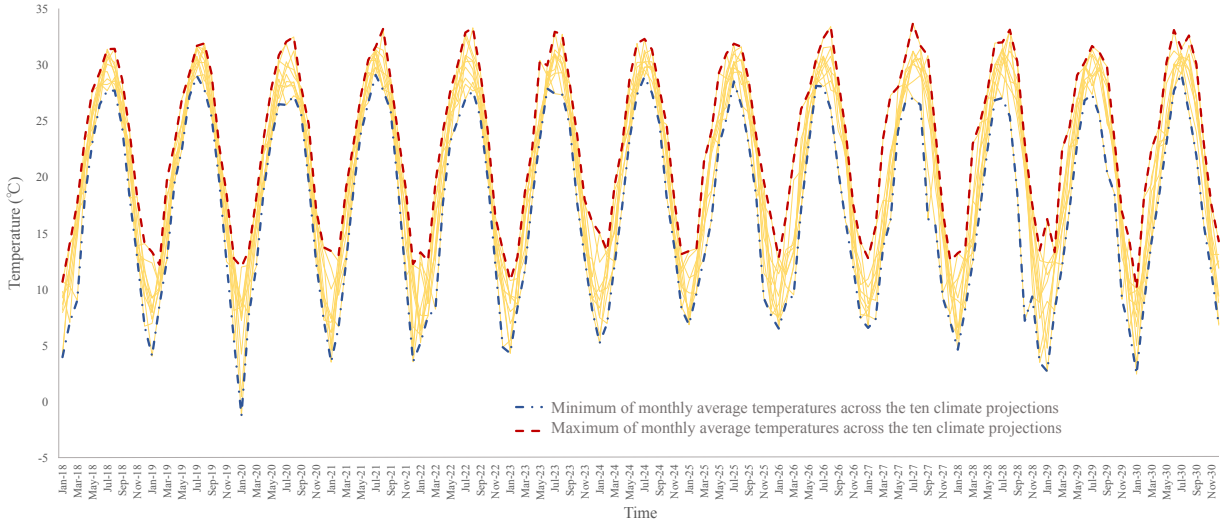


Figure B.1: The monthly average temperatures for the City of Knoxville, Tennessee for the ten different climate projections from January 2018 to December 2030. The dashed lines present the maximum and minimum temperatures across the ten projections.

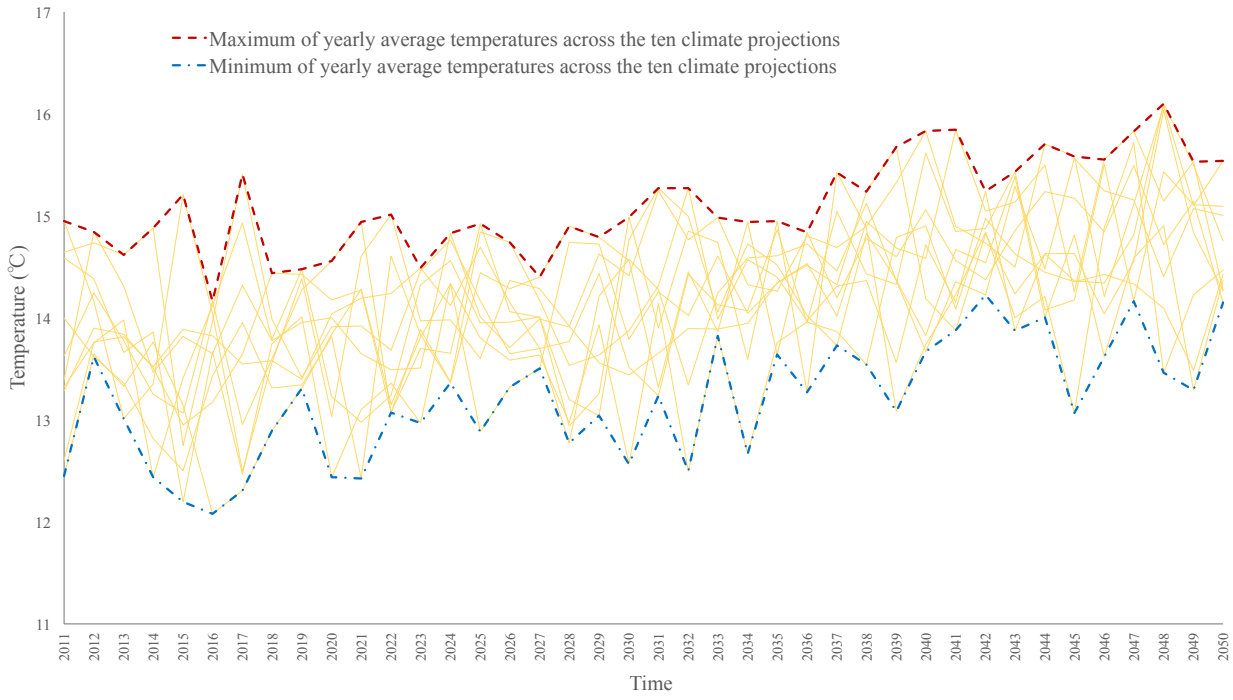


Figure B.2: The yearly average temperatures for the City of Knoxville, Tennessee for the ten different climate projections from January 2011 to December 2050. The dashed lines present the maximum and minimum temperatures across the ten projections.

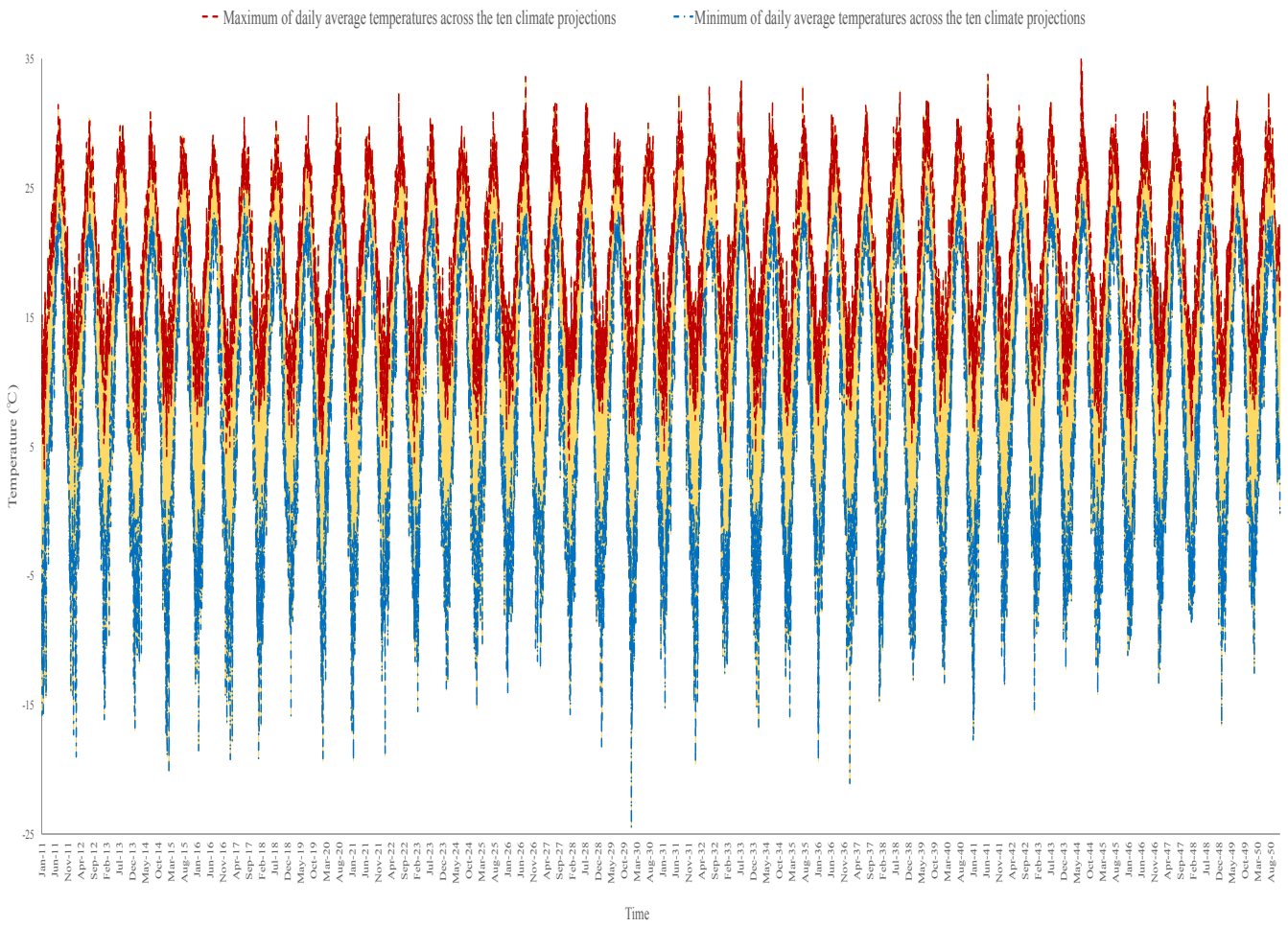


Figure B.3: The daily average temperatures for the City of Knoxville, Tennessee for the ten different climate projections from January 2011 to December 2050. The dashed lines present the maximum and minimum temperatures across the ten projections.

Appendix C:

Table C.1 shows the number of variables, constraints, and solution times for the three case studies shown in Table 5, for when $T = 10$ and $T = 20$ years.

Table C.1: The number of constraints, variables, and solution times for the three cases in Table 5.

	Number of constraints	Total number of variables	Number of binary variables	Run time (Seconds)	
				T = 10	T = 20
Case 1	1,868,267	1,453,098	415,168	438.9	442.2
Case 2	1,868,267	1,453,098	415,168	463.6	452.6
Case 3	1,868,267	1,453,098	415,168	422.2	446.9

Appendix D:

The level of requisite energy for the manufacturing process of PV panels has been throughly studied in the literature. Various studies have focused on the life cycle analysis (LCA) of PV panels [16], among which, [5] has been one of the most highly recognized and referenced works. Based on the report by [5], the manufacturing process of 1 m^2 of common PV systems (including the PV module, frame, and support) from extraction of raw material to finished product requires 1,500 kWh of energy. This level of energy consumption is based on the assumption made by the authors that all modules need to be mounted on Aluminum frames, resulting in a large increase in the amount of the energy consumption. However, more recently developed PV systems do not need to be installed on Aluminum frames, and can be mounted on cheaper and more environmental friendly options [16].

Based [72], most of PV panels in the U.S. are imported from Asia, with the highest percentage from China. [85] approximate the traveling distance for each individual panel from China to the U.S. to be equal to 21,005 km, 200 km of which is for freight trains, 50 km for lorry transit, and the rest is for freight ship transit. According to [**?**], shipping 1 ton of cargo for the given distances using their respective transportation type requires 1,589 kWh. Hence, considering that each individual PV panel weights between 10 kg to 20 kg [**?**], on average, shipping 1 m^2 PV panel from China to the U.S. requires 14.9 kWh of energy.

As for the end-of-life cycle of PV panels, as of 2018, the recycling industry for PV panels in the U.S. is still in its early days, as there is not enough PV panel waste generated to support a sustainable and profitable business [152]. For instance, there was only 6,500 tons of PV panel waste in the U.S. in 2016 [95]. Based on the U.S. regulations [95], PV panel waste falls under the general waste category. Therefore, due to lack of data, we do not consider any additional energy consumption for the end-of-life processing of PV panels.

Appendix F:

Property 1. For any remaining charge h, and battery temperature τ, the level of degradation due to charge/discharge increases in battery maximum available capacity, ℓ. That is, for a given level of charge/discharge a, a battery with a maximum available capacity $\ell + \varepsilon$ degrades more than a battery with a maximum available capacity ℓ. i.e.,

$$g(\ell + \varepsilon, h, a, \tau) \geq g(\ell, h, a, \tau). \tag{1}$$

Note that the difference in the degradation levels is smaller than the difference in the maximum available capacity. That is, for two batteries with maximum available capacities $\ell + \varepsilon$ and ℓ, we have

$$g(\ell + \varepsilon, h, a, \tau) - g(\ell, h, a, \tau) \leq \varepsilon. \tag{2}$$

We assume ε to be equal to capacity increment, δ. The degradation of the Li-ion battery follows the function given in Equation (2.3). Therefore,

$$g(\ell + \delta, h, a, \tau) - g(\ell_1, h, a, \tau) = (\ell + \delta)e^{-f_d} - \ell e^{-f_d} = \delta e^{-f_d} \leq \delta \tag{3}$$

This follows Equation (2.3), and the fact that e^{f_d} is always ≥ 1 [234].

In this paper, we let π denote the optimal policy. In addition, let $a_t^I(\ell, h, \phi)$ and $a_t^{II}(\ell, h, 1)$ denote the level of charge/discharge actions, and keep/replace actions, respectively.

Lemma 1. For any given day t, for $\phi = 1$, $R_t(\ell)$ is non-increasing in $\ell \geq \underline{\ell}$.

We define the salvage value function, $c_0(\ell)$, as a non-decreasing function in maximum available capacity, ℓ. That is, for any $\delta \geq 0$, $c_0(\ell + \delta) \geq c_0(\ell)$. As shown in Equation (2.5), for any given ℓ, $R_t(\ell)$ is calculated as the difference between a constant part, new battery cost and the income from a new battery starting at day t, and the salvage value, $c_0(\ell)$, which is a non-decreasing function in ℓ by the definition. Hence, $R_t(\ell)$ is non-increasing.

Lemma 2. For any given day t, and remaining available charge h, $V_t(\ell, h, 1)$ is non-increasing in $\ell \geq \underline{\ell}$.

For any given maximum available capacity ℓ, let π^{Δ} denote the set of actions starting in any state $s_t(\ell, h, \phi)$, where action $a_t^I(\ell - \Delta, h, \phi)$ and $a_t^{II}(\ell, h, 1)$, i.e., the level of charge/discharge,

and keep/replace, respectively, is taken in state $s_t(\ell, h, \phi)$ and all future actions are taken optimally. Let $U_t(\ell, h, \phi)$ be the total expected discounted cost to go starting from $s_t(\ell, h, \phi)$ following the charge/discharge and keep/replace actions given by π^{Δ}. We assume $\Delta = \delta$ and denote its relative set of actions by π^{δ}. We define $K_t^{\pi^{\delta}}(\ell, h)$ to be the expected cost to go from day t when the decision is to keep under π^{δ}. Note that the expected cost to go from day t when the decision is to replace, i.e., $R_t(\ell)$, is the same for π and π^{δ}. That is, for any given ℓ and Δ, $R_t^{\pi^{\Delta}}(\ell) = R_t(\ell)$. For instance, for $\ell = 0.9$ and $\Delta = 0.01$, $R_t^{\pi^{0.01}}(0.9) = R_t(0.9) = c - c_0(0.9) + \lambda \cdot V_t(\bar{\ell}, h_0, 0)$. Hence, starting from $s_t(\ell, h, 1)$ where $\ell = \underline{\ell} + \delta$, by Equations (2.4) - (2.6), we have

$$U_t(\underline{\ell} + \delta, h, 1) = \min\left\{R_t(\underline{\ell} + \delta), K_t^{\Pi^{\delta}}(\underline{\ell} + \delta, h)\right\} \leq R_t(\underline{\ell} + \delta) \leq R_t(\underline{\ell}) = V_t(\underline{\ell}, h, 1). \tag{4}$$

Note that $V_t(\ell, h, 1)$ is the total expected discounted cost to go starting from $s_t(\ell, h, \phi)$ under the optimal policy, i.e., $V_t(\underline{\ell} + \delta, h, 1) \leq U_t(\underline{\ell} + \delta, h, 1)$. Hence,

$$V_t(\underline{\ell} + \delta, h, 1) \leq U_t(\underline{\ell} + \delta, h, 1) \leq V_t(\underline{\ell}, h, 1). \tag{5}$$

Now we suppose that for any given t, h, and $\ell = \underline{\ell}, \underline{\ell} + \delta, \underline{\ell} + 2\delta, ..., \underline{\ell} + (k-1)\delta$ we have

$$V_t(\ell + \delta, h, 1) \leq V_t(\ell, h, 1). \tag{6}$$

Next, we show that $V_t(\ell + \delta, h, 1) \leq V_t(\ell, h, 1)$ for $\ell = \underline{\ell} + k\delta$. First, we have

$$\begin{aligned}
&U_t(\ell + \delta, h, 1) = U_t(\underline{\ell} + (k+1)\delta, h, 1) = \\
&\min\left\{R_t(\underline{\ell} + (k+1)\delta), K_t^{\pi^{\delta}}(\underline{\ell} + (k+1)\delta, h)\right\} = \\
&\min\Bigg\{c - c_0(\underline{\ell} + (k+1)\delta) + \lambda \cdot V_t(\bar{\ell}, h_0, 0), \\
&\lambda \cdot \sum_{y \in y(x)} V_t([\underline{\ell} + (k+1)\delta - g(\underline{\ell} + (k+1)\delta, h, \theta, \tau)], h + \theta, 0) P_y^t(y)\Bigg\},
\end{aligned} \tag{7}$$

where θ is the sub-optimal charge action in $s_t(\underline{\ell} + (k+1)\delta, h, 1)$, i.e., $\theta = \min\{a^I(\underline{\ell} + (k+1)\delta - \delta, h, 1), y\} = \min\{a^I(\underline{\ell} + k\delta, h, 1), y\}$. To simplify, we define $g(\underline{\ell} + k\delta + i\delta, h, \theta, \tau) \equiv \hat{g}(i)$.

For example, $g(\underline{\ell}+(k+1)\delta, h, \theta, \tau) \equiv \hat{g}(1)$. Hence, Equation (7) can be rewritten as

$$\begin{aligned} U_t(\underline{\ell}+(k+1)\delta, h, 1) = \min\Big\{ & c - c_0(\underline{\ell}+(k+1)\delta) + \lambda \cdot V_t(\overline{\ell}, h_0, 0), \\ & \lambda \cdot \sum_{y \in y(x)} V_t([\underline{\ell}+(k+1)\delta - \hat{g}(1)], h+\theta, 0) P_y^t(y) \Big\}. \end{aligned} \tag{8}$$

Recall from Equation (2) that the difference in the degradation level of two batteries with different maximum available capacities does not exceed the difference in their maximum available capacity. As a result, for $\Delta = \delta$, from Equation (2) we have

$$g(\ell+\delta, h, a, \tau) - g(\ell, h, a, \tau) \leq \delta. \tag{9}$$

Hence, $\hat{g}(1) \leq \hat{g}(0) + \delta$, and

$$\underline{\ell}+(k+1)\delta - \hat{g}(1) \geq \underline{\ell} + k\delta - \hat{g}(0). \tag{10}$$

Therefore, from Equations (11)-(10), we have

$$\begin{aligned} & U_t(\underline{\ell}+(k+1)\delta, h, 1) = \min\Big\{ c - c_0(\underline{\ell}+(k+1)\delta) + \lambda \cdot V_t(\overline{\ell}, h_0, 0), \\ & \lambda \cdot \sum_{y \in y(x)} V_t([\underline{\ell}+(k+1)\delta - \hat{g}(1)], h+\theta, 0) P_y^t(y) \Big\} \leq \\ & \min\Big\{ c - c_0(\underline{\ell}+k\delta) + \lambda \cdot V_t(\overline{\ell}, h_0, 0), \lambda \cdot \sum_{y \in y(x)} V_t([\underline{\ell}+k\delta - \hat{g}(0)], h+\theta, 0) P_y^t(y) \Big\} \\ & = V_t(\underline{\ell}+k\delta, h, 1) = V_t(\ell, h, 1) \end{aligned} \tag{11}$$

Recall that $U_t(\ell+\delta, h, 1)$ is the total expected discounted cost to go starting from $s_t(\ell+\delta, h, 1)$ under π^δ, and $V_t(\ell+\delta, h, 1)$ is the total expected discounted cost to go starting from $s_t(\ell+\delta, h, 1)$ under the optimal policy. Hence,

$$V_t(\ell+\delta, h, 1) \leq U_t(\ell+\delta, h, 1) \leq V_t(\ell, h, 1). \tag{12}$$

This follows from Equation (2.4) and (2.7), assumption of induction, Lemma 1, and the properties of minimum.

Corollary 1. For any given day t, and remaining available charge h, $K_t(\ell, h)$ is non-increasing in $\ell \geq \underline{\ell}$.

Let ℓ^1 and ℓ^2 denote maximum available capacities for two batteries, where $\ell^1 \leq \ell^2$. Let $\hat{A}_t^{1\,\ell_1}$ and $\hat{A}_t^{1\,\ell_2}$ denote the set of all possible actions when $\ell = \ell^1$ and $\ell = \ell^2$, respectively. It is trivial that $\hat{A}_t^{1\,\ell_1} \subseteq \hat{A}_t^{1\,\ell_2}$. Let $\hat{a}^{\ell_1} \in \hat{A}_t^{1\,\ell_1}$ denote the optimal action for which $K_t(\ell_1, h)$ is minimum. Let $\hat{a}^{\ell_2} \in \hat{A}_t^{1\,\ell_2}$ denote the optimal action for which $K_t(\ell_2, h)$ is minimum. If $\hat{a}^{\ell_2} = \hat{a}^{\ell_1}$, based on Property 1 and Lemma 1, $K_t(\ell_2, h) \leq K_t(\ell_1, h)$. If $\hat{a}^{\ell_2} \neq \hat{a}^{\ell_1}$, based on properties of minimum, the value for $K_t(\ell_2, h)$ under action $\hat{a}^{\ell_2}$ has to be smaller than or equal to the value for $K_t(\ell_2, h)$ when taking an action equal to $\hat{a}^{\ell_1}$. Hence, $K_t(\ell_2, h) \leq K_t(\ell_1, h)$.

Corollary 2. For any given day t, and maximum available capacity ℓ, $K_t(\ell, h)$ is non-increasing in h.

For any given *ell*, let h_1 and h_2 denote remaining available charges for the battery, where $h_1 \leq h_2$. It is trivial that $\hat{A}_t^{1\,h_2} \subset \hat{A}_t^{1\,h_1}$. Let θ_1 shows the charge level for which $K_t(ell, h_1)$ is minimum and $h_1 + \theta_1 = M_1$. Let M_2 be the final charge level for which $K_t(\ell, h_2)$ is minimum. If $M_1 = M_2$, then $\ell'^1 \leq \ell'_2$, and based on Lemma 1, $K_t(\ell, h_2) \leq K_t(\ell, h_1)$. If $M_1 \neq M_2$, then $K_t(\ell, h_2)$ must be smaller than $K_t(\ell, h_2)$ where $M_1 = M_2$, due to properties of minimum. Hence, $K_t(\ell, h_2) \leq K_t(\ell, h_1)$.

This corollary states that once we find a ℓ^* for a given h for which $R_t(\ell^*) \leq K_t(\ell^*, h)$, we can assume that $R_t(\ell^*) \leq K_t(\ell^*, h') \quad \forall h' \in [0, h]$. This also shows that for when $K_t(\ell^*, h) \leq R_t(\ell^*)$, we can assume that $K_t(\ell^*, h') \leq R_t(\ell^*) \quad \forall h' \in [h, 1]$.

Theorem 1. For any given day t, and remaining battery capacity h, $V_t(\ell, h, 1)$ is of threshold type policy. That is, there exists a maximum available capacity ℓ^* such that

$$V_t(\ell, h, 1) = \begin{cases} K_t(\ell, h), & \text{if} \quad \ell \geq \ell^*, \\ \\ R_t(\ell), & \text{otherwise}, \end{cases} \tag{13}$$

From Equation (2.5), $R_t(\ell)$ is constant in ℓ. By Corollary 1, for any remaining charge available h, $K_t(\ell, h)$ is non-increasing in ℓ. In Equation (2.4), we define $V_t(\ell, h, 1)$ as the minimum of $K(\ell, h)$ and $R(\ell)$. Hence, the result follows.

Note that this only holds if we consider a fixed salvage value for all ℓ, or we find a salvage value function which by considering the real cost of electricity cost, the increase in the salvage value of the battery based on ℓ is smaller than the added value due to the extra capacity.

Vita

Mohammad Ramshani was born in Tehran, Iran. He graduated in 2014 with a Masters degree in Systems Engineering from the University of Economic Sciences, Tehran, Iran. In the fall of 2015, he joined Dr. Xueping Li's group as a graduate assistant at the Department of Industrial and Systems Engineering of University of Tennessee, Knoxville (UTK). He is expected to complete his Doctor of Philosophy degree in 2019. His research interests include logistics and supply chain management, simulation, stochastic programming, and stochastic processes. He has published several peer-review journal and conference papers. He is a student member of the Institute for Operations Research and Management Sciences (INFORMS). In 2018, he worked as an Operations Research Analyst Co-op at Monsanto Company.